AD NUMBER

ADB016707

NEW LIMITATION CHANGE

TO

Approved for public release, distribution unlimited

FROM

Distribution authorized to U.S. Gov't. agencies only; Test and Evaluation; JUN 1975. Other requests shall be referred to Picatinny Arsenal, Attn: SARPA-TS-5, Dover NJ 07801.

AUTHORITY

USAARDC ltr, 5 Jun 1978

FINAL REPORT

DESIGN OF EXPLOSION BLAST CONTAINMENT VESSELS FOR EXPLOSIVE ORDNANCE DISPOSAL UNITS

B. Dale Troit, Joseph E. Backofen, and John J. White, III

June 1975

PICATINNY ARSENAL
Dover, New Jersey 07801

Contract No. DAAA21-72-C-0129

BATTELLE
Columbus Laboratories
505 King Avenue
Columbus, Ohio 43201

The findings of this report are not to be construed as an official Department of the Army position.

DISPOSITION

Destroy this report when no longer needed. Do not return it to the originator.

Unclassified

SECURITY CLASSIFICATION OF THIS PAGE (When Data Entered)

REPORT DOCUMENTATION PAGE

READ INSTRUCTIONS BEFORE COMPLETING FORM

1. REPORT NUMBER

2. GOVT ACCESSION NO.

3. RECIPIENT'S CATALOG NUMBER

(9)

4. TITLE (and Subtitle)

(6) DESIGN OF EXPLOSION BLAST CONTAINMENT VESSELS FOR EXPLOSIVE ORDNANCE DISPOSAL UNITS,

5. TYPE OF REPORT & PERIOD COVERED

Final Report. 9 Sep 1971 — 30 Jun 75

6. PERFORMING ORG. REPORT NUMBER

7. AUTHOR(s)

(10) B. Dale Frott, Joseph E. Backofen, Jr. and John J. White, III

8. CONTRACT OR GRANT NUMBER(s)

(15) Contract No. DAAA21-72-C-0129 new

9. PERFORMING ORGANIZATION NAME AND ADDRESS

Battelle-Columbus Laboratories
505 King Avenue
Columbus, Ohio 43201

10. PROGRAM ELEMENT, PROJECT, TASK AREA & WORK UNIT NUMBERS

(11) Jun 75

11. CONTROLLING OFFICE NAME AND ADDRESS

U.S. Army
Picatinny Arsenal
Dover, New Jersey 07801

(12) 114p.

12. REPORT DATE

13. NUMBER OF PAGES

14. MONITORING AGENCY NAME & ADDRESS(if different from Controlling Office)

15. SECURITY CLASS. (of this report)

UNCLASSIFIED

15a. DECLASSIFICATION/DOWNGRADING SCHEDULE

16. DISTRIBUTION STATEMENT (of this Report)

Distribution limited to U.S. Government Agencies only (test and evaluation; June 1975). Other requests for this document must be referred to Picatinny Arsenal, Attn: SARPA-TS-S, Dover, N.J. 07801

17. DISTRIBUTION STATEMENT (of the abstract entered in Block 20, if different from Report)

DDC RECEIVED MAR 1 1977 A

18. SUPPLEMENTARY NOTES

19. KEY WORDS (Continue on reverse side if necessary and identify by block number)

Explosive containment vessels
Blast containment vessels
Explosive ordnance disposal
Elastic response of vessels

20. ABSTRACT (Continue on reverse side if necessary and identify by block number)

Completely enclosed spherical containment vessels in 2.0-ft-diam, 0.5-in.-wall, 3.0-ft-diam, 0.73-in.-wall, and 4.5 ft-diam, 1.0-in.-wall were designed and tested. A computer program was written to calculate the maximum response of spherical vessels to symmetric internal blast loads including elastic and plastic strains. Good agreement between calculation and experiment was obtained for both elastic and plastic vessel deformations.

(Continued)

DD FORM 1 JAN 73 1473 EDITION OF 1 NOV 65 IS OBSOLETE

Unclassified

SECURITY CLASSIFICATION OF THIS PAGE (When Data Entered)

407080

20. (Continued)

The effectiveness of two 60% dynamites in producing stress on the vessel walls was found to be a function of the scaled distance to the vessel walls. Their effectiveness increased from ~0.5 at a scaled distance of 2.5 ft/lb$^{1/3}$ to ~0.8 at a scaled distance of 1.3, relative to 50/50 Pentolite at 0.73 to 0.80 g/cm^3.

The maximum strain produced by a suitcase-shaped charge with dimensions in the ratio 1:2:3, was found to exceed the average effect of compact cylindrical-shaped charges as a function of the scaled distance. The factors were 1.3 to 1.4 at a scaled distance of 1.80 ft/lb$^{1/3}$ to slightly over 3 at a scaled distance of 0.9 ft/lb$^{1/3}$.

The single-shot failure limit for the 2.0-ft vessels was determined at between 6.5 and 7.0 lb of Composition C-4. The two-shot failure limit was determined at between 5.0 and 6.0 lb of C-4, for vessels of A-516, Grade 70 steel. The single-shot limit corresponds to the maximum wall stress from the calculated confined explosion gas pressure exceeding the static ultimate strength of the vessel material.

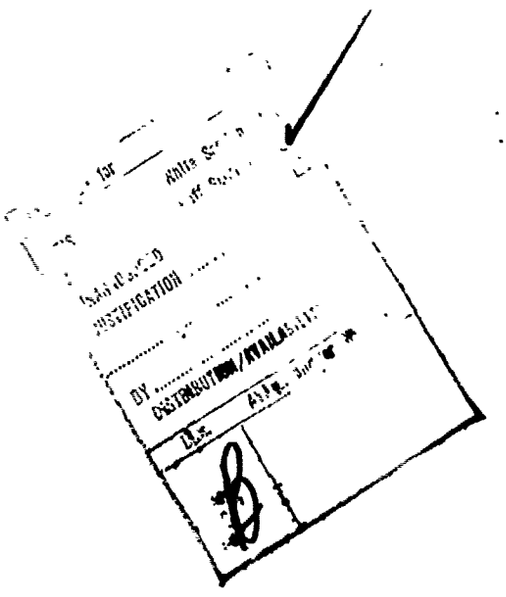

SUMMARY

This report describes an experimental and analytical investigation of the design and performance of spherical vessels for containment of explosive blast for application by explosive-ordnance disposal teams. During this program a total of eight spherical steel containment vessels were fabricated. The diameters and wall thicknesses investigated were 2.0 ft with 0.5-in. walls, 3.0 ft with 0.75-in. walls, and 4.5 ft with 1.0-in. walls. The vessel ports were approximately one radius in diameter and completely closed by flat steel doors overlaying the ports from the inside.

During the course of this program a computer code was developed which calculated the maximum elastic-plastic response and residual plastic strain of spherical, thin-walled vessels in response to an internal, triangular shock wave followed by a static internal pressure. The code in its present form uses measured shock-wave parameters from Pentolite and static pressures which may be calculated for a number of explosives.

The relative effectiveness of four explosives was studied in the 3.0- and 4.5-ft-diameter vessels. The relative effectiveness as used here is the ratio of first-cycle maximum strains produced in the vessel wall. The Pentolite used in this investigation (a granular form with a bulk density of 0.73 to 0.80 g/cm^3) produced an elastic response 20 to 24 percent less than the response predicted analytically for full-density Pentolite, independent of the charge and vessel size. The relative effectiveness of both DuPont Special Gelatin, 60% Strength and Gelex-1 dynamites was very similar. Both showed increasing effectiveness with decreasing scaled distance relative to the Pentolite investigated. Their effectiveness relative to the low-density Pentolite increased from $\sim$0.5 at a scaled distance of 2.5 ft/lb$^{1/3}$ to $\sim$0.8 at a scaled distance of 1.3 ft/lb$^{1/3}$. The 3FA black powder investigated produced very small vessel responses in comparison to the detonating explosives.

The relative effectiveness of charges in a suitcase geometry (relative dimensions 1:2:3) as compared to cylinders with $\ell/d = 1$ was found also to be a function of the scaled distance. The response of the spherical vessels to these asymmetric charges was found to be highly anisotropic. In that part of the vessel which showed the maximum response to the suitcase-shaped charges (directly opposite the major flat charge face), the relative effectiveness varied from $\sim$1.3 to 1.4 at a scaled distance of 1.80 ft/lb$^{1/3}$ to slightly over 3 at a scaled distance of 0.9 ft/lb$^{1/3}$.

The effectiveness of expanded vermiculite and small glass bottles as blast-attenuating vessel filler materials was investigated in a preliminary way, in a 4.5-ft-diameter vessel. The relative

effectiveness was measured by the first-cycle strain for the filled vessel divided by the first-cycle strain for the unfilled vessel. For vermiculite, in single shots at each charge level, the effectiveness changed from 0.21 with 2 lb of Pentolite to 0.66 at 8 lb of Pentolite to 0.48 at 10 lb of Pentolite. From this preliminary information, the effectiveness of the vermiculite is shown to be decreasing with increasing charge size, however, the upper limit of charge size for which a vermiculite fill will still be beneficial is not clear from the present data.

Small glass bottles (1 to 8 oz) were investigated as a shock-attenuating filler in a single 8-lb Pentolite shot. Although the vessel response was complex, it was judged that the glass was of little benefit in this role.

Plastic deformation as measurable by changes in distance between fiducial marks on the vessel surface ($\pm$0.05 percent) was first observed (0.7 percent) on the 3.0-ft-diameter vessel at a charge load of 6.5 lb of Special Gelatin, 60% Strength dynamite in a suitcase-shaped charge. This vessel successfully contained four additional charges at greater loads than this up to a maximum of 12 lb of the same charge type, with a maximum accumulated residual plastic strain of 2.7 percent. At the conclusion of these tests, this vessel was still free of catastrophic damage and has been in use for test firings at Picatinny Arsenal for nearly three years.

A series of tests was conducted to determine the single-shot failure limits on four 2.0-ft-diameter vessels. For spherical Composition C-4 charges, the failure limit was found between 6.5 lb (4.86 percent residual strain) and 7.0 lb (catastrophic failure). An elastic-plastic computer code calculation produced good agreement with the recorded plastic strains for these vessels using 80,000-psi yield strength for these vessels, which is appreciably in excess of the static properties of 53,300 psi (0.2 percent offset) yield and 75,300-psi ultimate tensile strengths. This difference is attributable to strain-rate effects on the mechanical properties. The calculated confined explosive gas pressure in these vessels brackets 75,000-psi maximum wall stress between 6.5 and 7.0 lb of C-4. Thus, it appears that the ultimate failure of these vessels may have been influenced by the confined gas pressure working against the static properties of the steel, while the initial plastic strain was produced by the initial shock wave working against strain-rate-hardened material.

TABLE OF CONTENTS

TABLE OF CONTENTS
(Continued)

LIST OF TABLES

TABLE OF CONTENTS
(Continued)

Page

LIST OF TABLES
(Continued)

LIST OF FIGURES

TABLE OF CONTENTS
(Continued)

Page

LIST OF TABLES
(Continued)

TABLE OF CONTENTS
(Continued)

Page

LIST OF FIGURES
(Continued)

TABLE OF CONTENTS
(Continued)

Page

LIST OF FIGURES
(Continued)

DESIGN OF EXPLOSION BLAST CONTAINMENT VESSELS FOR EXPLOSIVE ORDNANCE DISPOSAL UNITS

B. Dale Trott, Joseph E. Backofen, and John J. White, III

INTRODUCTION

This study was initiated in September 1971 with the objective to develop design information for a completely enclosed spherical blast containment vessel. Included in the initial objective was the development of the relative elastic response of spherical vessels to Pentolite, nitroglycerin-base and ammonium nitrate dynamites, and black powder, as well as the relative effects of a suitcase-shaped charge versus a compact charge shape. These effects were to be evaluated in the range of elastic response of the vessels. In the special case of nitroglycerin-base dynamite in a suitcase-shaped charge, the charges required to produce significant plastic deformation of a vessel were to be determined. As these objectives were realized, an improved design for an access-port closure mechanism (the single-pin door support), which originated with Mr. Jon Petry of Picatinny Arsenal, was developed, implemented, and evaluated at Battelle in a 4.5-ft-diameter vessel in a subsequent contract modification. In a further contract modification, the effects of two blast-attenuation filler materials were investigated, and a series of four small (2.0-ft diameter) vessels were fabricated to determine the failure limits of the evolving design. Hydrostatic tests were also conducted on the 4.5-ft-diameter vessel to verify the performance of the dynamic strain gages installed on this vessel. This is the final report on this work.

During the time this work was in progress a computer code to evaluate the elastic-plastic response of spherical vessels to internal blast loading was developed. Portions of the development of this analysis, which is based on the work of Baker[1], were supported by this program. The "Analysis" section of this report describes the basis for this predictive tool and shows some representative effects.

The "Vessel Design and Construction" section gives the details of vessel designs and design methodology developed in this program as well as the details of their construction, with emphasis on the welding procedures used.

The "Experimental Procedures" section describes the details of the strain-gage instrumentation used on the vessels, the means for measurement of plastic strains, and provides a detailed description of the explosive charges and the hydrostatic test used to calibrate the strain gages. Also included in this section is a short chronological test summary of all charges fired in the total of eight vessels fabricated for this program.

The "Experimental Results and Discussion" section presents the experimental results obtained in this program together with the matching analytical predictions where applicable.

ANALYSIS OF RESPONSE OF SPHERICAL VESSELS

The analysis of the response of spherical vessels to internal blast loading is based on the work of W. E. Baker[1]*. It is based on the following assumptions:

- Spherical symmetry
- Thin-walled vessel
- Shock-wave loading by a triangular shock wave followed by a static pressure in the vessel
- Undamped vibration
- No gravitational stresses
- The vessel material is elastic-plastic with linear work-hardening.

Because the initial objectives of the program were directed toward understanding the elastic response of the vessels, the analysis was carried out in three stages. First, the elastic response of a vessel to a triangular shock wave with no following static pressure was analyzed, later the elastic-plastic response was added, and finally the static-pressure effect was included. The complete analysis which has been conducted since the inception of this program has been partially supported by in-house funds and funds from the Naval Explosive Ordnance Disposal Facility, as well as by this program. Hence, a separate report describing the complete analysis is being prepared and will be distributed in the near future. The following brief description outlines the method of analysis used. For further details, the complete analysis should be consulted. The objective of the following analyses is the determination of the maximum displacement and stress, and, in the case of plastic deformation, the residual deformation and strain after all internal loading is removed.

Elastic Response

The elastic differential equations of motion of a spherical vessel driven by a triangular shock wave are:

---

* References are given at the end of the report.

$$\rho ha \frac{d^2 u_1}{dt^2} + 2h\sigma = ap(t) \text{ for } 0 \leq t \leq T_s, \tag{1}$$

and

$$\rho ha \frac{d^2 u_2}{dt^2} + 2h\sigma = aP_s \text{ for } t \geq T_s, \tag{2}$$

where ρ = density of vessel metal
h = vessel wall thickness
a = radius of vessel
u_1, u_2 = displacement of vessel wall before and after $t = T_s$, respectively
t = time
σ = tangential stress in vessel wall
$p(t) = P_r(1 - t/T_s)$
P_r = peak reflected shock pressure
T_s = time when the triangular shock wave terminates in the static pressure
P_s = static pressure following the shock wave.

These differential equations were solved using LaPlace transforms to yield equations of motion for the vessel for $0 \leq t \leq T_s$ and $t \geq T_s$ with the aid of the following boundary conditions and auxiliary relations:

$$\left.\begin{aligned} u_1 &= 0 \\ \frac{du_1}{dt} &= 0 \end{aligned}\right\} \text{ at } t = 0, \tag{3}$$

$$\left.\begin{aligned} u_1 &= u_2 \\ \frac{du_1}{dt} &= \frac{du_2}{dt} \end{aligned}\right\} \text{ at } t = T_s, \tag{4}$$

$$\sigma = \frac{E}{1 - \nu} \varepsilon = \frac{E}{1 - \nu} \frac{u}{a}, \tag{5}$$

where

E = Young's modulus
ν = Poisson's ratio.

Depending on the duration of the driving pressure pulse, the maximum response of the vessel may occur either before or after the end of the driving pulse. The quantity which governs this response was derived to be:

$$\omega T_s = 2.3311,$$

where

ω = fundamental breathing mode frequency

$$\omega = [2E/\rho a^2(1 - \nu)]^{1/2} . \tag{6}$$

If this quantity is positive or negative the maximum in response occurs either during or after the forcing period, T_s, respectively. The conditions for the maximum response were found by the usual techniques for evaluating maxima using the equation of motion for the appropriate time period.

The maximum elastic response of a spherical vessel thus found was programmed for computer evaluation initially and then later the elastic portion of the analysis was included in the present elastic-plastic computer program.

Data for the magnitude and duration of the driving air shock were obtained for 50/50 Pentolite explosive initially from the work of W. E. Baker, et al.[2], and later from the work of Goodman[3]. Little significant difference was found between these sources. The peak pressure, P_r, comes from experimentally measured peak normally reflected air shock data. The time duration, T, is calculated form experimentally measured impulse data so that the assumed triangular shock wave (returning to zero pressure) includes the measured impulse.

The time duration, T_s, is found from

$$T_s = T(1 - P_s/P_r). \tag{7}$$

This calculation may slightly overestimate the impulse delivered to the vessel wall by including P_s so early in time. However, for the values of P_s used, the inclusion of P_s changes the calculated results less than 1 percent from those calculated with $P_s = 0$ within the elastic range of response.

Values of the explosion gas pressure, P_s, were calculated using the appropriate subroutines included in the work of Proctor[4]. In his study, Proctor shows that his method for calculation of the explosion gas pressure produces values in good agreement with experimental data obtained by several investigators.

Figure 1 shows the calculated elastic response for several vessels. It was noted that the calculated variation in maximum stress, σ, with weight of explosive, W, approximated a family of straight lines all with the same slope. It was decided that a simple empirical fit of the computer-calculated points would be a useful tool. Such a fit can be expressed by an equation of the form

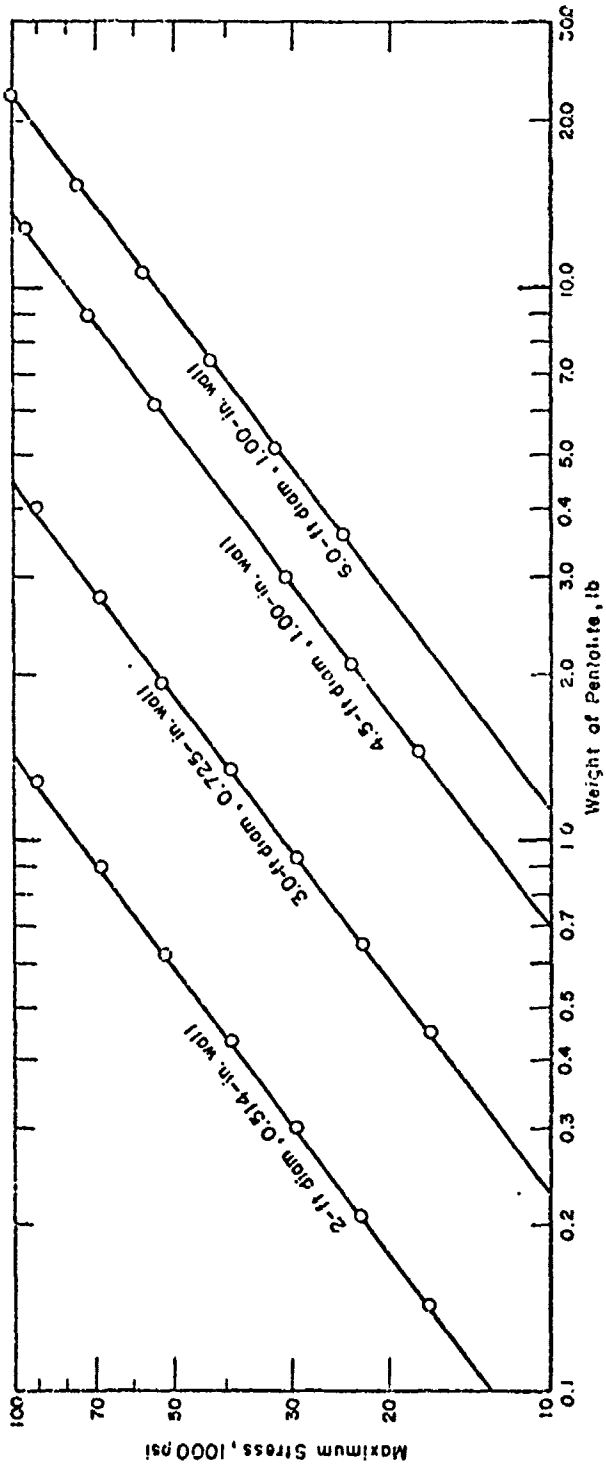

FIGURE 1. CALCULATED ELASTIC RESPONSE FOR SEVERAL VESSELS

$$\log \sigma = \log A + n \log W, \tag{8}$$

where the constant A is a function of the vessel wall thickness, h, and diameter, ϕ. Measurement of the slopes, n, of lines fitted to selected computer calculations showed that, indeed, n was nearly constant, independent of h and ϕ, having an average value of 0.768. The method used for calculation of σ showed that, if other variables were held constant, σ was proportional to 1/h. Thus, th form for A was selected as:

$$A = g(\phi)/h, \tag{9}$$

where $g(\phi)$ is the function of ϕ to be determined from Equations (8) and (9). It is easy to show that $g(\phi)$ is given by:

$$g(\phi) = h\sigma/W^n = h\sigma/W^{0.768}. \tag{10}$$

Values for $g(\phi)$ were evaluated from the calculated values of σ for three vessels as shown below:

ϕ (ft)	h (in.)	W (lb)	σ (psi)	$g(\phi)$	$\bar{g}(\phi)$
3.0	0.50	0.3	18,100	22,815	22,920
		1.0	46,000	23,000	
		10.0	269,000	22,947	
4.5	0.75	1.0	18,000	13,500	13,570
		10.0	106,000	13,563	
		30.0	248,000	13,648	
6.0	1.00	3.0	21,000	9,032	9,126
		10.0	53,800	9,179	
		100.0	315,000	9,169	

The above evaluation shows that $g(\phi)$ is nearly independent of W and varies regularly with ϕ. A log-log plot of $g(\phi)$ versus ϕ for the three average values of $g(\phi)$ is shown in Figure 2. The near-linear relationship obtained may be expressed by the form:

$$\log g = \log D + m \log \phi, \tag{11}$$

where D and m are constants. Graphical evaluation of D and m leads to the following expression for g, after slight rearrangement:

$$g = 9.80 \times 10^4/\phi^{1.324}. \tag{12}$$

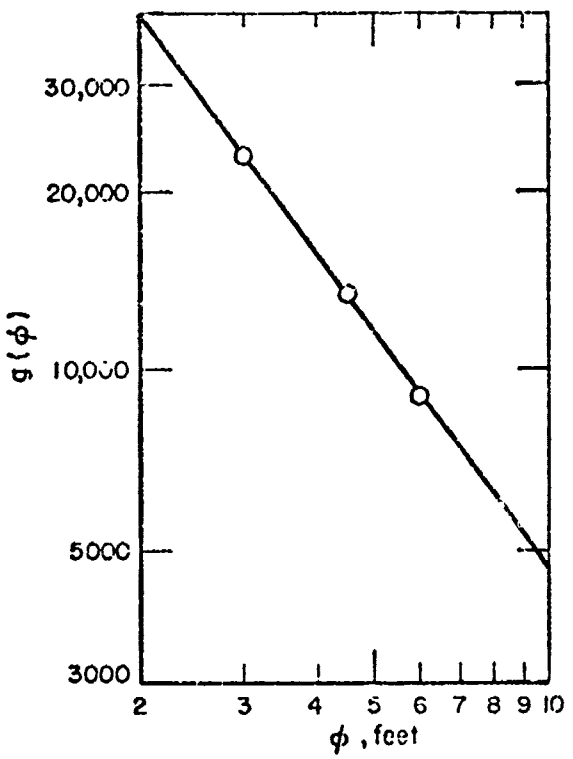

FIGURE 2. PLOT SHOWING RELATION OF LOG $g(\phi)$ AND LOG ϕ

Putting Equations (12) and (9) into (8) yields the following relatively simple relation between the maximum stress σ, in psi, the weight of Pentolite, W, in pounds, the vessel diameter, ϕ, in feet, and wall thickness, h, in inches.

$$\sigma = 9.80 \times 10^4 \, W^{0.768}/h\phi^{1.324}. \qquad (13)$$

The straight lines through the calculated points shown in Figure 1 were calculated using Equation (13). The degree of fit obtained shows the derived empirical equation fits the calculated data quite well over the practical range of maximum stresses shown.

It should be noted that the high stress values used in some of the above calculations do not imply that real materials are expected to remain elastic to these stress levels. They merely indicate what the response would be if they did. For real materials which yield plastically above their elastic limit, the above expression will obviously predict meaningless results. To predict the plastic response of vessels, an elastic-plastic analysis is necessary.

Elastic-Plastic Response

Early experiments in this program showed that if permanent plastic deformation of a blast containment vessel is allowed, the blast from much greater explosive charge weights can be contained a limited number of times for a given weight vessel. Blast containment chambers for some explosive ordnance disposal applications are expected to be portable units in which minimizing the vessel weight is of considerable importance. Furthermore, these vessels are expected to actually contain the blast from an explosion relatively infrequently. Hence, utilization of a vessel designed to plastically deform without rupture for a limited number of charges, can yield considerable weight advantages over a vessel designed to remain elastic during charge containment. Thus, an analysis of the expected performance of a containment vessel loaded into the region of plastic deformation becomes a valuable design aid.

The elastic-plastic response of the spherical vessels was analyzed using the same equations given previously for the elastic portion of the response.

The elastic-plastic model for material behavior used in this analysis assumes purely elastic behavior up to a yield stress, σ_y, followed by a linear work-hardening portion of the curve, characterized by a slope or plastic modulus, S. Thinning effects of the vessel wall due to plastic strain have been neglected.

The differential equations of motion of the vessel for stresses above σ_y are:

$$\rho h a \frac{d^2u}{dt^2} + \frac{2Sh}{a}u + 2h\,(\sigma_y - S\varepsilon_y) = ap(t), \tag{14}$$

for

$$t_y \leqslant t < T_s\ ,$$

and

$$\rho h a \frac{d^2u}{dt^2} + \frac{2Sh}{a}u + 2h(\sigma_y - S\varepsilon_y) = aP_s, \tag{15}$$

for

$$t \geqslant T_s \text{ and } t > t_y\ ,$$

where ε_y is the strain at yielding given by:

$$\varepsilon_y = \frac{(1 - \nu)}{E} \sigma_y , \tag{16}$$

and the other quantities are as previously defined. As in the elastic analysis, these equations were solved using standard LaPlace transform techniques. The resulting equations of motion were matched to their elastic counterparts at the time, t_y, when the yield stress, σ_y, was reached. The matching boundary conditions were that both the wall displacement and velocity were continuous on transition to plastic behavior.

The maximum plastic response may be reached by three possible paths:

(1) The yield stress is exceeded before the end of the forcing period, T_s, and the maximum deformation is reached before the end of the forcing period.

(2) The yield stress is exceeded before the end of the forcing period but the maximum deformation is not reached until after the end of the forcing period.

(3) The yield stress is not exceeded until after the end of the forcing period, and, hence, the maximum deformation is reached after the end of the forcing period.

The details describing the way in which it is possible to determine which of the above paths will be followed, for any combination of vessel, material, and shock-wave parameters, are given in the complete description of the analysis referenced previously.

Once the route to the maximum response has been determined, it is a straightforward matter to determine the actual maximum response parameters by standard techniques from the appropriate equation of motion.

After the maximum elastic-plastic stress, σ_m, and strain, ε_m, are reached, subsequent oscillations of the vessel are assumed to occur elastically with no Bauschinger effect. Hence, the residual plastic strain, ε_r, is found by allowing elastic recovery with the usual elastic modulus back to zero stress:

$$\varepsilon_r = \varepsilon_m - \frac{(1 - \nu)}{E} \sigma_m . \tag{17}$$

The last term in the above equation represents the elastic recovery. The elastic recovery for steel is quite small, as shown in the tabulation below.

Maximum Stress, psi	Elastic Strain Recovery, percent
50,000	0.12
75,000	0.18
100,000	0.24
125,000	0.30
150,000	0.36

Hence for loads which produce appreciable plastic strain, the elastic recovery is small and plots of the residual plastic strain differ only slightly from plots of the maximum strains produced.

Figure 3 shows an example of the calculated effect of the contained explosion gas pressure on the residual plastic strain produced in two vessels. In both of the examples shown, the effect of the confined explosion gas pressure is nil until the residual plastic strain exceeds 0.5 percent. In both cases this does not occur until an explosive load equal to nearly 3 times that required to exceed the yield strength of the material has been reached. For larger explosive loads the confined explosion gas pressure becomes the dominant factor in determining the total strain of the vessels. This is the result of not only the increasing confined explosion gas pressure but also the increasing time to reach the maximum deformation of the vessels with increasing charge loading. The latter effect allows more time for the confined explosion gas pressure to be effective in delivering impulse to the expanding vessel.

Ultimately, of course, the confined explosion gas pressure will exceed the yield strength of the vessel and therefore be capable of producing significant plastic deformation of the vessel in the absence of shock-wave effects. This is the expected mode of vessel deformation and ultimate failure when deflagrating explosives, such as black powder or propellants, are contained.

In conclusion, the present analysis in computerized form is capable of conducting parametric analyses of the predicted performance of spherical vessels for variations in vessel diameter and wall thickness, material yield strength, and work-hardening coefficient and provides as output information the time of yielding and the time of maximum deformation after shock-wave impingement, the maximum vessel wall deflection and strain, and the residual plastic vessel wall deflection and strain.

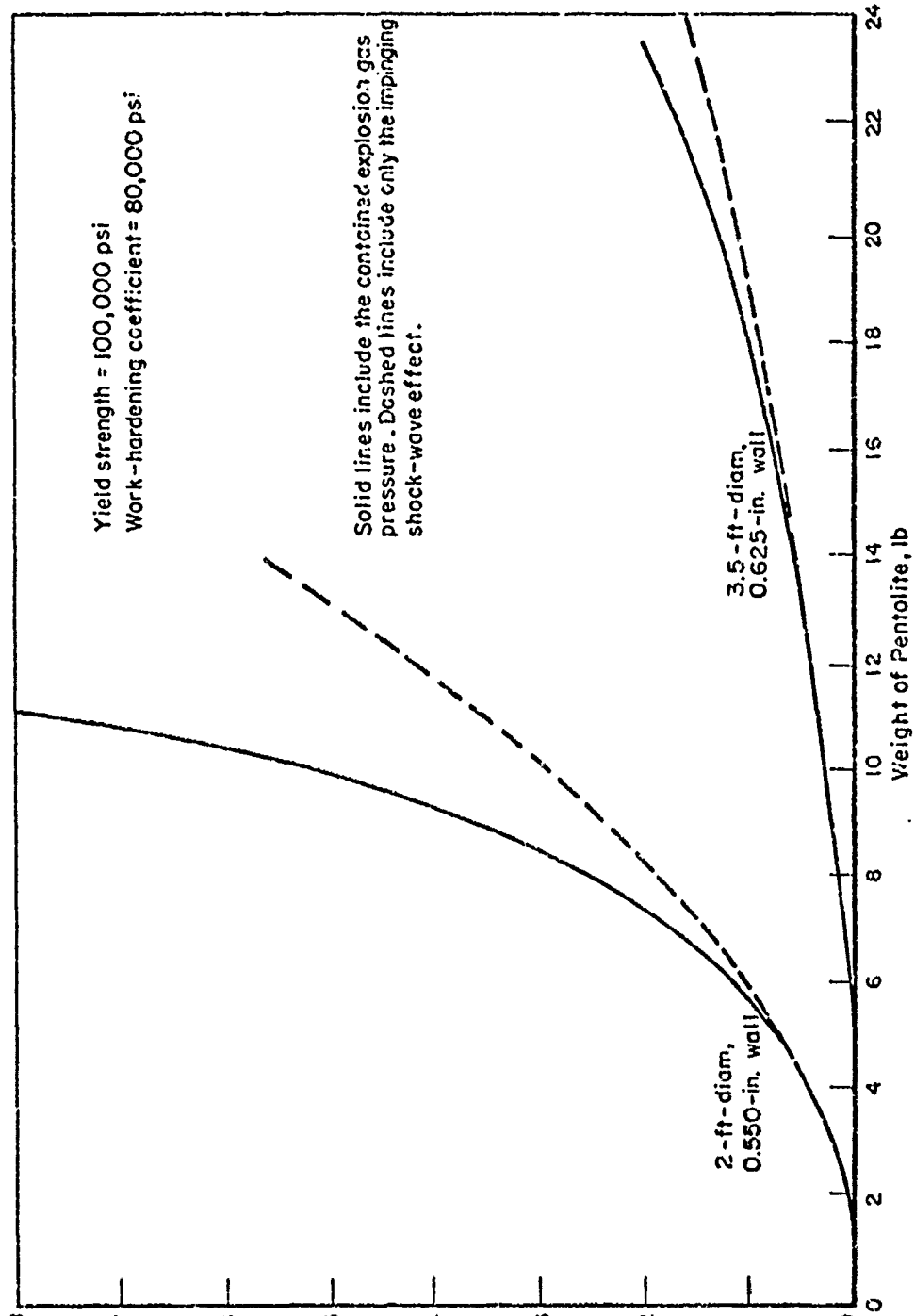

FIGURE 3. CALCULATED EFFECT OF THE CONTAINED EXPLOSION GAS PRESSURE ON THE RESIDUAL PLASTIC STRAIN PRODUCED IN TWO VESSELS

Also included in the output is information regarding the degree of oxidation of the explosive detonation products by the air contained in the vessel, according to Proctor's model for calculation of the explosion gas pressure, together with the calculated explosion gas pressure and the vessel wall stress, calculated on a static basis, which this gas pressure would produce. The analysis does not include the effect of vessel volume increase due to expansion by the shock wave on the calculated static pressure, nor does it include the effect of vessel wall thinning on the resultant deformations and stresses. These effects are small, however, for small deformations. The analysis also does not include a fracture or failure criterion for a vessel; this must be determined experimentally for each vessel design. An upper limit for the explosive load which will produce vessel failure may be readily inferred, however, as the explosive load which produces a stress from the confined explosion gas pressure equal to the ultimate tensile strength of the vessel calculated at the point of minimum wall thickness.

VESSEL DESIGN AND CONSTRUCTION

This section contains descriptions of the eight vessels fabricated for this program and the design criteria for sizing the parts.

Containment Vessels

Eight spherical containment vessels were fabricated for this program. The pertinent parameters of these vessels are summarized in Table 1. The vessels were fabricated in two lots of four vessels each, widely separated in time.

Figure 4 is a schematic top view of Vessels 1 and 3. As shown, the port was reinforced by a simple tube. The door included a tab for the attachment of two hinge blocks. Two hinge straps, as shown, were welded to the reinforcing tube before the tube was welded into the hemisphere. This design was generated prior to the development of the port reinforcement criteria given in the next section. The thickness of the flat door was chosen at twice the thickness of the vessel. This was known to be too thin to remain undistorted; however, a bulging distortion of the door should strengthen it against further distortion. In order to be certain that the door overlap on the inside of the reinforcing tube was not lost as a result of bulging the door, the doors in both vessels were made 1 inch larger in diameter than the OD of the reinforcing tube.

No supporting feet or attachments other than lifting lugs were welded to Vessels 1 through 4 initially. They were supported on cradles formed of 1/2-in. steel plate and depended on friction to maintain the orientation of the vessel in its cradle.

Vessel 4 was fabricated exactly like Vessel 3, except without a door.

Figure 5 is a schematic side view of Vessels 3a through 6a, drawn to scale. Vessel 2 is qualitatively very similar in design. It differs in the details of the location of the cross-pin, shape of the built-up parts between the door and the adjusting bolts, and the supporting feet. The caster wheels shown in Figure 5 were used on Vessels 3a through 6a. In Vessel 2, the casters were replaced by small feet welded to the vessel. These were cut from 1-in. plate and provided a 1 by 2.5-in. supporting area to rest on the rim of the cradle previously fabricated. The feet were necessary on this vessel to maintain its orientation in the cradle because of the relatively greater weight of the reinforcing ring and door in this design. The detailed design criteria for this single-pin door support design are given later.

TABLE 1. EXPLOSION CONTAINMENT VESSEL PARAMETERS

Vessel No.	Nominal Inside Diameter, ft	Specified Wall Thickness, in.	Actual Wall Thickness (Average), in.	Inside Diameter of Port, in.	Door Thickness, in.	Closure Design	Materials		
							Vessel	Port Reinforcing Ring	Door
1	4.5	0.75 min	∿1.0	26.5	1.50	Fig. 4	ASTM A-537 -72A	Mild steel	Mild steel
2	4.5	0.75 min	1.00	--	4.0	Fig. 5	ASTM A-537 -72A	ASTM A-516 Grade 70	ASTM A-516 Grade 70
3	3.0	0.5 min	∿0.72	17.5	1.0	Fig. 4	ASTM A-537 -72A	Mild steel	Mild steel
4	3.0	0.5 min	0.725	17.5	None	--	ASTM A-537 -72A	Mild steel	--
3a-6a Inclusive	2.0	0.55 rolled gage	∿0.495 ± 0.012	12.0	2.25	Fig. 5	ASTM A-516 Grade 70[a]	ASTM A-537 -72B[b]	ASTM A-537 -72B[b]

(a) Plus specified minimum 12 ft-lb Charpy value at -40 F.

(b) Except for gage.

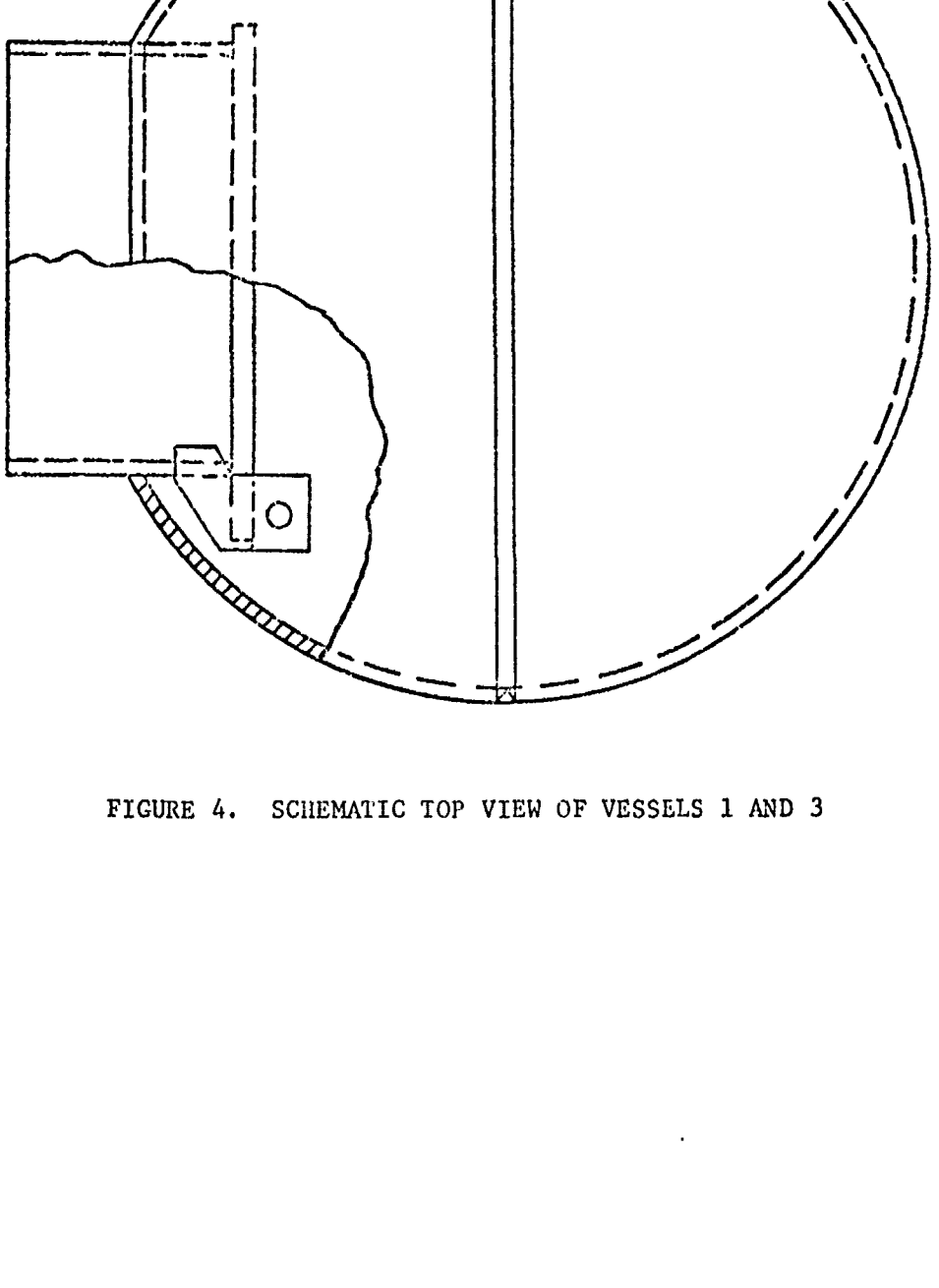

FIGURE 4. SCHEMATIC TOP VIEW OF VESSELS 1 AND 3

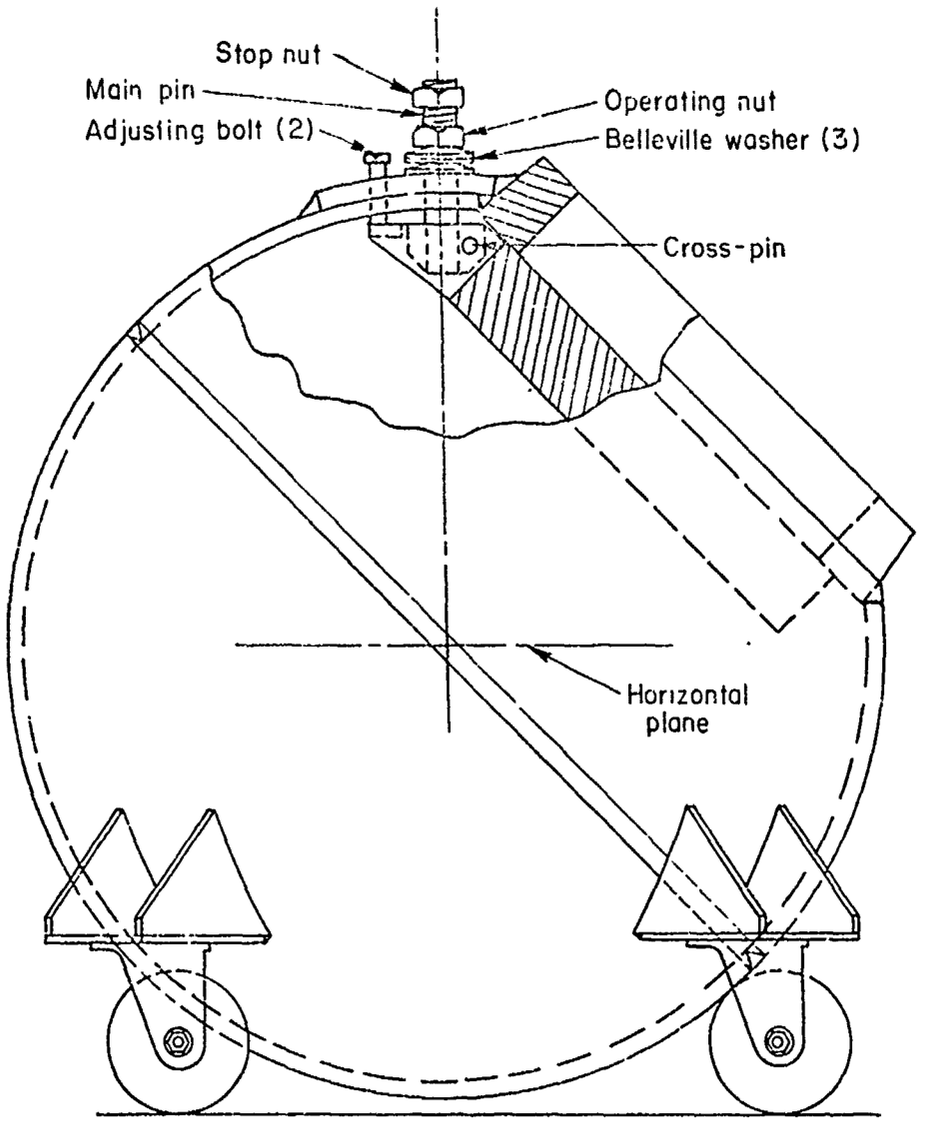

FIGURE 5. SCHEMATIC SIDE VIEW OF SPHERICAL CONTAINMENT VESSEL WITH SINGLE-PIN DOOR SUPPORT MECHANISM

The single-pin door support idea was originated by Mr. Jon Petty of Picatinny Arsenal, the technical monitor on this program. The details of the operating mechanism were supplied by the first two authors. The operation of the single-pin door mechanism is given in the following paragraphs.

The adjusting bolts shown in Figure 5 are initially adjusted, together with the operating nut on the main pin, to provide a good fit of the door against the inside of the reinforcing ring. Free play built into the cross-pin allows the two adjusting bolts to bring both sides of the door into contact with the reinforcing ring. The block attached to the bottom of the support pin and the built-up box which surrounds the block and is welded to the door are designed to hold the door at only a slightly smaller angle to the main pin than the fully seated position. The adjusting bolts only provide for the final seating of the door against the ring, by rotation of the door on the cross pin.

The stop nut is also initially adjusted to allow the door to rotate around the inside of the vessel with small clearance when the operating nut is backed off against it. The stop nut is then locked in place with Loctite (for the 2-ft-diameter vessels) or a mechanical clamp built into the nut (for the 4.5-ft-diameter vessel).

With these initial adjustments made, and the door closed, as shown in Figure 5, the door is opened simply by rotation of the operating nut. The door is lowered for clear rotation initially, then further rotation of the operating nut, now against the stop nut, forces rotation of the main support pin and door through ~90 deg to the open position.

To close the door, the operating nut is merely rotated in the opposite direction. The door is rotated to its closed position by the initial rotation of the operating nut because of the jamming action of the stop nut and operating nut together. When the door rotates to its proper position to close completely, it contacts a door stop attached to the reinforcing ring. Continued rotation of the operating nut frees it from the stop nut and raises the door to the fully closed position. As the door rises, the adjusting bolts are again contacted and bring the door to an accurate seat angle against the ring.

This mechanism has worked exactly as described through 43 shots in Vessel 2, and similarly in the smaller vessels, Nos. 3a through 6a.

Material Selection

Steel was selected as the vessel material on the basis of cost, strength, fabricability, and availability. The selection of a specific grade of steel for the primary vessel was based on five considerations: (1) a high level of toughness, as measured by the Charpy notch-bar impact test, at low ambient temperature, (2) weldability, (3) cost, (4) availability,

and (5) the fact that steels with good impact properties at low temperatures must be good-quality steels. This provides additional assurance that deformation of the steels will not be adversely affected by unacceptable defects or improper processing.

The first choice steel grade selected is designated as ASTM A-537-72A, Class 1, or as ASME boiler steel SA-537A. This is a high-quality carbon steel with a nominal composition of 0.15 to 0.2 percent carbon, 1.2 percent manganese, 0.2 percent silicon, less than 0.02 percent sulfur, and less than 0.01 percent phosphorus. This steel, as specified by the American Society for Testing Materials (ASTM) or the American Society for Mechanical Engineers (ASME) boiler code, will have a minimum yield strength of 50,000 psi and elongation in 8 in. of 18 percent. In addition, this steel will have a guaranteed minimum Charpy notched-bar impact strength value of 12 ft-lb at a temperature of -75 F, a temperature far below expected ambient temperatures. Nominal values for impact strength at -75 F are about 30 ft-lb, and at -50 F about 55 ft-lb. This is a steel characterized by high levels of toughness even in the normalized heat-treatment condition (Class 1) that was specified for the vessel. This type of heat treatment was specified because it only requires heating to the specified temperature for the correct length of time and air cooling as compared with the more complicated heat treatments involving heating, quenching, and tempering, which can yield higher levels of impact strength. The shells of the first four vessels were constructed of this material, while the remaining parts were constructed from mild steel stocks on hand, except that the reinforcing ring and door for Vessel 2 were constructed of A-516 Grade 70 material as an alternate since no A-537 material could be located. ASTM A-516 Grade 70 material is quite similar to A-537 but a lower yield strength is allowable, and low-temperature toughness is not normally guaranteed.

The particular materials for the second lot of 2-ft-diamater vessels were selected on the basis of availability within the guidelines above. During the time of ordering these vessels (1974) steel availability was less than normal. However, the supplier of the hot-pressed hemispheres, Lukens Steel Co., did provide additional low-temperature Charpy impact property guarantees on the lot of A-516 Grade 70 material used for these vessels. The rings and doors for these vessels were fabricated from a section of 5-in.-thick plate of A-537-72B, Class 2, material. This was the only material available in the required sizes which fit the mechanical property requirements. This material is identical to A-537-72A, Class 1, except that it is supplied in the quenched and tempered condition and is somewhat stronger than the normalized material.

Vessel Wall Thickness

Table 2 gives ultrasonically measured wall thicknesses of vessels 1, 2, and 4. The results indicate that, if Vessel 3 was similar to Vessel

TABLE 2. MEASUREMENTS OF WALL THICKNESSES OF VESSELS 1, 2, AND 4

(All measurements are in inches[a])

Location[b]	Vessel No. 1 (4.5 ft I.D.)				Vessel No. 2 (4.5 ft I.D.)				Vessel No. 4 (3.0 ft I.D.)			
	Port Side		Opposite		Port Side		Opposite		Port Side		Opposite	
Pole	(c)		0.946	0.952	(c)		0.945		(c)		0.695	
15°	(c)		0.922	0.928	(c)		0.940	0.935	(c)		0.680	0.685
30°	(c)		0.928	0.970	(c)		0.945	0.930	(c)		0.675	0.675
45°			0.950	1.001	0.965	0.955	0.940	0.980	0.680	0.685	0.700	0.750
60°			1.005	1.035	1.000	0.980	0.985	1.015	0.710	0.720	0.720	0.715
75°					1.025	1.025	1.025	1.040	0.745	0.745	0.760	0.745
Adjacent to Weld							1.100	1.105	0.790	0.800	0.790	0.795
Weighted Average Wall Thickness						1.001					0.725	

(a) Thickness measurements were obtained by means of an ultrasonic pulse echo technique. Resolution was approximately 0.005 in. Surface roughness, however, limited the absolute accuracy to an estimated uncertainty of ± 0.01 in.

(b) The pole is the center of the pressed hemisphere; 90 deg is on the main girth weld. For each vessel, all measurements were taken along a single great circle. Where two measurements appear at the same angular location, they were taken on opposite sides of the pole. The first column is consistently for one side and the second for the other side of the pole of each hemisphere.

(c) Open port in this location.

TABLE 3. MEASUREMENTS OF WALL THICKNESSES OF VESSELS 3a THROUGH 6a

(All measurements are in inches)

Vessel No.	Lower Hemisphere, Adjacent to Weld	Upper Hemisphere	
		Adjacent to Weld	Adjacent to Port
3a	0.536	0.532	0.465
	0.534	0.537	0.457
	0.542	0.537	0.455
	0.540	0.530	0.436
4a	0.542	0.533	0.494
	0.547	0.537	0.475
	0.517	0.540	0.474
	0.541	0.547	0.487
5a	0.535	0.536	0.450
	0.543	0.520	0.447
	0.540	0.536	0.425
	0.537	0.516	0.418
6a	0.542	0.528	0.450
	0.525	0.528	0.450
	0.517	0.539	0.455
	0.531	0.539	0.462

4, it had an average wall thickness of 0.725. Note that the wall thickness shows appreciable variation, with the thickness generally increasing from the pole to the girth welds. The weighted average wall thickness was calculated based on the assumption that the observed variation was circularly symmetrical about the pole. Thus measurements near the girth weld received more weight than those at or near the pole.

Table 3 gives measured wall thicknesses of Vessels 3a through 6a. The four measurements at each location identified were taken at equally spaced locations around the periphery of the vessels before welding. No ultrasonic thickness surveys were made on these vessels.

Fabrication and Welding

All vessels were fabricated by welding together a pair of hot-pressed hemispherical heads. The ports were welded into holes machined into one of the hemispherical heads.

The initial fabrication of the first four vessels was done completely in the Battelle-Columbus Machine Shops. The hemispheres were welded into spheres using multipass, full-penetration welds deposited by the MIG process. The vessel ports were initially welded in using the same process. After welding, the four vessels were stress relieved at 1125 $\pm$ 25 F for 1 hr followed by furnace cooling to 600 F. They were shot-blasted to remove the heat-treatment scale.

This lot of vessels was intended to be a scaled-down version of a 6-ft-diameter, 1-in.-wall vessel with a port large enough to allow the insertion of a 2-ft cube containing a charge. The data developed were to allow predictions of the performance of the 6-ft vessel.

In a subsequent contract modification, Vessel 2 was modified by removal of the original sleeve, similar to Vessel 1, and installation of the present port and door. This welding and all subsequent welding was performed in the Battelle-Columbus Welding Development Laboratory.

The port was welded into Vessel 2 using the shielded metal arc process. The multipass weld was built up using the stringer bead technique. The welding parameters used were as follows:

Preheat temperature: 300 to 400 F
Interpass temperature: 400 to 600 F
Electrode: E9018-M, 5/32-in. diameter
Arc voltage: 24 volts
Welding current: 150 amps
Heat impact: 30 to 45 kJ/in.

This technique was chosen to produce welds with the minimum of residual stresses, and a fine-grained weld so that postwelding heat treatment could be eliminated.

The principal structural welds in the second lot of vessels (Nos. 3a through 6a) were done by the Battelle Welding Development Laboratory. The welding procedure used for these vessels is given here in some detail, since the same procedure can be used for vessel welds with wall thicknesses from 3/16 to 3 in.

The same procedure was used in making the weld attaching the door ring to the sphere and the girth weld between two hemispheres. This procedure, No. P-75-A, is included as Appendix A. The reinforcing ring was welded into one hemisphere before welding the hemispheres together to provide easy access to the inside surface of the weld.

A preheat temperature of at least 250 F was used prior to any welding. The steps following preheat were as follows:

- The ports to be welded were tacked in place using E-8016-C3 covered electrode.
- The root pass was deposited from the vessel inside surface using the shielded-metal-arc process and E-8016-C3 covered electrode.
- The root bead was ground out to sound metal from the outside.
- The ground surface of the root pass was dye-penetrant-inspected to insure removal of any lack of fusion in the base of the root pass. Areas showing any indication of lack of fusion were reground and rechecked until sound metal was ensured.
- The second weld pass was deposited from the outside by shielded metal arc using the same electrode material.
- The joint was completed using Hobart FabCO 81 cored wire electrode in a semi-automatic gas metal-arc welding process.
- The face of each pass was cleaned by power wire brushing to remove slag between welding passes.
- The completed joint was radiographically inspected according to Section VIII, Pressure Vessels Division 1 of the ASME Boiler and Pressure Vessel Code, 1974.

On the girth weld, the vessels were mounted on a rotating fixture after tacking to allow all welds to be deposited in the flat position.

Door and Reinforcing Ring Design

General Criteria

The design formulas for the reinforcing ring and door were derived using an average wall thickness of the vessel and the following constraints:

- The formulas were based upon a static internal pressure loading.
- The sphere was assumed to act as a thin shell, which is completely valid only for shells having a ratio between the radius to the median surface and the thickness greater than or equal to 60 ($a_s/t_s > 60$)[2] The stress in the shell was then given by the following formula:

$$\sigma_s = pa_s/2t_s \tag{18}$$

where

σ_s = uniform stress in the sphere

p = static internal pressure

a_s = radius to the median surface of the sphere

t_s = thickness of the spherical shell.

- The door was designed to a stress at the outer surface of the center of the door equal to that in the sphere so that gross deformation and subsequent shifting of the bearing support line with the ring would not occur.
- The ring was designed so that the sphere and the ring would have equal static deflection at their welded junction under an internal pressure.
- All eccentricities within the ring and sphere junction were minimized for a static loading.

The average wall thickness of the vessels was used even though there was a significant variation in true wall thickness from the center to the edge of each hemisphere because it was both conservative and the best number available so that the design could proceed before the hemispheres were delivered.

It is noted that obtaining reliable actual wall-thickness information from suppliers of formed hemispheres is not an easy matter.

Formed hemispheres are characteristically supplied for pressure-vessel applications in which the minimum wall thickness is the applicable criterion. With the uncontrollable variations in wall thickness which occur during the forming operation, manufacturers characteristically use an appreciable extra thickness for the original blank to insure that the quoted minimum is exceeded at the thinnest portion of the final fabrication, since weight is not normally a factor in pressure-vessel applications. In this work, however, minimum weight is one of the primary considerations. For purposes of determining the average wall thickness which will be realized in a vessel, the manufacturer's quoted inside diameter and estimated (not guaranteed) shipping weight seems to provide the best indication of what the average wall thickness of the vessel is likely to be for design purposes. Consideration must be given to the expected minimum wall thickness as well, since the hot-spinning process, for example, appears to lead to much larger and more uncontrollable variations in wall thickness than hot pressing in a die.

Steps in Design

This section includes the design guidelines developed for the vessels fabricated in this program. The performance of the vessels tested to date using these guidelines appears to be generally satisfactory, although additional experience with them is desirable before they can be regarded as firmly established. The vessels fabricated for this program were not sized with the intention of containment of a specified blast load, since no design criteria for this purpose existed at the inception of this program. However, the results of this research now allow choice of a vessel diameter and wall thickness expected to accomplish a specific containment objective. In addition, the size of the opening desired is selected on the basis of the expected end use of the vessel. Currently, our judgment for most applications is that the port opening should not exceed the radius of the vessel.

Figure 6 illustrates the geometry of the junction between the sphere, reinforcing ring and door.

The size of the bearing surface b between the ring and the door is the first quantity to be determined. For a first estimate, the following expression was used:

$$b_1 = (\sigma_s/\sigma_b)(a_d/a_s)t_s, \tag{19}$$

where

σ_b = the lower of the compressive yield-stress values for the door and ring materials.

a_d = radius of the port.

The remaining quantities were defined in Equation (18).

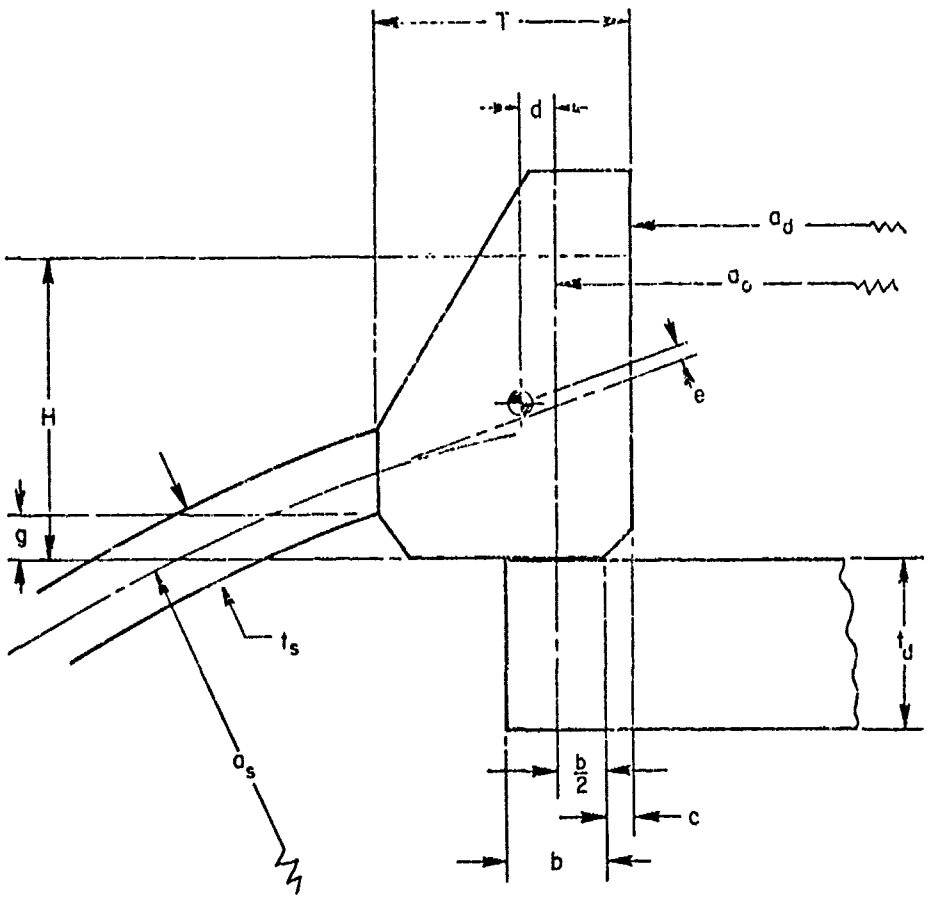

FIGURE 6. GEOMETRY OF THE JUNCTION BETWEEN THE SPHERE, REINFORCING RING, AND DOOR

The value of b was then refined using the following formula wherein a_o was substituted for a_d:

$$a_o = a_d + b_1/2 \tag{20}$$

$$b = (\sigma_s/\sigma_b)(a_o/a_s)t_s, \tag{21}$$

where

a_o = approximate location of the bearing stress load line assuming c is equal to zero in Figure 6.

The thickness of the flat plate door, t_d, was determined from the following formula for small deflections[5], which considers not only bending of the plate but also shearing strain and lateral pressure effects on the edge of the door.

$$t_d = \left[\frac{3}{4} (3 + \nu)\, a_o^2/(a_s/t_s - \frac{1}{2}(\frac{3 + \nu}{1 - \nu})) \right]^{1/2}, \tag{22}$$

where ν is Poisson's Ratio ($\nu = 0.27$ for steel). The objective in the design of the door was to provide a part that would support both the dynamic load and the static load of a contained explosion without deforming so much that the load line geometry between the door and the ring was destroyed. The stress found in the sphere was used as the maximum value of stress to be found in the door. This occurred at the outer surface of the center of the door.

The first approximation of the reinforcing-ring cross section was generated with the assumption that the centroid of the ring would lie close to the radius, a_s. The following formula, which was derived from references 5, 6, and 7 for a thin ring, which has a thickness-to-radius ratio less than 1:5, and a sphere, was used for the first estimate of the cross section of the ring, which would deform the same amount at its centroid as the sphere, if the sphere had continued to the same location:

$$A = \frac{a_s t_s}{(1-\nu)} \cos \phi_o \sin \phi_o, \tag{23}$$

where

$$\phi_o = \sin^{-1}(a_o/a_s). \tag{24}$$

This rectangular area, A, then allowed a reasonable engineering estimate for the thickness of the ring, T, to be made. If the ratio, T/a_o, violated the thin-ring criterion, the following formula, based on a thick ring with the deflection matched at the point of contact with the hemisphere, was used to determine the height, H, of the ring:

$$H = \frac{2E_s t_s}{E_r(1-\nu)} \left[\frac{\sqrt{a_s^2 - (a_d + T)^2}}{2} - g \right] \frac{1}{a_s} \left[\frac{1 + (1 + \frac{T}{a_d})^2}{(1 + \frac{T}{a_d})^2 - 1} - \nu \right] \quad (25)$$

where E_r and E_s are Young's Modulus of the ring and sphere, respectively, and the other quantities are as shown in Figure 6. The area and the rough dimensions of T and H are next represented on a drawing, such as Figure 6. Using this drawing, the shape of the ring cross section was changed from simply rectangular to accomplish the following two objectives while keeping the cross-sectional area, A, of the ring constant:

- Make the transition or change in cross section between the sphere and the ring as smooth as possible to avoid large stress concentrations.
- Make the sum of the moments caused by the bearing load from the door and the loading by the sphere as near equal to zero about the centroid of the ring cross section as possible, to minimize the tendency of the ring to twist under load.

The second objective was expressed by the equation:

$$e = d \frac{a_o}{a_s} \quad (26)$$

where

e = perpendicular distance from the projected load line from the junction of the sphere and ring to the centroid

d = perpendicular distance from the projected door/ring bearing line to the centroid of the ring.

A rapid solution for the ring sizes and shapes required for cost and sizing purposes was facilitated by adjusting a_o through use of the internal chamfer, c, on the inside surface of the ring (see Figure 6).

$$a_o = a_d + c + b/2. \quad (27)$$

The final iteration checked the validity of the values calculated for the bearing surface, door thickness, cross section of the reinforcing ring, and the balance of the moments about the centroid of the reinforcing ring. Thus, the design of the reinforcing ring and door was completed for the 4.5- and 2.0-ft containment chambers.

In the 4.5-ft vessel number 2, it was expected that the wall thickness, t_s, of the vessel was 0.75-inch, and the reinforcing ring was designed for this thickness. When the original port was removed, allowing micrometer measurements to be made, it was found that this vessel was thicker than 0.75 inch. The ultrasonic thickness survey of wall thickness, as shown in Table 2, was then performed, showing that the average wall thickness was 1.00 inch. Thus, the reinforcing ring was undersigned by the above criteria by ~25 percent. The reinforcing ring had already been machined, however, and the decision was made to install the ring anyway, since the design criteria given here were new and as yet unproven.

In the 2-ft-diameter vessels, numbers 3a-6a, the reinforcing rings were designed for a vessel wall thickness of 0.55 inch. In this case, the wall thickness measurements conducted on the vessels after their arrival suggested that the average wall thicknesses are somewhat less than this value, and the reinforcing rings may be overdesigned by about 10 percent.

Single-Vertical-Pin Door Mechanism Design

General Criteria

Figure 5 illustrates the major components of a single vertical-pin door mechanism. For the initial weight estimations, the mechanism weight was taken as 10 to 15 percent of the weight of the door with the higher value used for the 4.5-ft-diameter vessel.

The following were the general design criteria for the mechanism:

- In the closed position the main pin, belleville springs, and adjusting bolts must hold the weight of the door and some arbitrary seating pressure of the door against the ring.
- In the open position the main pin must be able to support an expected loading factor for rough handling multiplied by the weight of the door.
- The belleville springs should have enough deflection left when holding the door in the closed position to allow the vessel wall to move outward the sum of the maximum elastic deflection predicted by the computer program and the movement of the cross pin caused by the elastic deflection of the door. Under no circumstances should the belleville springs be flattened out when the door is closed.

- The general arrangement of the main pin and cross pin should be as close to the door as possible to reduce the loads caused by the dynamic interaction of the door and chamber.

- The main pin bearing support should be long enough (usually greater than one diameter) to allow free motion of the door both up and down without binding caused by the fact that the support is resisting a moment on the pin caused by the off axis weight of the door.

- Plastic deformation of the chamber may enlarge the pin support bearing. This must be considered for the expected usage and lifetime of the chamber.

- In the region of the penetration of the sphere by the main pin and the adjusting bolts a doubler plate or possibly two should be used so that the stress level in the region is lower than that in the rest of the chamber. If the vessel is to have a long lifetime, this region should be held within the elastic capability of the material so that the hole sizes for the adjusting bolts and main pin support do not change.

Steps in Design

The main pin was sized by the combined bending and tensile load caused by the open door. The weight of the door and a value of ten loading factor was applied to the geometry of the pin door for each chamber designed.

The main pin was then checked for the stress caused by the load from the adjusting pin, main pin, door geometry while supporting the weight of the door and the arbitrary seating pressure against the ring. In general, the arbitrary seating pressure was actually determined from the capabilities of the adjusting bolts and main pin.

The support for the main pin was designed using a close running fit for the hole. A thin strip of bearing area (0.25 inch) was assumed at both ends of the support. The bearing stress on these surfaces was then designed to approximately 20,000 psi for the moment caused by the off axis door, with the loading factor applied, by varying the length of the support. If the support length became unreasonably long, the diameter of the pin was increased as was done for the 4.5 ft vessel.

The belleville springs were then selected to fit the diameter of the main pin and transmit the maximum tensile load in the pin to the outer surface of the chamber with only a nominal deflection. The number of belleville springs used were determined by the requirement that the sum of the remaining available deflection to flattening out for all the springs was set above the sum of the expected maximum elastic deflection of the chamber wall and the axial thrust caused by the edge rotation of the door and the geometry of attachment through the cross pin.

The cross pin and minor plate parts of the built-up connection were then designed so that they transmitted the loads corresponding to the maximum load in the main pin without yielding.

The outer doubler plate (and inner doubler plate, if required) were fabricated from the material removed from the hemisphere that received the reinforcing ring. They were conservatively laid out to cover the entire region from the reinforcing ring to at least a distance no closer than two to three times the diameter of the closest penetration through the chamber wall.

The threads on the driving nut for the main pin were selected with a ramp angle such that it is easy to open and close the door. Additionally, the low ramp angle was chosen so that the nut was resistant to movement during the dynamic loading cycle of the chamber.

EXPERIMENTAL PROCEDURES

Instrumentation and Diagnostics

To follow the performance of the spherical vessels evaluated during this program, two types of diagnostics were employed: strain gages were attached at various locations on the vessels and a network of fiducial marks was placed on the vessels to obtain information on the plastic strain distribution.

Strain-Gage Locations

The dynamic response of the vessels to internal blast loading was followed with strain gages, located as shown schematically in Figures 7 and 8. These locations were chosen to provide strain data: (1) near the closure port, (2) directly opposite the closure port, (3) at points off the edges and major flat face of suitcase-shaped charges, and (4) at various locations around the vessel surfaces.

The layout of the strain gages for Vessels 1 and 3 was identical (See Figure 7). Gage 1 was installed approximately 3.5 wall thicknesses from the edge of the closure port. Gage 3 was located directly opposite the closure port. In order to study the effects of suitcase-shaped charges, it was planned to orient the charges to provide response data at locations relatively free of effects of the vessel port at least on one edge. Gages 2 and 4 were thus positioned at 90 and 180 degrees, respectively, from Gage 1. Suitcase-shaped charges were suspended in the vessels so that the normal to their major flat was directed toward Gage 2. Assuming cylindrical symmetry of the vessels about the port axis, the location of Gages 1 through 4 permitted the study of the angular response of the vessel design for the case of spherical and near-spherical charges. A fifth strain gage was located near the center of the flat door to follow its response.

The positions of the strain gages mounted on Vessel 2 are shown in Figure 8. After the experience gained with Vessels 1 and 3, the location of Gage 4 was changed in order to monitor the hoop stresses generated in the port reinforcing ring at a point 90 degrees from the door support pin. Gage 1 was installed closer to the closure weld, due to the location of the support pin and its outer surface reinforcing plate. No gage was installed on the door of Vessel 2, because experience with Vessels 1 and 3 showed that water from the escaping detonation product gases condensed on the gage and rendered it inoperative.

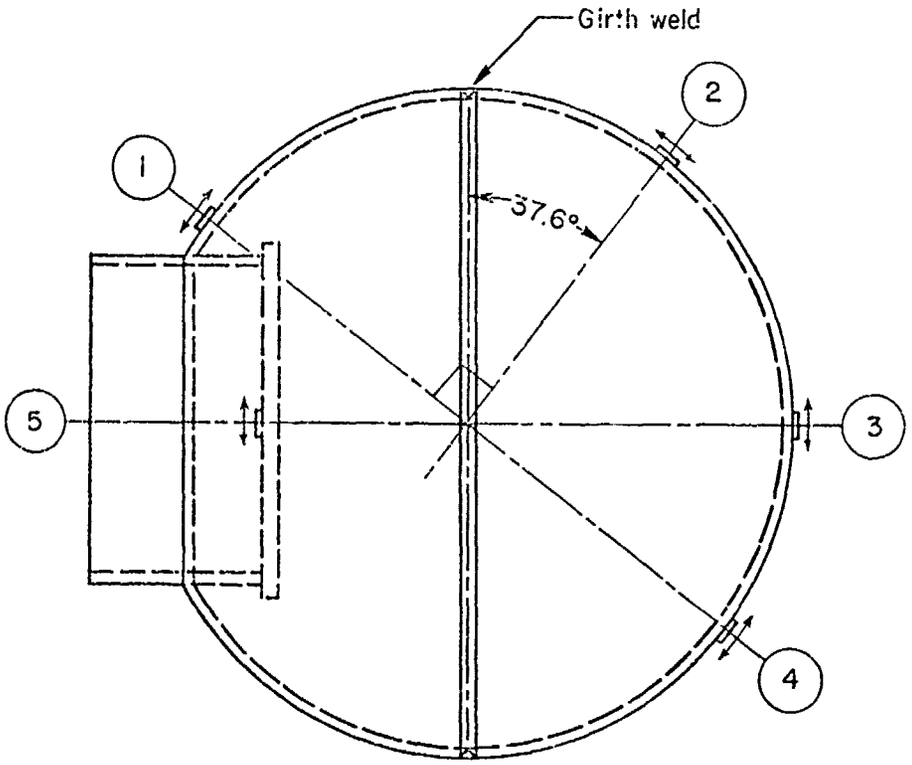

FIGURE 7. SCHEMATIC VERTICAL SECTION THROUGH THE CENTERLINE OF VESSELS 1 AND 3 SHOWING STRAIN-GAGE LOCATIONS

Gages were installed to measure the strain component in the plane of the paper.

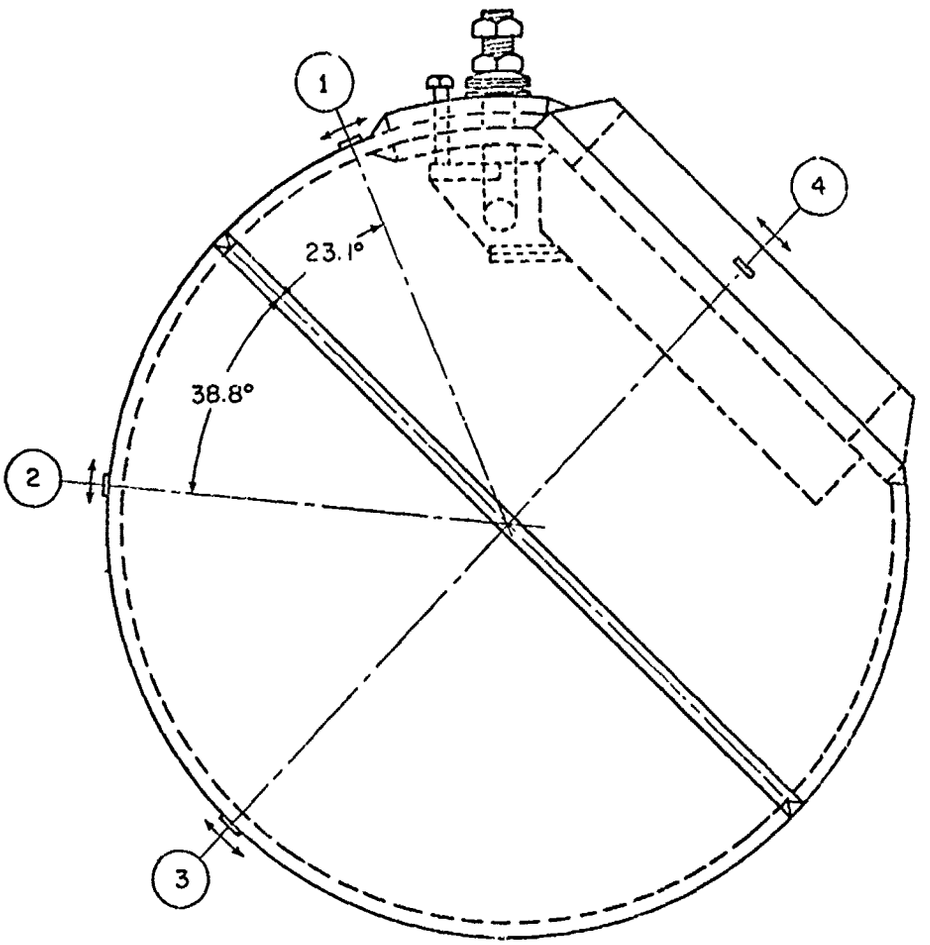

FIGURE 8. SCHEMATIC VERTICAL SECTION THROUGH THE CENTERLINE OF VESSEL 2 SHOWING STRAIN-GAGE LOCATIONS

Gages were installed to measure the strain component in the plane of the paper.

Strain Gage Description and Installation Procedures

The strain gages employed throughout this program are 350-ohm, 1/4-in. gage length from Micro-measurements Corp. The gages installed on Vessels 1 and 3 were Type EP-08-250BF-350. These gages, which are special annealed constantan foil, have a quoted strain range of ±20 percent in this size. They were chosen in order to follow the possibly large plastic strains which the vessels might encounter. They were cemented to the vessels (using Micro-Measurements' M-200 adhesive) on areas which had been previously ground, sanded, polished, and carefully cleaned. The gages were connected to the measuring bridge equipment using a three-wire temperature-compensating circuit. (Three wires of a foil-shielded four-wire cable were used.) In these installations, the ends of the connecting cable wires were soldered directly to the strain-gage tabs using established strain-gage soldering technique. The cables were securely taped to the vessel adjacent to the gages to prevent accidental stress on the cable-gage connection.

This gage installation on the first containment vessels tested worked satisfactorily for small charges; however, as the explosive shock load on the vessels increased, failures due to the connecting wires being torn from the gages were encountered. It appeared that the mass of the connecting wires was so great that the momentum imparted to them by the initial outward movement of the vessel caused the wires to be torn from the gages. This problem was ameliorated to some extent by securing the gage leads to the vessel between layers of insulating tape with 1/2 inch steel bands. The bands were secured tightly around the vessel using a banding tool such as is used to reinforce packing cases with steel bands. As the loads increased, this technique was still inadequate, and failure of the gage cement was also encountered. To solve these problems, a different gage installation technique was used on Vessel 2.

The strain gages installed on Vessel 2 were Micro-Measurements' Type EA-06-250AE-350. They were selected because of the better temperature compensation with steel which they offer as well as somewhat better stability, although they are limited to ±5 percent strain. The surface preparation for installation of the gages was similar to that used previously. The gages were cemented to the vessel with EPY-500 epoxy cement (from BLH Corp.) which requires an elevated-temperature curing cycle with pressure maintained on the bonding surface during curing. The latter was accomplished by means of silicone rubber pressure pads held under pressure with steel banding straps around the vessel. The temperature was monitored at each gage with a Chromel-Alumel thermocouple spot-welded to the vessel adjacent to each gage location. The heat-curing cycle consisted of maintaining a temperature >300 F and <350 F for one hour. Heating and temperature control was done manually with the aid of a large hand-held natural gas burner attached to the end of a flexible hose. The flame was applied to the inside of the vessel to reduce the possibility of accidental overheating. The temperatures of all gages were monitored continuously with the aid of a multipoint strip-chart recorder. Due to the large thermal mass of the vessel,

temperature changes at the gage locations were gradual, and no difficulty was encountered in maintaining the temperature within the required limits on all gages for the prescribed time period. This heating system required approximately 45 minutes to raise the temperature to 350 F. The epoxy cement proved to be very reliable and no gage cement failures have been observed on this vessel to date.

After Vessel 2 suffered a hole blown in the bottom and it was repaired, all gages except Gage 2 were still in good condition although the lead attachments had been broken. A new gage in the Number 3 location was installed using the above procedure.

A new method for gage lead attachment was also employed on Vessel 2. The three-wire temperature compensating circuit was retained. Short (2-in.) lengths of fine, 32-gauge varnished copper wire were used to connect the gages to the shielded cable wires, using the minimum possible amount of solder, to minimize the mass of the leads attached to the gages. Again, the cable was securely taped to the vessel with duct-tape immediately adjacent to the gage to prevent accidental damage to the gage connections. This seemingly fragile gage connection has proven to be very reliable through the considerable number of shots fired in Vessel 2, although care in handling is necessary to prevent damage from sources extraneous to the internal blast loads on the vessel.

Strain-Gage Measurement

Two problems which required solutions in developing a reliable dynamic strain-gage measurement system were the provision of a timely trigger for the recording oscilloscopes and provision of sufficient gain and band-pass capability to record the low-amplitude gage signals free from excessive electrical noise. The best solution found to date for the oscilloscope trigger is provided by the functioning of a fast switch on the electric detonator, connected to the oscilloscopes through a fast capacitor discharge circuit. The switch is formed by the metallic detonator sheath and a 0.007-in.-thick copper foil wrapped partially around the detonator. One electrical lead is attached to the detonator sheath by simply wrapping two turns of bared hook-up wire around the detonator sheath near the lead end. The other electrical lead is soldered to the copper foil after forming it to the required radius but before installing on the detonator. The switch assembly is completed by placing the foil around the detonator near the base charge end and securing it with 1/4-in.-wide strips of masking tape. Electrical insulation and the small required standoff is provided by two wraps of 1/4-in.-wide masking tape placed on the detonator under the edges of the copper foil. The assembly is completed by an ohmmeter check that the switch leads are open. As the detonator base charge explodes, the expansion of the sheath momentarily makes electrical contact between the sheath and copper foil.

The detonator switch is attached to the oscilloscopes through the capacitor discharge circuit shown in Figure 9. This circuit produces

a fast-rising pulse of >30 V peak with a duration of ∿1 μsec, which is adequate to trigger the oscilloscopes used for recording the dynamic wave forms.

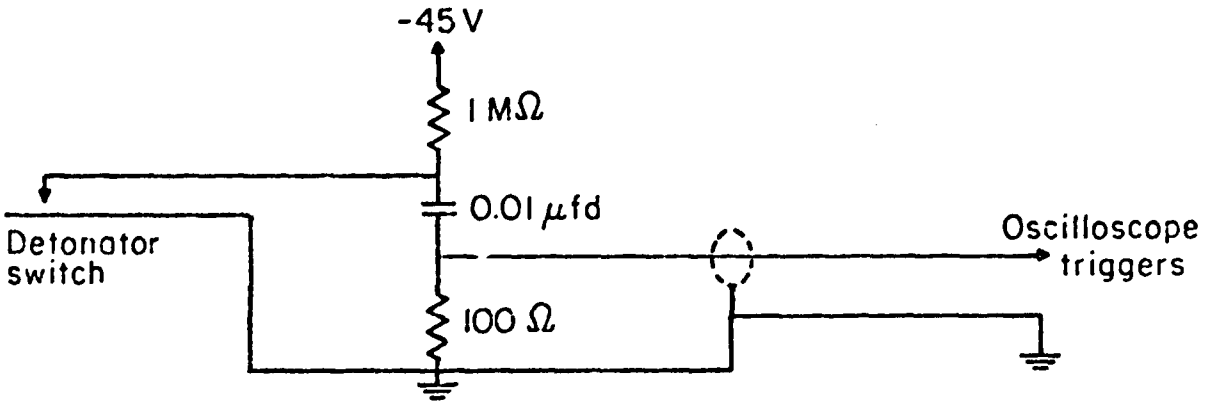

FIGURE 9. CAPACITOR DISCHARGE CIRCUIT FOR OSCILLOSCOPE TRIGGERS

The use of this switch trigger circuit is desirable from at least two standpoints. It allows replacement of the high-energy, fast pulse discharge required to produce reliably fast detonator functioning with a low-voltage battery source which does not cause annoying or dangerous electrical transients to appear in the high sensitivity, strain-measuring circuitry. It also produces a scope trigger at the time of detonator functioning with a time jitter estimated at <4 μsec based on high-speed photography of detonator functioning. With a knowledge of the detonation time of the explosive, this allows direct measurement of the time to first response of the vessel from the strain-gage records.

In practice, the initiation and trigger system first employed was a 100-j, 5-kV fast capacitor discharge pulser unit to fire the electric detonator. In use, the pulser was fired by a time-delay generator 100 to 200 μsec after the oscilloscopes were triggered to provide a section of noise-free base-line on the oscilloscope records from which the dynamic strain could be measured. This trigger system was employed on all shots in Vessels 1 and 3 and on shots 201 to 209 in Vessel 2.

All following shots used the foil-switch trigger. The foil switch trigger was adopted when it appeared that an occasional electrical transient from the high-voltage pulser could affect the strain-gage signal outputs for several milliseconds after pulser firings, although the transient effects normally disappeared in a few tenths of a millisecond, before the first strain signal arrived at the gage.

Several different systems were used to amplify and condition the strain-gage signal prior to recording it. The first used were Daytronic Model 870 strain-gage amplifier modules, which appeared to lack the necessary response in this application, and were not used after Shot 108 in Vessel 1. A second system which gave better results was the Ellis Model BAM-1 strain-gage amplifier and indicator. This is a small, battery-

powered amplifier with response from dc to 20 kHz. One of these amplifiers was used in connection with a Tektronix Model 555 oscilloscope to record strain-gage data in Shots 101 through 109 with the Daytronic modules on the other three channels, and two of them were used to record data for all remaining shots in Vessel 1, all shots in Vessel 3 and for Shots 201 through 219 in Vessel 2.

The Ellis amplifier also may be used as a static strain indicator, and on the gage channels in which it was installed it provided the capability for monitoring accumulated plastic strain in the vessels, although calibration of the bridge balance potentiometer directly in terms of strain is somewhat inconvenient.

In an effort to reduce the high-frequency noise content of the dynamic strain-gage outputs, a Daytronic Model 723 band-pass filter was used on all of the shot channels recorded using the Ellis amplifiers beginning with Shot 118 in Vessel 1, and all shots in Vessel 3. The Model 723 was used as a two-channel, low-pass filter. In general, the upper cut-off frequency was set at ∿3 or more times the calculated fundamental frequency of the vessel or part being studied, to avoid loss of meaningful signal information. The noise level of this and other available filters was too high to allow their use with the strain-gage signal before amplification and thus could not be used on channels recorded directly by an oscilloscope. Since no significant improvement of record quality with respect to reduction of scatter on repetitive shots, and an apparent extended recovery time following electrical transients was sometimes apparent, the use of this filter was abandoned for later shots in this program.

The simplest dynamic strain-measurement system appears to be the use of the dynamic strain gage in a full bridge circuit made up using three precision 350-ohm resistors supplied by Micro-Measurements for bridge completion resistors. The bridge is powered by either 12 or 24 Vdc from automotive-type wet cell batteries, although large dry cells may be used with slightly reduced stability. The bridge output is monitored directly by a Tektronix Model 502A oscilloscope arranged for differential input of the signal from the bridge. This oscilloscope provides a dc to 1 MHz band width, and sufficient vertical amplifier gain (∿1 mV/cm is the maximum necessary) to eliminate the need for a separate preamplifier. This system was first used on Shot 109 and on two gage channels for all remaining shots in Vessel 1, all shots in Vessel 3, and for Shots 201 through 219 in Vessel 2. It was used on all four gage channels for the remainder of the shots in Vessel 2. Generally, this system showed less transient upset by the pulser firing the detonator than the Ellis amplifier system, but more high-frequency (>20 kHz) noise than the signals from the Ellis amplifier, presumably because of its greater band-pass capability.

Dynamic Strain-Gage Accuracy

Calibration of the dynamic strain-gage output was accomplished using the standard shunt calibration techniques. The applicable equations for calculation of the value of shunt resistor, R_c, required to produce change in bridge balance equivalent to that produced by a change in strain, $\Delta\varepsilon$, was derived to be

$$R_c = R_g\,(1/f\Delta\varepsilon - 1), \tag{28}$$

where R_g = resistance of the strain gage

and f = the strain-gage factor relating the fractional change in gage resistance $\frac{\Delta R}{R}$ to the change in strain $\Delta\varepsilon$

$$f = \frac{\Delta R}{R} \Big/ \Delta\varepsilon \tag{29}$$

Thus, oscilloscope calibration was accomplished simply by temporarily connecting a resistor decade box, dialed to the value of R_c calculated from Equation (28) to provide the desired strain calibration step, $\Delta\varepsilon$, and adjustment of the oscilloscope vertical gain to produce the desired deflection of the baseline. The strain step consistantly used that which would provide a 3-cm deflection on the oscilloscope screen. This step was conducted very carefully with iterative, alternate adjustment of the oscilloscope baseline position and vertical gain because of the interaction which normally occurs between these controls. With use of a value of R_c calculated to at least 4 significant figures and dialed into a precision General Radio Decade Resistance Box, the gain repeatability was good to $\sim$3 percent over the screenface. This calibration was performed immediately before each shot. When a series of shots was being performed which required no change in the strain calibration from shot to shot, it was found that the gain of the amplifier and oscilloscopes was very stable from day to day.

The repeatability of dynamic strain measurements from shot to shot deserves some comment. Initially, when the first measurements were being taken, this question was addressed experimentally. A granular form of 50/50 Pentolite was being fired in small repetitive charges contained in plastic bags squeezed and taped into a compact shape. Variations in the recorded maximum dynamic strains of more than ±20 percent were observed on 0.73-lb Shots 110 through 115 and 118 through 121. After failing to find the source of this large variability anywhere in the measuring system, the container for the charges was changed to cardboard right circular cylinders with carefully controlled dimensions, so that not only the charge weight

but also the charge geometrical shape and density were controlled. The next series of charges, Shots 122 through 126, showed a reproducibility good to approximately ±10 percent for the maximum strains. Most, if not all, of this scatter is judged to be caused by noise superimposed on the strain signal from various sources such as cable vibrations and acoustic pickup by the oscilloscopes. It is further judged that over the bank of data collected, which spans nearly a 3-year time period and several different sets of measuring equipment, that ±15 percent is a reasonable error limit to assign individual datum points, although probably many of the data are better than this, and occasional datum points probably have more uncertainty than this from not fully understood sources.

Fiducial-Mark Networks and Measurement

In order to obtain information about the residual plastic deformation of the vessels and the strain distribution over the surface of the vessels, a network of fixed points for measurement, (fiducial marks) were placed on the surface of each vessel. Numbers were assigned to each mark and measurements between pairs of adjacent marks were recorded before testing and periodically repeated during testing to follow the progress of deformation (if any) of the vessels as a result of contained detonations.

The marks were arranged insofar as possible, along three orthogonal great circles on the surface of the sphere. One of these was always parallel with and adjacent to the main girth weld, and on some vessels there were two circles formed, one on either side of the weld. A second great circle was placed in a vertical plane. The orientation of the third orthogonal circle is specified by the first two.

Vessels 1 and 2 used identical networks; Vessel 3 included the same network as 1 and 2 plus some additional marks. On all of these vessels the fiducial marks consisted of a pair of fine scribed lines, one of which located the edge of the steel measuring tape to a repeatable position while the second at right angles served as an index line for measurement. Measurements were made by stretching a steel tape tightly along the surface of the vessel, holding an even number of inches over one line and reading the inches and fractions on the other line. Checks showed this system to yield reproducible readings to better than ±1/32 of an inch over the somewhat irregular, hot-formed vessel surfaces, so long as the same steel tape was used. Differences slightly larger than this were found between different steel tapes. These measurements provided a reasonably accurate measure of the average vessel surface strain between marks as the tape was forced to follow the vessel surface. The marks on Vessels 1 and 2 were typically ∿43 in. apart leading to an approximate measurement uncertainty of ±0.07 percent. The marks on Vessel 3 were typically ∿29 in. apart leading to a maximum uncertainty of ±0.1 percent. The system of marks used on Vessels 1 and 2 is shown in Figure 24 located in the "Results" section for convenience of reference.

A different type of fiducial mark was used on Vessels 3a through 6a, as well as a layout that differed in detail from the previous lot. Each mark on these vessels was formed by a finely pointed prick punch. Each mark was assigned an identifying number as before. Measurements were made, however, with the aid of a dial-gage-indicating vernier caliper equipped with sharp points which were inserted in a pair of adjacent prick-punch marks for measurement. Thus, this measurement was actually a measurement of the chord distance between adjacent marks and would lead to some ambiguity in interpretation in terms of vessel metal strain in the case of radical shape changes or local changes in vessel curvature. Spherical-shaped charges were fired in these vessels, however, and no such difficulties in interpretation occurred. This system has the advantage of greatly increased speed of measurement at no loss in accuracy. Individual measurements were typically near 10 in. They were measured with a repeatability of ± 0.002 in., in most cases, although because of certain irregularities in some punch marks the repeatability could vary as much as ± 0.005 in. leading to an uncertainty of ± 0.02 to 0.05 percent. Figure 28 located in the "Results" section shows the mark layout used for Vessels 3a through 6a, inclusive.

Explosive Charges

The relative effects of four different explosives--three detonating explosives and black powder--on the response of the containment chambers was investigated during this program. These explosives were arranged into several charge shapes for evaluation of charge-shape effects.

The initial, and most extensively used explosive in this program, was a loose, granular form of 50/50 Pentolite from DuPont or Trojan. Considerable variation in the bulk density of this material is possible by light crushing and vibratory packing. An intermediate density from the standpoint of that which could be achieved by the above methods was selected and efforts were made to reproduce this density. As a result the Pentolite bulk density was held in the ranges from ~0.73 to 0.80 g/cm^3, except for one charge each at 0.695 and 0.83 g/cm^3 which was outside this range. Examination of the data showed no discernible effect of this variation in density.

Two dynamites were investigated: DuPont Special Gelatin, 60% Strength; and DuPont Gelex-1, 60% Strength. These were removed from their stick wrappers and hand-packed into cardboard containers to be free of apparent voids. The most frequently occurring as-fired density of the gelatin was 1.65 g/cm^3 with a range from 1.64 to 1.69 g/cm^3. The Gelex charge density as-fired was 1.25 ± 0.01 g/cm^3. Both of these dynamites form and pack easily which accounts for the good uniformity of density achieved.

With the exception of some initial shots with Pentolite in plastic bags, all of the above explosives were packed into 1/16-in.

cardboard containers for firing. Two basic charge shapes were used -a cylinder and a suitcase. The cylinder charges were right-circular cylinders whose diameters were made nearly equal to their length. Whenever possible, commercially manufactured cardboard tubes were utilized so that there was some slight variation in length:diameter ratio. All cylinder charges were hung in the center of the vessels from eyebolts welded inside the vessels for this purpose. The cylinder axis was vertical with respect to gravity.

The suitcase-shaped charges were sized for the desired charge weight and density with the edge lengths maintained in the ratio 1:2:3. These relative dimensions approximate the relative dimensions of many suitcases. They were hung in the center of the vessels with the longest dimension horizontal and tilted so that the largest flat face was normal to the direction to the No. 2 gage in each case.

The fourth explosive investigated was 3FA black powder, with a bulk density near 1.09 g/cm^3. The charges were placed in either glass containers or pipe sections with steel end caps. The first black powder shot (Shot 314) was initiated by a detonator and Detasheet booster. The remainder were squib-initiated.

Hydrostatic Test Procedures

In order to verify the performance of the strain gages installed on Vessel 2 and obtain a calibration of their response to internal pressure, the vessel was sealed and pressurized with liquid. Because this vessel was not designed to be sealed to hold hydrostatic pressure, and because the door-ring combination was found to be warped out of flatness, this task proved to be quite difficult. Three distinct sealing problems had to be solved: The main 26-in.-diameter port, the 2-in.-diameter support pin, and the two 1-in. adjusting bolts threaded completely through the vessel skin and reinforcing plates. These were solved as follows:

The gaps between the ring and door in the overlap area were filled with epoxy putty and glue following careful cleaning of the door. A supplemental external bar and bolt connected to the center eyebolt on the door provided the necessary additional clamping pressure to affect a seal.

The support pin was O-ring-sealed, using a small triangular copper gasket to bridge the gap between the vessel and the pin and prevent O-ring extrusion. The initial clamping pressure on the O-ring required to effect the seal was provided by a specially fabricated split collar which was clamped around the support pin inside the vessel to compress the O-ring against the inner end of the pin support sleeve.

The adjusting bolts were sealed with epoxy glue in the threads. In order to make this seal, it was necessary to insert short threaded plugs cut from bolts and screwed nearly to the bottom of the threads. These plugs formed cups of the threaded holes to hold sufficient epoxy to fill the entire threaded gap between the bolt and vessels when the bolts were inserted.

The vessel was connected to a high-pressure pump and a Baldwin-Lima-Hamilton 0 to 10,000 psi SR-4 pressure transducer, through 0.083-in.-bore, high-pressure tubing. The conditioned pressure signal was recorded on a strip chart recorder. The vessel was initially filled with water though one of the adjusting bolt-holes after other seals and connections were complete. The final bolt-hole was then sealed in, as described above, completing the closure. The four strain gages on the vessel were connected to a Budd Model 350 strain indicator through a Vishay Instruments Model SB-1 switch and balance unit, and the strain readings initially zeroed with the switch and balance unit.

Figure 10 shows the experimental results for the hydrostatic test of Vessel 2. The pressure was initailly increased to 1500 psi in order to insure that the seals were satisfactory. Decreasing-pressure data were obtained by shutting off the pump, opening the drain valve until the desired pressure was achieved, and reading the chart recorder and strain indicator within 1 to 2 minutes. Except for the creep data discussed below, the readings equilibrated in less than a minute and remained quite steady. Increasing pressure data involved shutting off the pump and completing the readings in 1 to 2 minutes. The initial increasing-pressure data closely approximated the initial decreasing-pressure data, thus indicating that little plastic deformation occurred for pressures less than 1500 psi. Above 1500 psi the first cycle data have a downward curvature, indicative of plastic response. At 2725 psi, the reinforcing ring (see Figure 5) had a strain of 1720×10^{-6} and creep behavior became quite noticeable in the strain-gage readings. A decision was made to recycle to lower pressures because the nonlinear results obtained for all gages suggested that the elastic limit of the vessel had been exceeded, and it was desired to keep the plastic deformation of the vessel small.

After several minutes of creep observations, from an initial pressure of 2725 psi, the second cycle of data was taken. Two phenomena characteristic of plastic flow were immediately obvious. The second-cycle data did not follow the path of the first cycle but traced a curve nearly parallel with the elastic portion of the first cycle. As a consequence of this parallel behavior, the zero pressure intercept with the strain axis increased significantly. This typical plastic phenomenon is known as residual strain. It was also observed that the decreasing-pressure data had a slight upward curvature, while the increasing-pressure data had a slight downward curvature. Creep behavior was noticeable once again when the pressure was increased to 2725 psi.

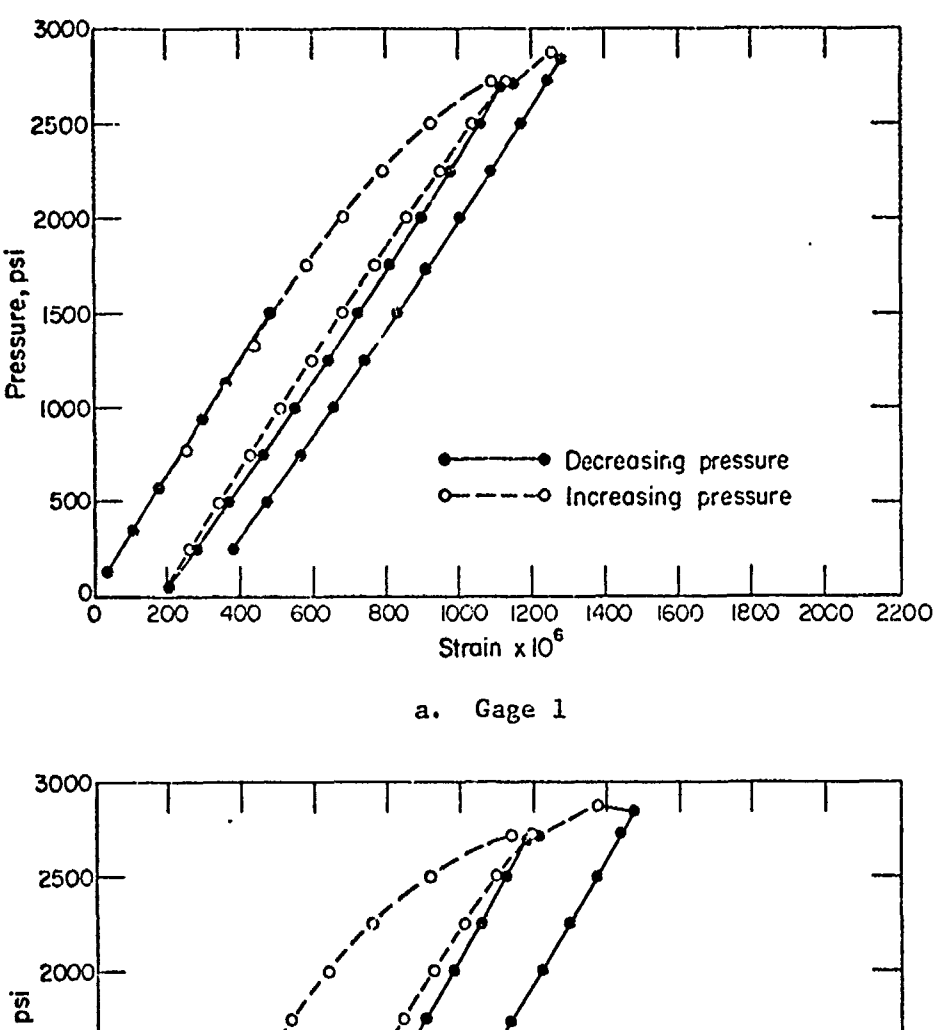

a. Gage 1

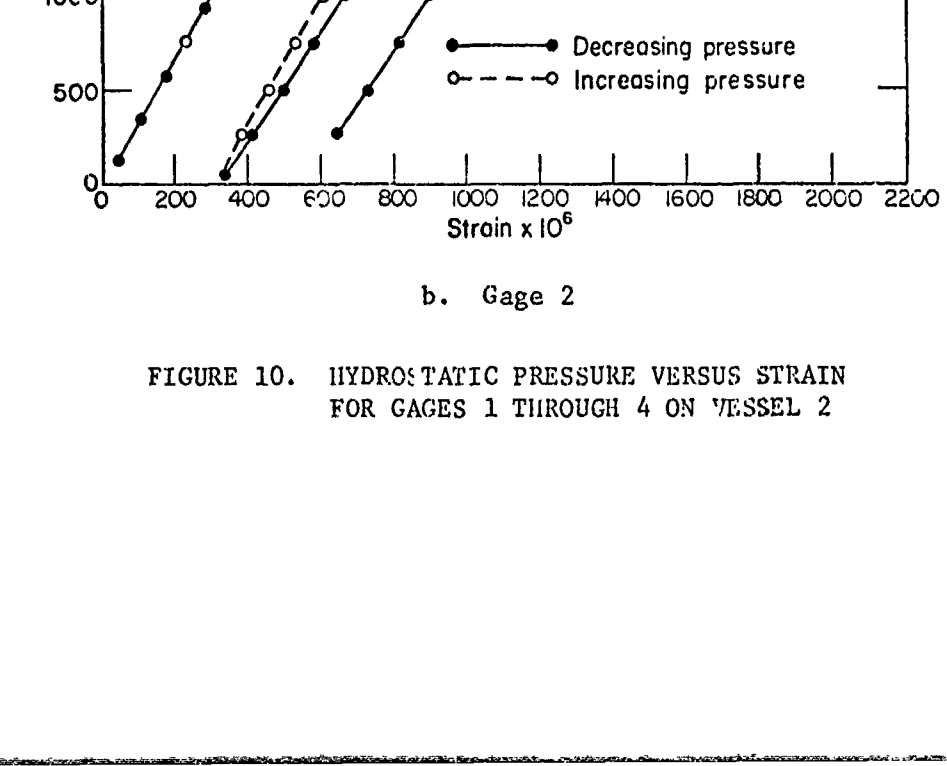

b. Gage 2

FIGURE 10. HYDROSTATIC PRESSURE VERSUS STRAIN FOR GAGES 1 THROUGH 4 ON VESSEL 2

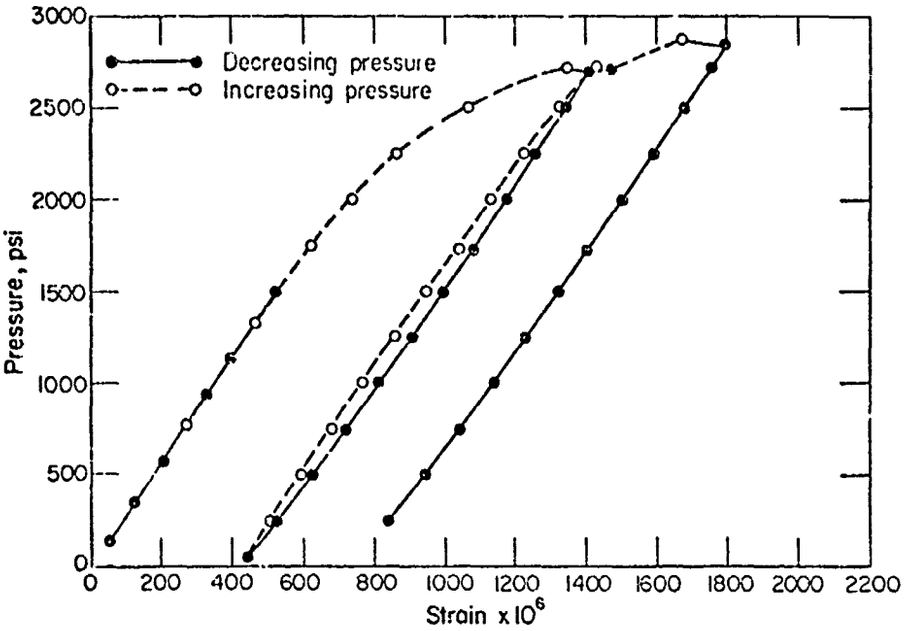

c. Gage 3

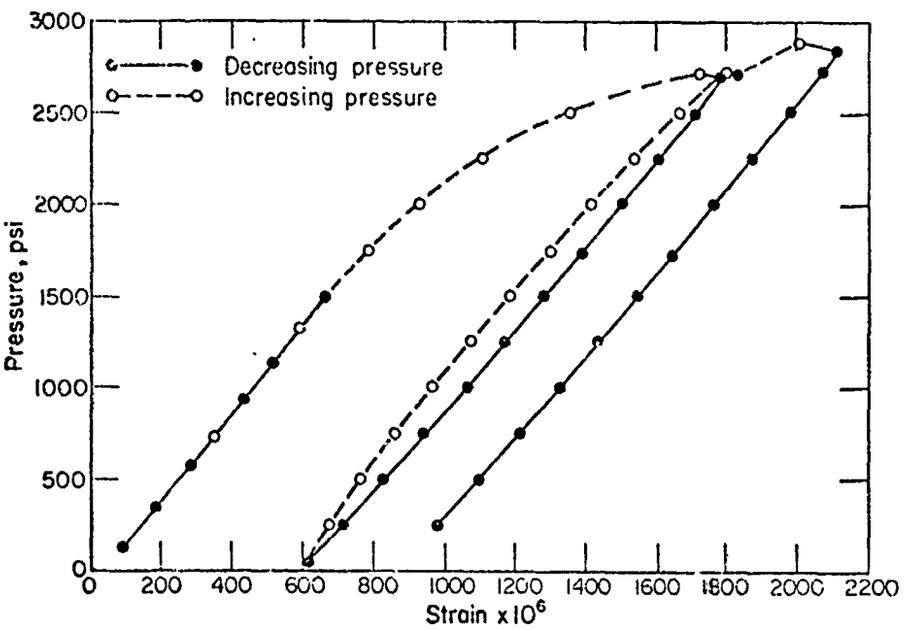

d. Gage 4

FIGURE 10. (Continued)

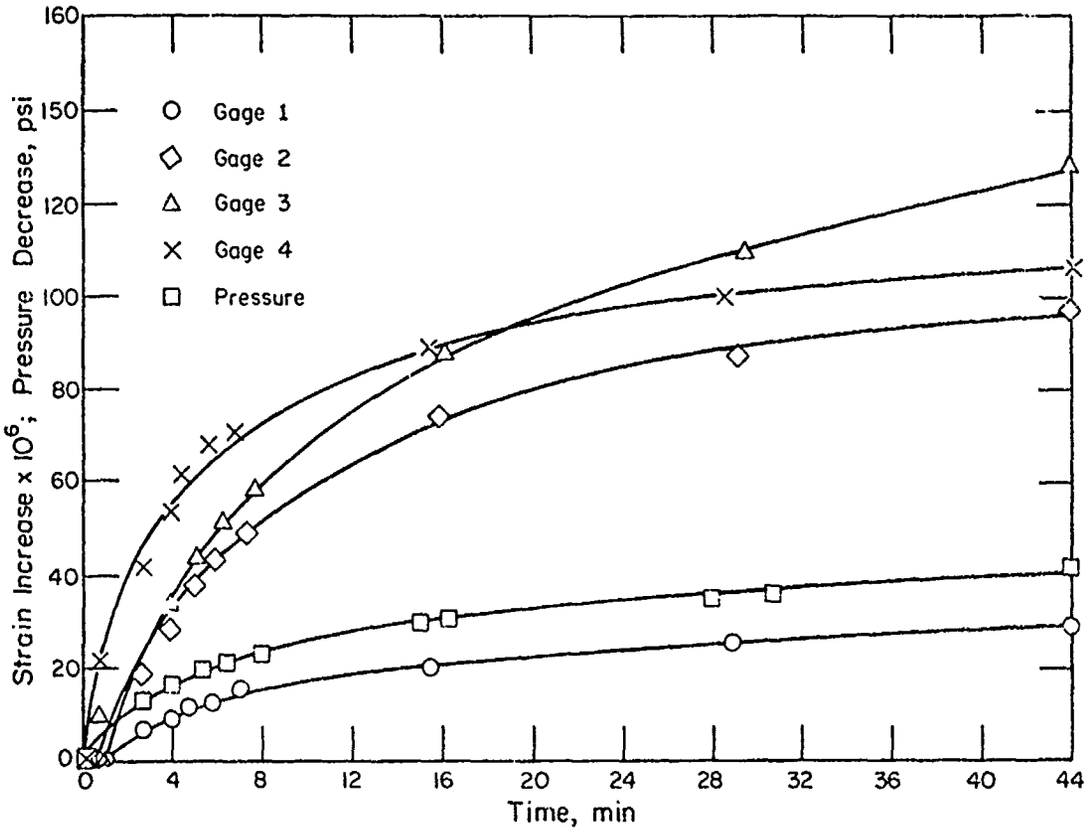

FIGURE 11. THIRD-CYCLE CREEP DATA FROM THE HYDROSTATIC TEST OF VESSEL 2

Initial pressure in the vessel was 2885 psi.

In order to demonstrate the progressive nature of both the work hardening and the accumulation of residual strain, a third cycle of data was taken. The pressure was increased to 2885 psi, the pressure at which the strain in the ring (as shown in Figure 10) was equal to 2000×10^{-6} or 0.2 percent. Creep data were recorded (as shown in Figure 11) for 45 minutes and then decreasing-pressure readings were taken to complete the experiment. The third-cycle data were parallel with the second cycle data and another large increment of residual strain was observed. Because of requirements to perform additional tasks with Vessel 2, it is judged that hydrostatic testing at higher pressures would introduce undesirably large residual strains and the test was terminated. Hysteresis loops and creep following deformation into the plastic region are normally found in studies such as this.

An elastic analysis has been performed on the hydrostatic test data, and the results are summarized in Table 4. Strain intercepts and pressure-strain slopes were obtained from Figure 10. The initial cycle results are unambiguous. The results quoted for the second cycle represent the average of the decreasing- and increasing-pressure data. There are no increasing-pressure data for the third cycle, however it was assumed that a hysteresis loop similar to that of the second cycle would have obtained. The near equality of the slopes in the second and third cycle supports this assumption.

The last line of Table 4 gives a prediction from elastic theory using standard material parameters. For Gages 1 through 3, these predictions were based on the thin-walled-sphere equation for strain:

$$\epsilon_s = \frac{P}{2} \frac{(1-\nu)}{E} \frac{a_s}{t_s} , \tag{30}$$

where ϵ_s is the strain in the surface dimensions, P is the hydrostatic pressure, ν is Poisson's ratio, E is Young's modulus, a_s is the radius of the vessel, and t_s is the wall thickness. The pressure-strain slope is given by:

$$\text{Slope} = \frac{P}{\epsilon_s} = \frac{2E}{(1-\nu)} \frac{t_s}{a_s} . \tag{31}$$

The predictions in Table 4 employed $E = 30 \times 10^6$ psi, $\nu = 0.28$, $a_s = 27.5$ in., and the thickness data given in Table 2. Due to the scatter in the reported thickness measurements, the values for t_s used in the predictions were 1.000 in. for Gages 1 and 2 and 0.945 in. for Gage 3.

It may be recalled that the design of the reinforcing ring was based on an equal static strain criterion for the ring and sphere, under the assumption that the sphere thickness was 0.75 in. After the ring for Vessel 2 was fabricated, ultrasonic wall-thickness measurements showed that the average wall-thickness was in fact 1.00 in. Thus the

TABLE 4. ELASTIC ANALYSIS OF THE HYDROSTATIC TEST ON VESSEL 2

Cycle	Gage 1	Gage 2	Gage 3	Gage 4
		Summary of Strain Intercepts[a], units of microstrain		
Initial	-8	10	8	45
Second	190	323	431	598
Third	295	560	755	864
		Summary of Pressure-Strain Slopes[b], units of microstrain		
Initial	3.05×10^6	3.40×10^6	2.89×10^6	2.42×10^6
Second	2.89×10^6	3.14×10^6	2.75×10^6	2.26×10^6
Third	2.87×10^6	3.11×10^6	2.73×10^6	2.25×10^6
Prediction[c]	3.04×10^6	3.04×10^6	2.87×10^6	2.28×10^6

(a) Accuracy of 10 microstrain.

(b) Accuracy of 3 percent.

(c) Accuracy of 5 percent.

cross-sectional area of the reinforcing ring was 25 percent less than it should have been to meet the equal-strain criterion, and the strain in the ring, ε_r, was expected to exceed the strain in the sphere, ε_s, at points well removed from the port, by a factor of 1/0.75. The predicted value for the slope of the ring data (Gage 4) shown in Table 4 is based on this factor.

Comparison of the measured and predicted slopes given in Table 4 shows that good agreement was obtained and that the strain gages which had been in service on the vessel for a considerable time were still providing reliable data.

Chronological Test Summary

Tables 5 through 8 show all of the shots fired on this program. Chronologically, the first 39 shots, all with dynamic strain-gage instrumentation were fired in Vessel 1. At Shot 139, using 4.4 lb of DuPont Special Gelatin, 60% Strength dynamite, the electrical leads on Gage 3 were broken off, and testing of this vessel was temporarily interrupted to repair the gage.

Table 7 shows the shots fired in Vessel 3. After Shot 316, testing was temporarily suspended due to the requirements of another program for the test facility. When the strain gages were reconnected, it was found that Gages 3 and 4 on the vessel were inoperative. It appears that they were damaged in movement of the vessel rather than by explosive blast. Testing was continued employing Gages 1 and 2 only. At Shot 323, using 5.5 lb of DuPont Special Gelatin, 60% Strength dynamite, Gage 2 popped completely off the vessel. Testing continued through Shot 328 when testing of this vessel was terminated. This vessel was subsequently shipped to Picatinny Arsenal for further evaluation.

Testing was resumed on Vessel 1. The large charge sizes employed in the last four shots were based on scaling from the results of previous testing, and estimated to be just below the elastic limit for Vessel 1. Following Shot 142, the weld along the upper right side of the port sleeve was observed to be leaking gas intermittently over a distance of ~1 ft. Shot 143 blew the entire closure sleeve and door from the vessel. Post-failure inspection showed that incomplete weld penetration had been obtained on the vessel-sleeve weld, causing the premature failure.

After a several-month delay, a program extension was secured and Vessel 2 was modified to include a better designed reinforcing ring and a 4-in.-thick door, swung on a single vertical pin. Stresscoat* was

*Stresscoat is a product of Magnaflux Corp.

TABLE 5. CHARGES FIRED IN VESSEL 1[a]

Shot Nos.	How Many	H.E. Weight lb	H.E. and Charge Type	Description
				H.E. Types
101-102	2	0.4	P L	P = 50/50 Pentolite, loose granular
103-109	7	0.8	P L	C-4 = Composition C-4
110-115	6	0.73	P L	Gn = DuPont Special Gelatin, 60%
116	1	1.10	P L	Strength dynamite
117	1	0.98	C-4 B	Gx = DuPont Gelex-1, 60% Strength
118-121	4	0.73	P L	dynamite
122-126	5	0.73	P C	
127-128	2	0.73	Gn C	Charge Types
129-130	2	0.73	Gx C	
131-132	2	1.10	P C	L = Charge in thin plastic bag taped
133	1	1.677	P C	to compact shape
134	1	2.54	P C	B = Formed into an approximate sphere
135	1	3.20	P C	C = Packed into a 1/16-in.-thick
136	1	3.86	P C	cardboard cylinder with length =
137	1	4.40	P C	diameter
138	1	4.40	Gn C	S = Suitcase-shaped charge in 1/16 in.-
139	1	4.40	Gn C	thick cardboard; relative
140	1	6.50	P B	dimensions were 1:2:3
141	1	16.0	Gn B	
142	1	16.0	Gn S	
143[b]	1	16.0	Gn S	

(a) Vessel 1 was 4.5 ft in diameter with a 1-1/2-in.-thick door and an average wall thickness of 1 in.

(b) Shot 143 blew out the reinforcing sleeve and door of the vessel.

TABLE 6. CHARGES FIRED IN VESSEL 2[a]

Shot No.	Explosive Weight, lb	Charge Type[b]
201[c]	0.30	P C
202[c]	0.40	P C
203[c]	0.55	P C
204[c]	1.60	P C
205[c]	2.0	P C
206[c]	2.5	P C
207	1.0	P C
208	1.0	P C
209	2.5	P S
210	3.2	P S
211	4 4	P S
212	6.0	P S
213	8.0	Gn S
214	10.0	Gn S
215	4.4	P C
216	6.0	P C
217	8.0	P C
218[d]	10.0	P C
219	1.95	P C
220	1.35	Gn C
221	1.95	P S
222	1.95	P S
223	10.0	P S
224	8.0	P S
225[e]	1.95	P C
226[e]	8.05	P C
	Hydrostatic Test	
227	2.0	P C
228	2.0	P C
229	1.94	P C
230	2.0	P C
231	4.4	P C
232	8.0	P C
233[f]	2.0	P C
234[f]	8.0	P C
235[e]	10.0	P C
236[g]	8.0	P C

(a) Vessel 2 was 4.5 ft in diameter, with a 4-in. thick door and an average wall thickness of 1 in.

(b) See Table 5 for an explanation of the charge types.

(c) Shots 201 through 206 were for check-out of vessel with stress-coat and were noninstrumented.

(d) Shot 218 blew a hole in the bottom of the vessel

(e) Vessel filled with vermiculite.

(f) Vessel half-filled with vermiculite.

(g) Vessel filled with glass bottles.

TABLE 7. CHARGES FIRED IN VESSEL 3[(a)]

Shot No.	Explosive Weight, lb	H.E. and Charge Type	Description
301	0.895	P C	H. E. Types
302	0.895	P C	
303	1.08	P C	P = 50/50 Pentolite, loose granular
304	1.23	P C	
305	1.38	P C	Gn = DuPont 60% Special Gelatin, 60% Strength dynamite
306	1.535	P C	
307	1.38	P S	
308	1.38	Gn C	Gx = DuPont Gelex-1, 60% Strength dynamite
309	1.38	Gx C	
310	1.535	Gn C	B = 3FA black powder
311	1.535	Gx C	
312	1.535	Gx C	Charge Type
313	1.535	Gx C	
314	1.0	B J	C = packed in a 1/16-in.-thick cardboard cylinder with length = diameter
315	0.95	B P	
316	2.4	B J	
317	3.7	B P	
318	1.535	Gn S	S = suitcase-shaped charge in 1/16-in.-thick cardboard; relative dimensions were 1:2:3
319	2.00	Gn S	
320	2.50	Gn S	
321	3.50	Gn S	
322	4.50	Gn S	J = packed in a glass jar
323	5.50	Gn S	P = packed in a pipe bomb
324	6.50	Gn S	
325	8.00	Gn S	
326	10.00	Gn S	
327	8.00	Gn S	
328	12.00	Gn S	

(a) Vessel 3 was 3.0-ft. in diameter, with an ~0.725-in. wall thickness; the flat door was 1.0 in. thick.

TABLE 8. CHARGES FIRED IN VESSELS 3a THROUGH 6a

Shot No.	Explosive Weight[b], lb	Vessel No.
401	5.0	3a
402	7.0	5a
403	6.0	4a
404	5.0	3a
405	6.5	5a
406	6.0	4a

(a) Vessels 3a through 6a had a 2-ft diameter, with a 2.25-in.-thick door and an average wall thickness of 0.495 in.

(b) All charges were Composition C-4, packed into spherical molds to a density of $\sim$1.55 g/cm^3.

applied to the vessel, and a series of six small shots was fired to determine the location of any areas of high stress. The results of the testing showed no definite areas of stress concentration. Consequently, the four strain gages were installed using two of the same relative locations used previously. These were Gages 2 and 3. Gage 1 was moved to a location approximately three wall thicknesses from the reinforcing plates around the hinge pin. This is approximately 18 inches closer to the weld than the Gage 1 in Vessel 1. The Gage 4 was installed on the reinforcing ring rather than on the vessel proper. Shots 207 through 218 were fired with strain-gage instrumentation. Shot 214 broke the weld holding the T-pin door support together. The door was opened using a chain through the external eyebolt, and a front loader to lift the door in place, secured by an external J-bolt through the door eyebolt and an external cross-bar across the port, for Shot 215 through 218. Using this system, control of the door was imperfect, and the support cord for the 10-lb Pentolite Shot 218, was apparently severed during door closure, allowing the charge to fall to the bottom of the vessel before firing. Shot 218 ripped a hole in the vessel but released no fragments. This damage is documented in Figure 12.

The hole in Vessel 2 was repaired by welding in a 28-in.-diameter spherical cap cut from an undamaged portion of Vessel 1. This diameter opening allowed removal of the door and repair of the door support T-pin, as well as removal of the deformed metal surrounding the hole. It was necessary to replace only Gage 3 of the four strain gages on the vessel. Testing continued through Shot 226 with dynamic instrumentation.

Again, after a several-month delay testing was resumed, this time to determine the calibration of the strain gages with hydrostatic pressurization in Vessel 2. The strain-gage results were found to agree with their calculated response to within ∿5 percent.

Finally, Shots 227 through 236 were fired in Vessel 2. The four 2.0-ft-diameter vessels were fabricated and tested to determine the maximum charge containment capability of spherical vessels of this type. These were tested in a final series of six shots, as shown in Table 8.

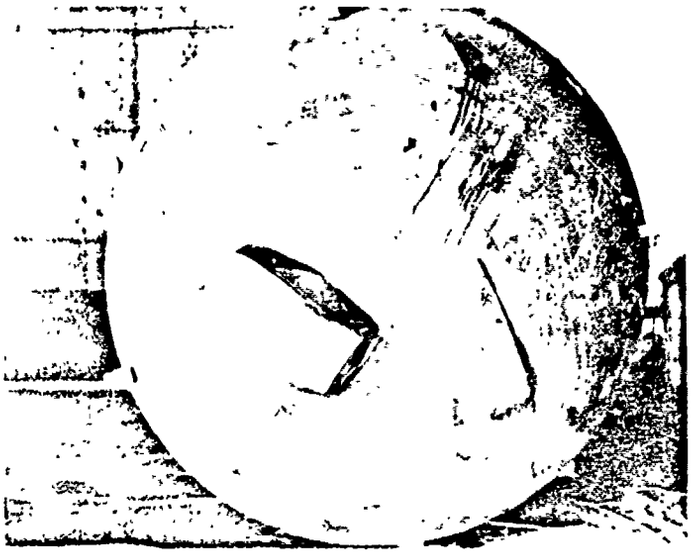

FIGURE 12. DAMAGE PRODUCED BY 10-LB OF PENTOLITE IN CONTACT WITH THE BOTTOM OF VESSEL 2

Vessel is viewed from the bottom in this photograph. The white bar on the vessel is 1 ft in length.

EXPERIMENTAL RESULTS AND DISCUSSION

A considerable volume of dynamic and post-shot measurement data was obtained. In this section the results have been separated into six parts for convenience. These are:

(1) The dynamic response of the vessel and door as observed by the strain gages and the variation of this response with maximum stress level attained.

(2) The initial maximum dynamic stresses and comparison with theory.

(3) Comparison of the strengths of the various explosives tested based on the measured vessel response.

(4) The effect of charge shape on vessel response.

(5) The evidence for plastic vessel response and comparison with theory.

(6) The effect of blast-attenuating filler materials

Dynamic Response of the Vessels

Typical strain-gage response records for small charges are shown in Figure 13 for a relatively small shot of 1.1 lb of Pentolite in the 4.5-ft Vessel 1. The different appearance of the upper and lower oscillographs resulted from the use of a low-pass filter on the gage outputs for the lower oscillographs to reduce the high-frequency noise component apparent on the upper trace. The filter cut-off frequencies were set at 1 kHz for Gage 5 and 6 kHz for Gage 3, both well above the natural frequencies of 318 Hz for the door (Gage 5) and 1971 Hz for the vessel, so that no meaningful data were removed by the filter. Firing of the charge detonator occurred at approximately 0.4 ms after the beginning of the oscillograph sweep. This is shown as a small spike on the upper photo and produces an initial negative transient on the lower photo due to an interaction with the low-pass filter. Instrument checks showed that this transient normally disappears in less than 0.4 ms, and thus the initial tensile peak should have been recorded free of spurious influences. However, the appearance of some traces makes this conclusion suspect. In later measurements all of the data were recorded without filtering, as in the upper photo.

The response of the door in oscillation was primarily tensile, as would be expected for a flat plate internally loaded. The static pressure inside the vessel would be expected to have a greater effect

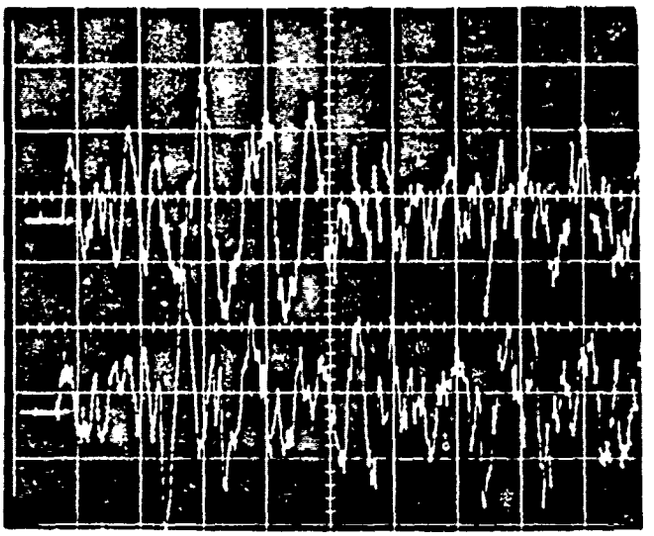

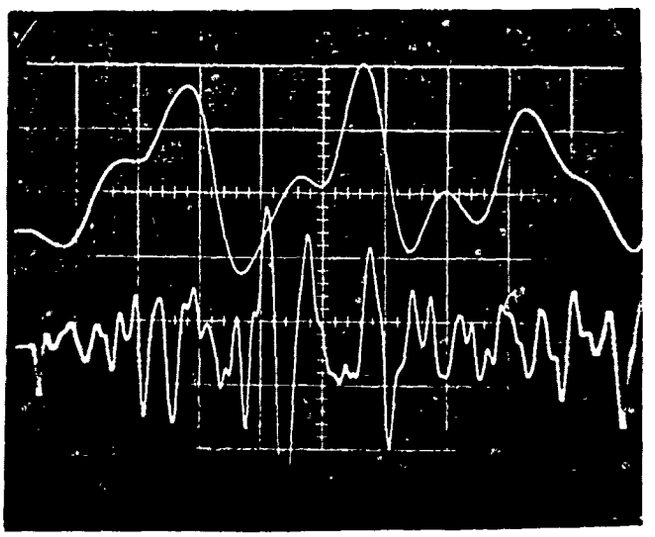

FIGURE 13. STRAIN-GAGE RECORDS FROM SHOT 131

The horizontal scale is 1 ms per major division. The vertical scales are 300 microstrain per major division for Gages 2 and 4, 600 for Gage 3, and 500 for Gage 5. The tensile strain direction is up.

on the door than on the vessel proper. The observed fundamental frequency of the door is in good agreement with a calculated natural frequency of 318 Hz for a circular disc simply supported at its edges. Note that the second maximum is larger than the first.

The response of the vessel after the first cycle is complicated. Note that large maxima occur at different times for the different gage locations and that these maxima are much larger than the initial maximum response. This is typical of all the low-amplitude gage records from all three vessels of the two sizes investigated. The later time maxima are often associated with several oscillations at approximately one-half the fundamental breathing-mode frequency. This lower frequency is associated with a bending-mode oscillation of the vessel. The bending-mode oscillation is excited apparently by the inertial restraint offered by the additional mass associated with the vessel closure port. The highest later-time maximum observed was always on Gage 3, located directly opposite the door. Further support for this later time strain maximum being the result of a bending-mode oscillation is provided by the following data. Maximum strains on Gage 3 of 8400 microstrain have been observed, with little, if any, residual plastic strain remaining in the vessel, as measured by changes in the external dimensions. If this strain were elastic, the stresses would have reached 330,000 psi, assuming spherical loading. The dynamic yield stress is probably 100,000 psi or less for the vessel material. If the strain were tensile throughout the wall thickness, residual plastic strain would be a necessity. However, if the surface strain were produced by an oscillatory bending stress, then only the outer (and inner) fibers of the material would suffer plastic strain, and the gradual decay of the oscillation could be expected to leave little residual strain. Small residual static strains, as noted on the static strain-gage indicators, were observed following shots in which the calculated elastic stresses exceeded 100,000 psi. These residuals were sometimes tensile and sometimes compressive in nature, which also agrees with a bending-mode oscillation.

To date, only a few strain-gage records have been obtained for the response of a vessel loaded into the plastic region. As the blast load increases, the overall maximum tensile strain response of the vessel shifts toward the first maximum of the response. This effect is shown in Figure 14 for Shot 142, 16 lb of DuPont Special Gelatin in the 4.5-ft-diameter Vessel 1. These records give evidence for residual deformation of the vessel, some of which remains unexplained at present. The shift in maximum response toward the first maximum is explained as follows: if the shock wave load becomes great enough to produce plastic deformation of the vessel in a breathing mode, two things happen. First the strain increases more rapidly than the stress due to exceeding the elastic limit, allowing the first-cycle strain to increase rapidly. Second the occurrence of overall plastic strain produces a very large and effective damping mechanism that rapidly attenuates further vibrations, until their amplitude drops below the elastic limit.

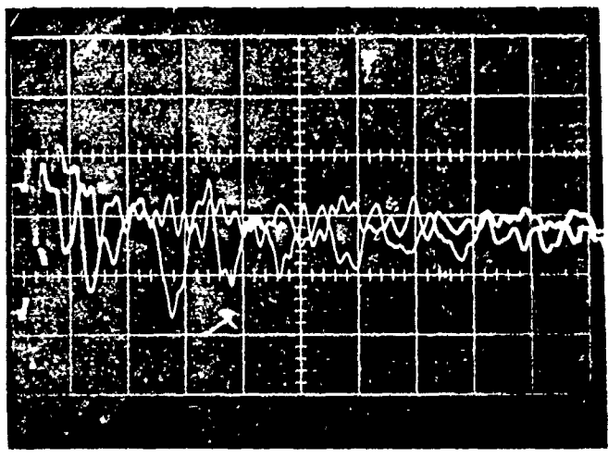

Gage 1

Gage 4

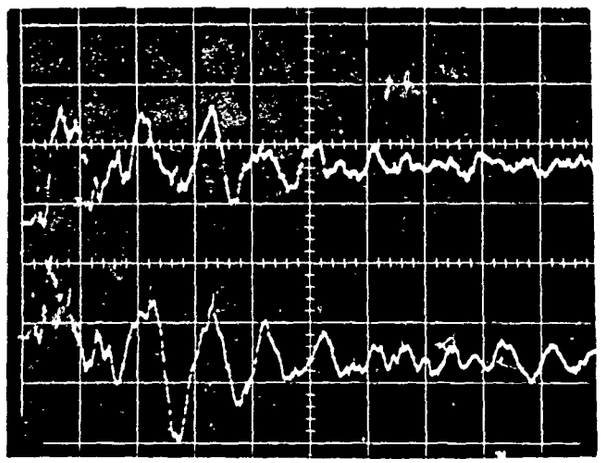

Gage 3

Gage 2

FIGURE 14. STRAIN-GAGE RECORDS FROM SHOT 142

The horizontal scale is 1 ms per major division. The vertical scales are 1600 microstrain per major division for Gage 1, 2000 for Gages 2 and 4, and 2400 for Gage 3. The tensile strain direction is up.

Maximum Dynamic Stresses

The initial maximum tensile strain reached in the dynamic responses of the spherical vessels is the significant quantity for comparison with the theory of the response of spherical vessels. At this time, no theory is capable of treating the late time maxima observed after several cycles of oscillation.

The most direct comparison with theory available from the present data is shown in Figure 15. This graph shows all the first-cycle maximum response data for compact Pentolite charges detonated in the 4.5-ft vessels, compared with calculated elastic-plastic responses for assumed 50,000 and 100,000-psi yield strengths in a 4.5-ft-diameter vessel with a 1.00-in.-thick wall. On this figure, both stress and strain are shown as ordinates. For elastic responses, either ordinate may be read. However, for the dashed portions of the predicted curves, above the assumed yield strength of the material, only the strain ordinate is applicable. The experimental data points, measured from oscilloscope records of strain-gage output, were plotted directly as strain data. These may be interpreted as stresses, with caution, since some of the upper points include some plastic strain components. The lower dashed line is a least-squares fit to all of the Pentolite data points except the highest points for 10 lb of explosive which showed deviation from linear behavior, and evidence for plastic strain which will be discussed later. The slope of the line fitted to the data appears to be in good agreement with the predicted slope. A statistical test of the difference between the predicted slope of 0.768 and the fitted line slope of 0.806 showed no significant difference at the 90 percent confidence level.

The difference in the predicted magnitude of stresses and the observed magnitudes averages about 24 percent, as shown in Figure 15. This difference is probably due to the lower blast-wave parameters to be expected from the low bulk-density Pentolite used in this program, compared with the full-density Pentolite used to generate the shock-wave data used in the analysis.

Figure 16 shows data for the 3.0-ft-diameter vessel similar to that shown in Figure 15. In this case the agreement in slope between the theoretical and measured response curves is more approximate, but there is little significance to the disagreement, because the data were obtained over a narrow range. In this case the experimental points lie about 20 percent below the theoretical curve. Within the accuracy of the data, the agreement between Figure 15 and 16 for the two vessel sizes is excellent and may be regarded as good confirmation of the scaling law used in the analytical prediction.

Figure 17 shows the first-cycle maximum response data for suitcase-shaped Pentolite charges and for DuPont Special Gelatin, 60%

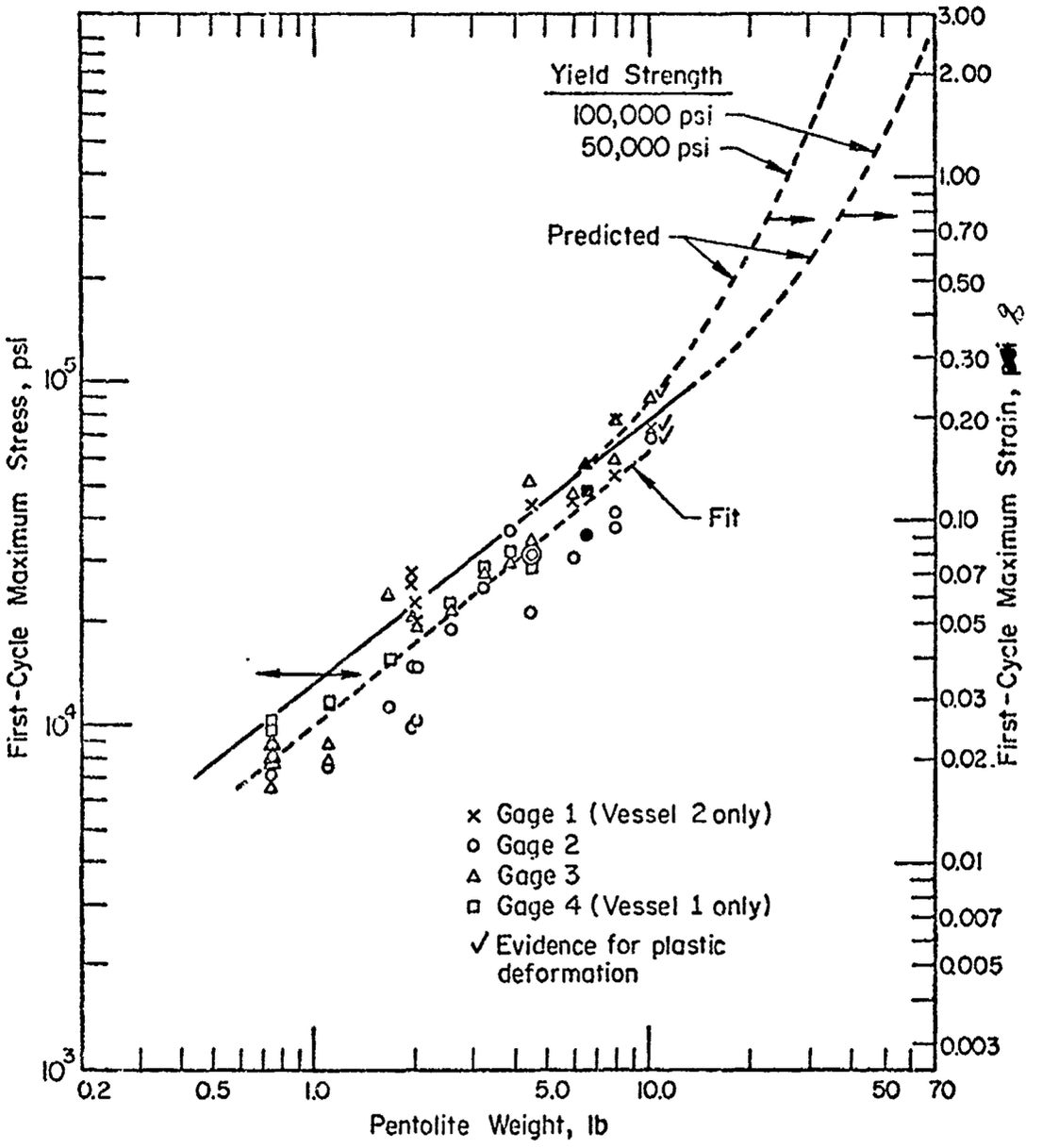

FIGURE 15. EXPERIMENTAL AND THEORETICAL FIRST-CYCLE RESPONSE OF THE 4.5-FT-DIAMETER SPHERICAL VESSELS TO COMPACT PENTOLITE CHARGES

Average vessel wall thickness was 1.0 in.

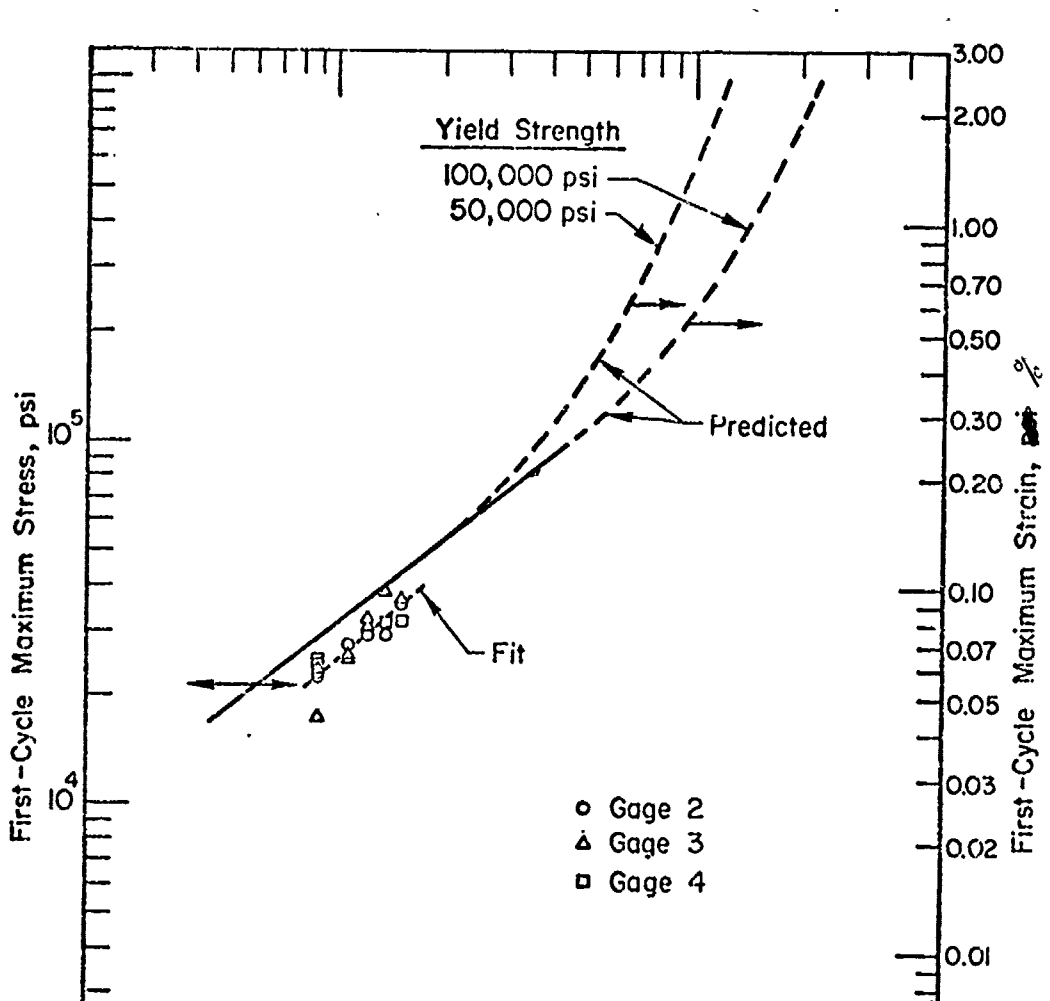

FIGURE 16. EXPERIMENTAL AND THEORETICAL FIRST-CYCLE RESPONSE OF A 3.0-FT-DIAMETER SPHERICAL VESSEL TO COMPACT PENTOLITE CHARGES

Average vessel wall thickness was 0.725 in.

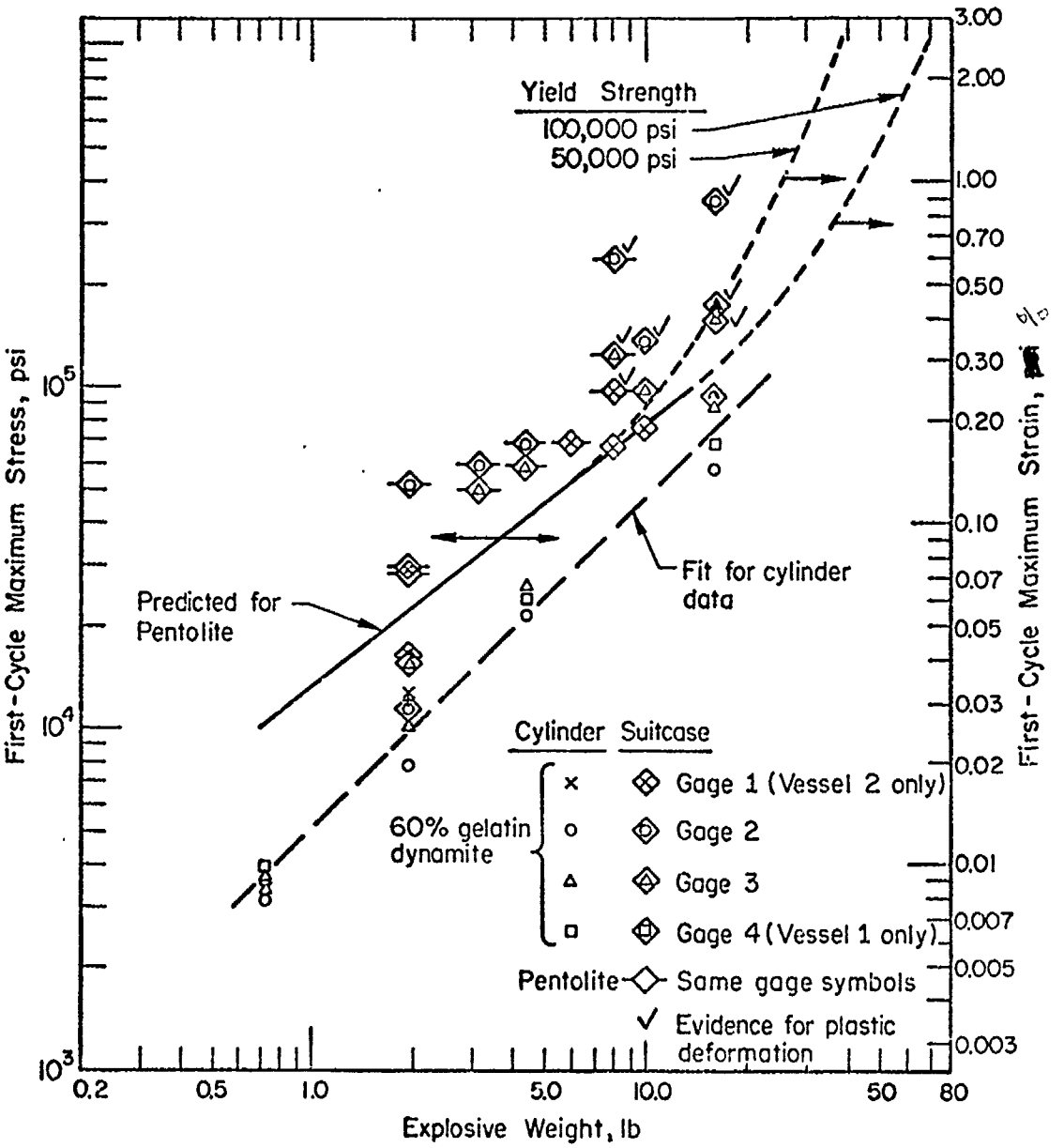

FIGURE 17. EFFECT OF CHARGE SHAPE ON FIRST-CYCLE RESPONSE OF THE 4.5-FT-DIAMETER SPHERICAL VESSELS TO SPECIAL GELATIN, 60% STRENGTH DYNAMITE CHARGES

Average vessel wall thickness was 1.0 in.

strength dynamite in both cylindrical and suitcase-shaped charges detonated in the 4.5-ft-diameter Vessels 1 and 2. The calculated curves for Pentolite are also shown for comparison. Note that the normal to the major flat face of the suitcase-shaped charges was directed toward Gage 2 except in one 16-lb gelatin dynamite shot in which the major flat face was inadvertently directed 37.6 deg toward the door from vertical instead of toward the rear. The data points from this shot are shown filled. The slower shock-wave attenuation off the major flat face of the charge normally gives rise to a larger vessel response in line with this shock than at other locations, as may be observed in the figure. The difference between Gage 2 response and that of other gages increases with charge size, as would be expected since the size of the flat charge face is increasing while the propagation distance to the vessel wall is decreasing. This effect is most pronounced when the two 16-lb dynamite suitcases with different orientations are compared. The response of the No. 2 gage facing the major flat face of the charge is more than 3 times greater than when the same gage is inclined 75.2-deg from this face. In both of these two shots, Gage 3 was 52.4 deg away from the direction to a major flat face and shows nearly the same response.

Figure 18 shows first-cycle maximum response data for Pentolite cylinders and suitcases of equal weight and the available gelatin dynamite data for the 3.0-ft-diameter Vessel 3. In both Figures 17 and 18 the dynamite data fall well below the Pentolite prediction at small charges but approach it at higher charges. The points with a √ showed evidence for plastic deformation. In many cases, the instrumentation was not ideally chosen to measure residual plastic strains with precision. Hence, there may have been small plastic strains in other shots as well which went undetected.

As described earlier, the first-cycle maximum strain is the strain calculated in the analysis. This is not, however, the maximum strain recorded, in general, by the strain gages. The maximum strains recorded by the strain gages occur at various times after the first-cycle maximum. The maxima occur at times after detonation ranging from ∿0.4 to 8.9 ms for both 4.5-ft-diameter vessels and from ∿0.3 to 4.8 ms in the 3.0-ft-diameter vessel. The time of occurrence of the maximum strain generally, but not without many exceptions, moves toward shorter times as the charge size increases. The time for maximum strain occurrences appears to be uncorrelated from gage to gage on the same vessel. However, the time of occurrence of the maximum for each gage is quite reproducible with minor exceptions. This behavior seems consistent with the excitation of a multimode vibration in each vessel which is characteristic of that vessel (size and weight distribution), but not currently known in detail. As the excitation decays, the maxima are created at each gage when two or more vibration modes have in-phase maxima at the strain-gage location.

Figures 19 through 21 show the maximum strains recorded for Pentolite and Special Gelatin, 60% strength dynamite in both cylindrical- and suitcase-shaped charges.

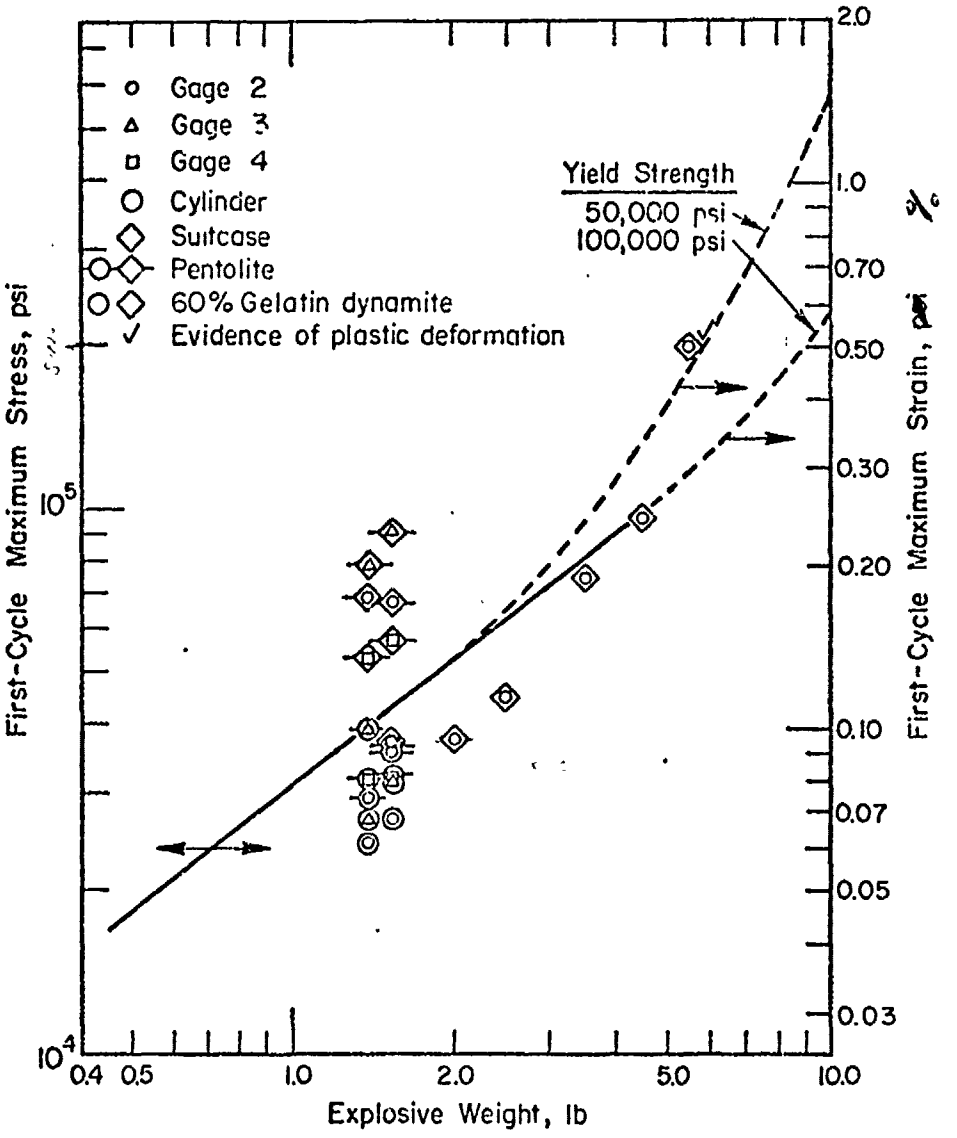

FIGURE 18. EFFECT OF CHARGE SHAPE AND COMPOSITION ON FIRST-CYCLE RESPONSE OF A 3.0-FT-DIAMETER SPHERICAL VESSEL

Average vessel wall thickness was 0.725 in.

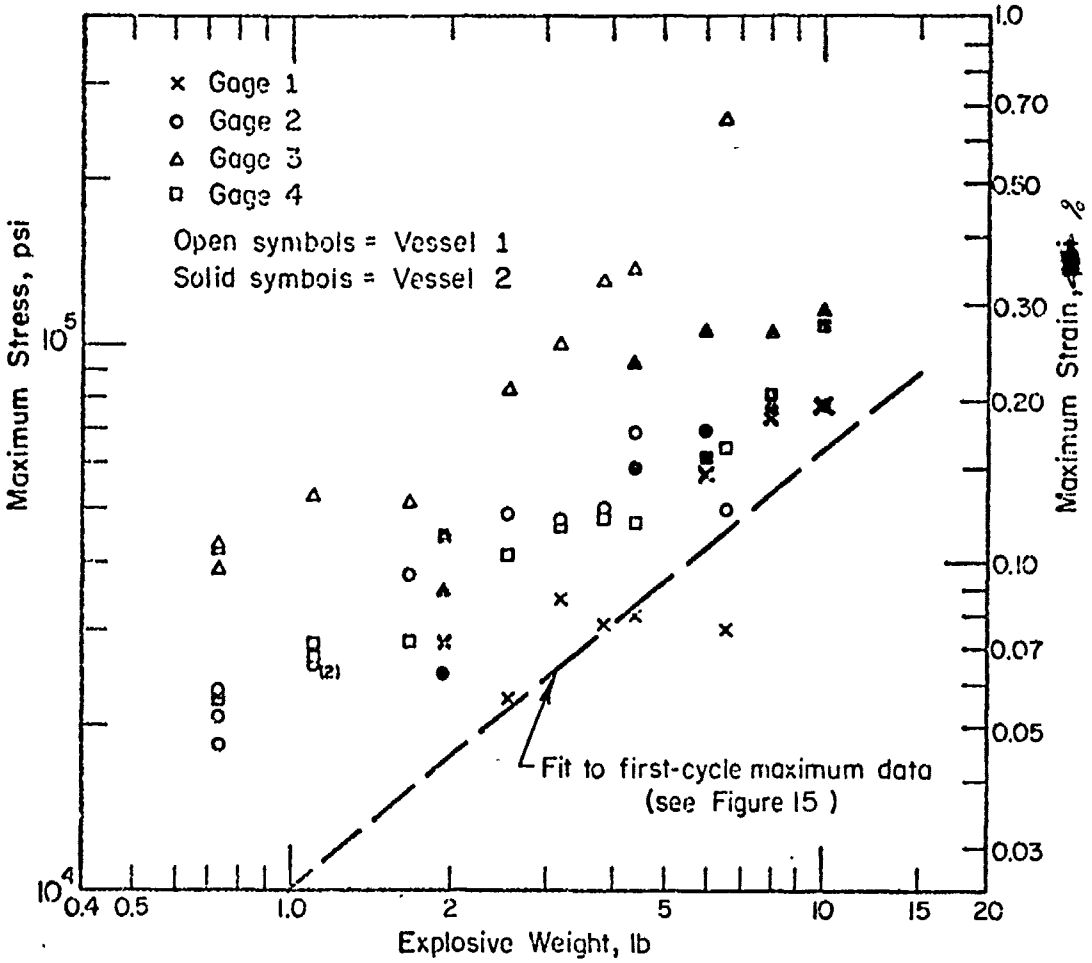

FIGURE 19. MAXIMUM STRAINS IN THE 4.5-FT-DIAMETER VESSELS FOR PENTOLITE CYLINDRICAL CHARGES

These maximum strains did not necessarily occur on the first cycle. Average vessel wall thickness was 1.0 in.

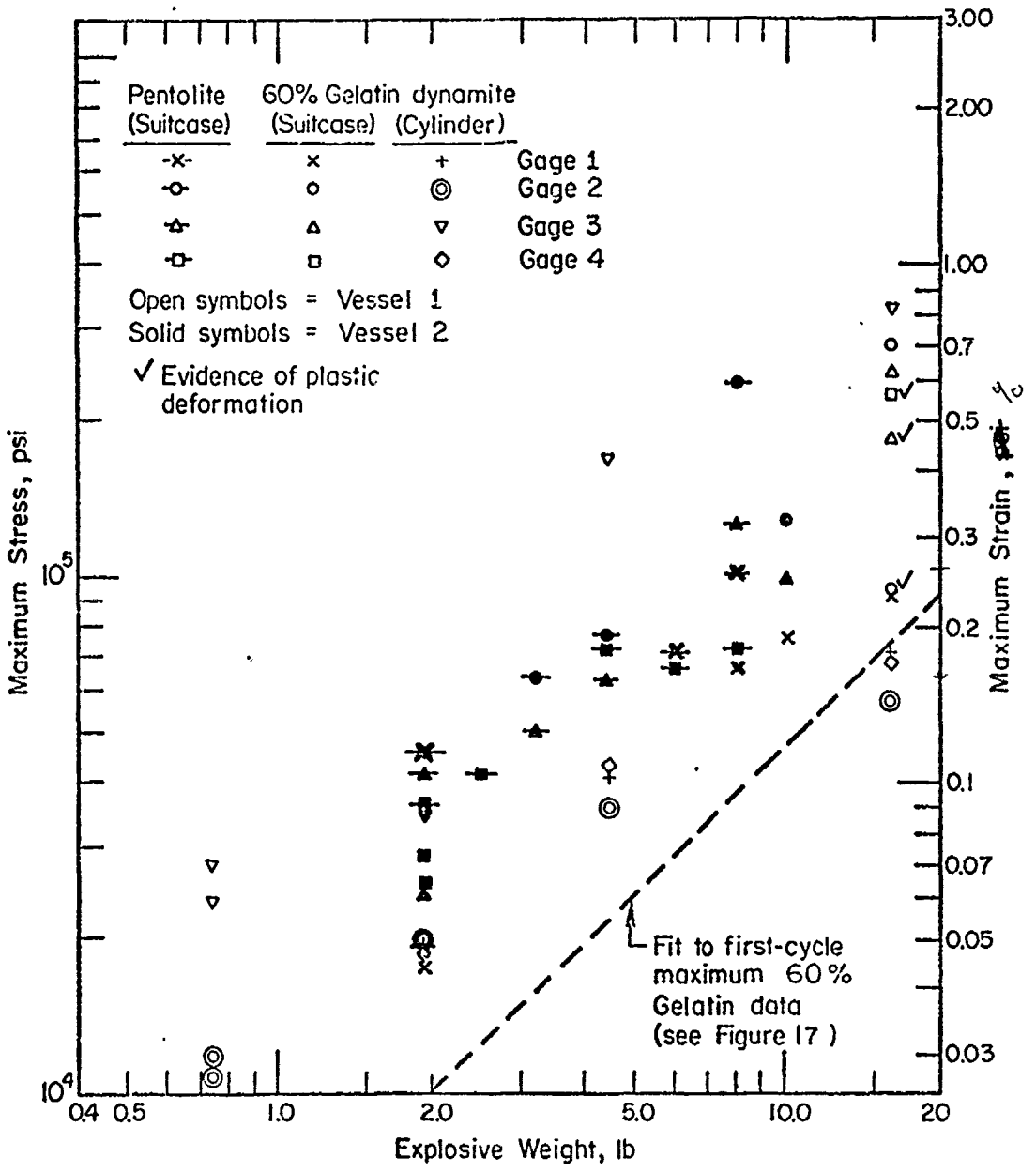

FIGURE 20. MAXIMUM STRAINS IN THE 4.5-FT-DIAMETER VESSELS FOR VARIOUS CHARGES

These maximum strains did not necessarily occur on the first cycle. Average vessel wall thickness was 1.0 in.

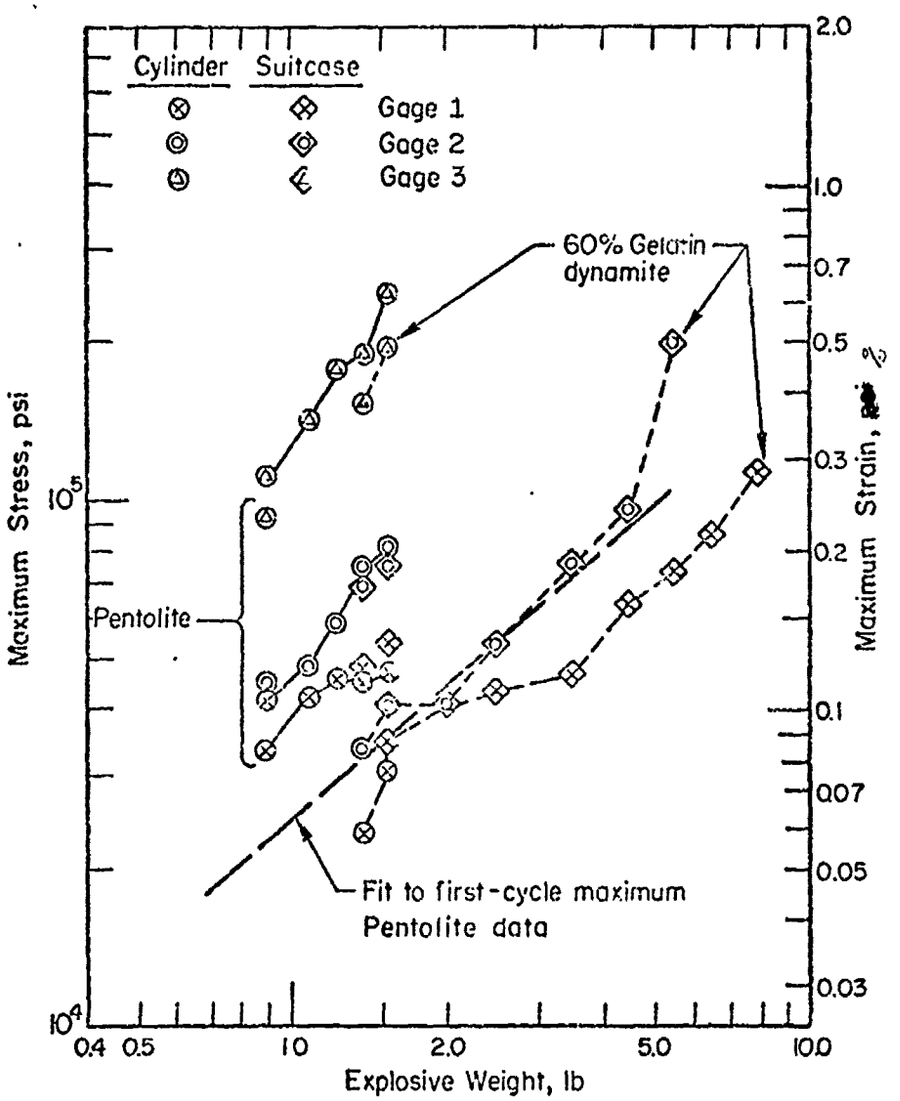

FIGURE 21. MAXIMUM STRAINS IN THE 3.0-FT-DIAMETER VESSEL FOR VARIOUS CHARGES

These maximum strains did not necessarily occur on the first cycle. Average vessel wall thickness was 0.725 in.

Figure 19 shows the maximum strains recorded by the various gages on the two 4.5-ft-diameter vessels tested, for Pentolite cylindrical charges. Figure 20 shows the same information for Pentolite suitcases and Special Gelatin dynamite cylinders and suitcases. On these figures the data from each of the two vessels have been identified because the response of Gage 3 is markedly different for the two vessels presumably because of their differing port designs and because Gages 1 and 4 were located at different points on the vessel surface. The data shown in Figures 19 and 20 were taken from the same set of shots used in plotting the first-cycle response shown in Figures 15 and 17, respectively. Also shown in Figures 19 and 20, for reference, are the lines fitted to the data shown in Figures 15 and 17, respectively.

The ratio of the overall maximum strain to the first-cycle maximum may be regarded as a magnification ratio. Examination of Figures 19 and 20 shows that the magnification ratio varies from about 1 to >4 for the various gage locations. It is significant that Gage 3, located directly opposite the port in each vessel, not only shows the largest magnification ratio for cylindrical charges but the largest change between vessels.* For Gage 3 the ratio is ≥4 on Vessel 1 and ∿2.5 on Vessel 2. There are two possible explanations for this difference in behavior. One is the obvious difference in the eccentric mass of the port and reinforcing ring in the two vessels. The other is the difference in charge orientation. In both vessels the cylindrical charges were hung with the cylinder axis vertical, which leads to the direction to Gage 3 being normal to the cylinder axis in one vessel and at ∿45 deg from the cylinder axis in the other.

In Figures 19 and 21, the peak strains as measured by the gages are plotted directly against the strain ordinate on the right of the figures. The stress scale shown on the left is for reference and is based on elastic strains in a spherical vessel. It is interesting to note that the maximum strains recorded exceed that required to produce 100,000-psi stress at between 3 and 4 lb of Pentolite in cylinders on Vessel 1, and near 1 lb on Vessel 3. The first small (60 to 100 με), residual plastic-strain increments were also found at these charge levels based on static strain-gage readings. Measurements of the fiducial marks, however, showed no measurable residual strain (±0.07 percent, or ±700 με) until after Shot 143, when two of ten fiducial lengths showed measurable strains under 0.2 percent. This information leads to the tentative conclusion that these maximum dynamic strains are exceeding the elastic limit of the material above the 3 to 4-lb charge levels in Vessel 1 and the 1-lb level in Vessel 3 but are not leading to plastic deformation detectable by static measurements because of their rapidly reversing and localized nature. It is believed that these strains are

---

*In Figure 20, for several sizes of suitcase charges, Gage 2 shows the largest maximum strains. Comparison of these points with the data for the first-cycle maxima shows that the Gage 2 magnification ranges from 1.64 at 1.95 Pentolite to 1.00 at 8 lb Pentolite, always less than for cylindrical charges.

real and can lead to low-cycle fatigue-type failures after a number of repeated shots at charge levels above about 3 lb of low-density Pentolite in the 4.5-ft-diameter vessel and 1 lb in the 3.0-ft vessel. Thus, caution should be exercised in the design of containment vessels intended for long-time use. In this context, "long-time use" cannot as yet be defined with precision, because no blast-containment-chamber fatigue-life data are known to exist.

Comparison of Explosive Strengths

Four different explosive compositions were fired in vessels in this program. In this section the data obtained to relate the effect of charge composition on the response of the vessels are presented.

Table 9 shows the strength of the two dynamites compared to the low-density Pentolite fired in this program. Explosive charges having the same weight and shape, fired in the same vessel are compared on the basis of maximum first-cycle responses. For each charge weight, and vessel size a scaled distance was calculated to allow comparison between vessel sizes.

Figure 22 shows the Special Gelatin/Pentolite comparison as a function of scaled distance. The Gelex-1 data are quite similar, as shown in Table 9. It is noted that the ratio of maximum first-cycle stresses appears to be a function of scaled distance, not simply charge size. The reason for this behavior is not currently understood but may be related to the nonideal detonation characteristics of the dynamite.

A total of four shots were fired using 3FA black powder in 3-ft Vessel 3. The shots are described in Table 10. No meaningful dynamic strains were recorded by the strain gages, possibly because the oscilloscope recording period was only 10 ms long and triggered by the pulser firing the initiator. The shots produced no measurable strain in the vessel, and sounded very quiet in comparison to other shots. The containers were fragmented in a fashion typical of black-powder explosions, and produced no dents or craters in the inside walls of the vessel. It is expected that relatively large charges of black powder of this type would be required to cause damage to vessels of the type developed in this program.

Effect of Charge Shape

Table 11 shows the results of comparing several pairs of charges of the same weight and composition of which one member of the pair was a suitcase-shaped charge and the other was a cylindrical-shaped charge. For each explosive weight a scaled distance was calculated for the purpose of comparing all results on a common coordinate system.

TABLE 9. COMPARISON OF STRENGTHS OF SPECIAL GELATIN AND GELEX-1 DYNAMITES AND PENTOLITE

Vessel No.	Diameter, 2R, ft	Charge Weight, W, lb	Charge Shape	Scaled Distance, $R/W^{1/3}$ ft/lb$^{1/3}$	First-Cycle Maximum Stress, σ, psi				Ratio: $\frac{\sigma_{Gelatin}}{\sigma_{Pentolite}}$		Ratio: $\frac{\sigma_{Gelex}}{\sigma_{Pentolite}}$		Data Source, Shot Nos.		
					Gage No.	Pentolite	Special Gelatin, 60% Strength Dynamite	Gelex-1, 60% Strength Dynamite	Indiv. Gage	Avg.	Indiv. Gage	Avg.	Pentolite	Spec. Gelatin	Gelex
1	4.5	0.73	C	2.499	2	7,780	3,570	4,760	0.459	.433	0.612	.577	122	127	129
					3	7,690	3,490	5,550	0.454		0.722		123	128	
					4	9,760	3,770	3,890	0.386		0.398		124		
													126		
1	4.5	4.40	C	1.373	2	30,160	21,190	26,190	0.703	.774	0.658	.834	137	138	139
					3	34,290	26,670	--	0.778		--				
					4	28,250	23,810	22,619	0.843		0.800				
2	4.5	1.95	C	1.801	1	27,660	12,740		0.461	.488			219	220	
					2	14,880	7,750		0.521						
					3	20,950	10,120		0.483						
					Ring[a]	14,160	19,270		0.654						
3	3.0	1.38	C	1.347	2	29,550	24,400	22,200	0.826	.756	0.751	.689	305	308	309
					3	39,300	27,000	26,200	0.687		0.667				
					4	31,700	--	20,600			0.650				
3	3.0	1.535	C	1.300	2	35,700	27,000	25,100	0.756	.808	0.703	.734	306	310	313
					3	36,500	31,400	29,500	0.860		0.808				
					4	32,100	--	22,200			0.691				
2	4.5	1.95	S	1.801	1	28,970	16,710		0.577	.569			222	221	
					3	28,450	15,990		0.562						
					Ring[a]	13,660	6,960		0.509						
3	3.0	1.535	S	1.300	2	67,300	37,430		0.556	.556			312	318	

(a) Gage 4 installed on reinforcing ring. Stresses for the ring were calculated from $\sigma_{ring} = E\varepsilon_{ring}$, where $E = 3 \times 10^7$ psi (Young's modulus).

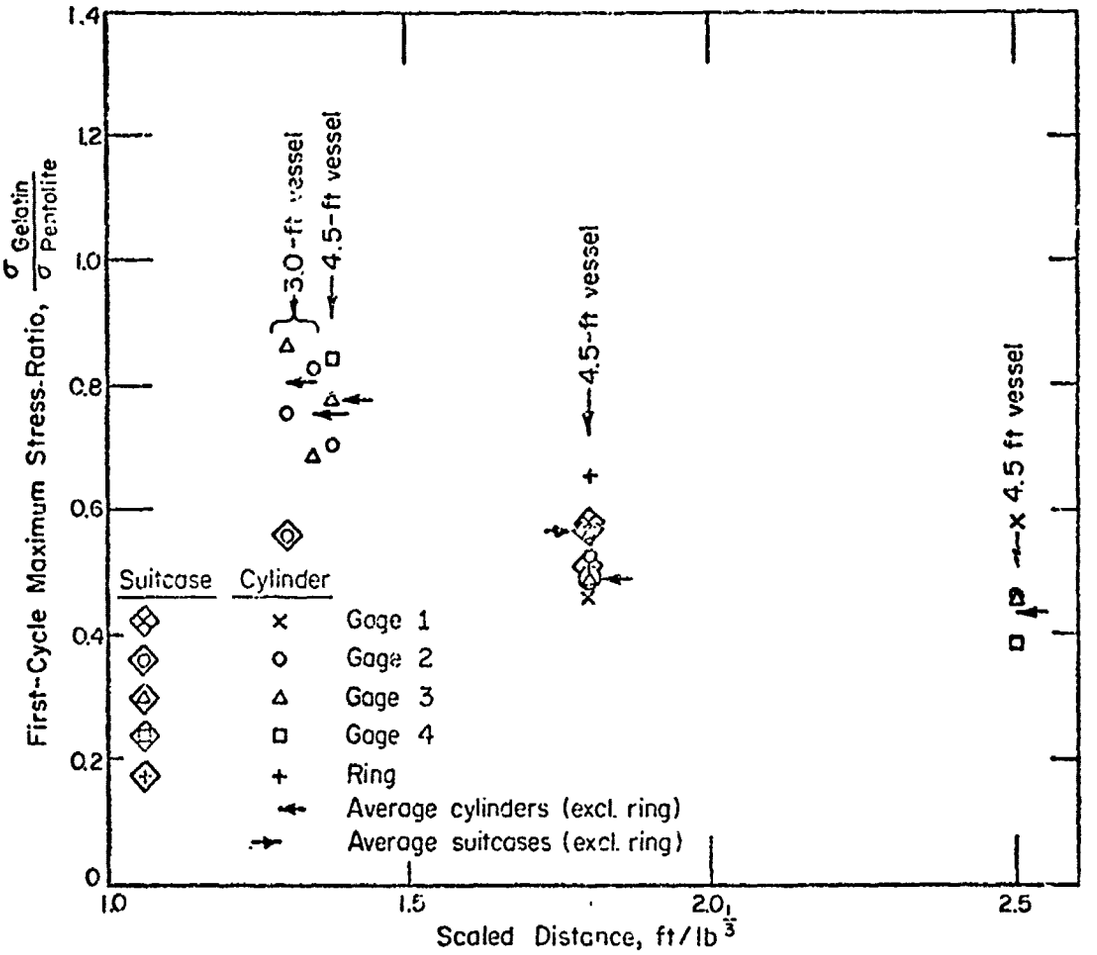

FIGURE 22. EFFECT OF CHARGE COMPOSITION ON FIRST-CYCLE VESSEL RESPONSE

TABLE 10. DESCRIPTION OF BLACK POWDER SHOTS FIRED IN 3.0-FT VESSEL

Shot No.	Black Powder Weight, lb	Container	Initiation
314	1.0	1-pint glass jar	Detonato with Detasheet[a] booster
315	0.95	1-5/8-in.-ID by 11-3/4 in.-long pipe section with steel end caps screwed on	Squib
316	2.4	1-liter round chemical flask	Squib
317	3.7	4-1/2-in. ID by 6-in.-long pipe section with 1/4-in.-thick steel plates welded on ends	Squib

(a) 5/8-in. diameter by 1/8-in. thick.

TABLE 11. COMPARISON OF EFFECT OF CYLINDER- AND SUITCASE-SHAPED CHARGES ON VESSEL RESPONSE

Vessel No.	Diameter, 2R, ft	Charge Weight, W, lb	Explosive[a]	Scaled Distance, $R/W^{1/3}$, ft/lb$^{1/3}$	Gage No.	First-Cycle Maximum Stress, σ, psi: Cylinder Shape	First-Cycle Maximum Stress, σ, psi: Suitcase Shape	Ratio $\frac{\sigma_{suitcase}}{\sigma_{cylinder}}$: Indiv. Gage	Ratio $\frac{\sigma_{suitcase}}{\sigma_{cylinder}}$: Average	Data Source, Shot Nos.: Cylinder	Data Source, Shot Nos.: Suitcase
1	4.5	16.0	Gn	0.893	2	57,400	187,150	3.260		141	142/143
					3	88,000	214,000[b]	2.432	2.991		
					4	68,300	224,000[b]	3.280			
2	4.5	1.95	Gn	1.801	1	12,740	16,700	1.312		220	221
					2	7,750	11,300	1.469	1.453		
					3	10,120	15,990	1.579			
					Ring[c]	9,270	6,960	1.332			
2	4.5	1.95	P	1.801	1	27,660	28,970	1.047			
					3	20,950	2o,450	1.358	1.202	219	222
					Ring[c]	14,160	13,620	0.966			
2	4.5	4.4	P	1.373	2	26,115	68,300	2 615			
					3	40,140	59,100	1.472	2.044	215/231	211
2	4.5	6.0	P	1.238	1	44,440	69,100	1.556			
					4	39,700	56,400	1.421	1.488	216	212
3	3.0	1.38	P	1.347	2	29,550	68,800	2.32		305	307
					3	39,300	78,500	1.997	1.999		
					4	31,700	53,300	1.681			
3	3.0	1.535	P	1.300	2	35,700	67,300	1.885			
					3	36,500	70,400	2.477	2.047	306	312
					4	32,100	57,100	1.779			

(a) Gn = DuPonc Special Gelatin, 60% Strength dynamite.
P = 50/50 Pentolite, loose granular.

(b) Shot 142 only.

(c) Gage 4 installed on reinforcing ring. Stresses for the ring were calculated from $\sigma_{ring} = E\varepsilon_{ring}$ where $E = 3 \times 10^7$ psi (Young's modulus).

Figure 23 shows the ratios from Table 11 plotted against scaled distance. The data show a great deal of scatter which is difficult to account for, but nevertheless a trend seems to be present toward the suitcase-shaped charge becoming relatively more effective as the scaled distance decreases (or charge size increases for a given vessel). This effect is easily understood for the Gage 2 position, opposite the largest flat face of the vessel but not so easily understood on the average.

The plastic-deformation results to be described later help to support and explain the large average dynamic gage response for suitcase-shaped charges oriented as in this program. Not only are localized plastic strains produced opposite the major flat faces of the charge, but the gneral deformation of the vessel in the plane normal to the longest charge axis face exceeds the deformation in the other two orthogonal planes of the vessel. The strain gages were located in the plane of largest deformation and, hence, their average response tends toward measurement of the average deformation in the plane of largest deformation not toward the average deformation of the entire vessel.

As understood in this way, the large relative effectiveness of suitcase-shaped charges to cylindrical (or spherical) charges, as shown in Figure 23, is probably valid data from the standpoint of containment-chamber design since the local maximum chamber distortion will control the ultimate chamber failure in the absence of manufacturing flaws.

Plastic Deformation

Plastic deformation of the vessels is indicated in three ways experimentally. The most reliable is the occurrence of plastic straining of the vessel as indicated by an increase of the measured dimensions between fiducial marks placed on the outer surface of the vessel. Other indications are a zero shift indicated by the static strain indicator used on some gages and shifts in the base line of oscillation observed on the oscillographs. The latter two effects have generally been small in magnitude but are consistent with the overall intrepretation.

In order to obtain evidence of plastic flow, charges of Special Gelatin, 60% Strength dynamite in suitcase geometry weighing 2, 2.5, 3.5, and 4.5 lb were fired in the 3-ft-diameter vessel. It was expected that 4.5 lb would produce significant plastic deformation of the vessel because the extrapolated first-cycle maximum stresses would exceed the ultimate static strength of the vessel. However, no plastic deformation, other than continued bulging of the door was noted. Consequently, similar charges weighing 5.5, 6.5, 8, and 10 lb were fired. Following the 10-lb

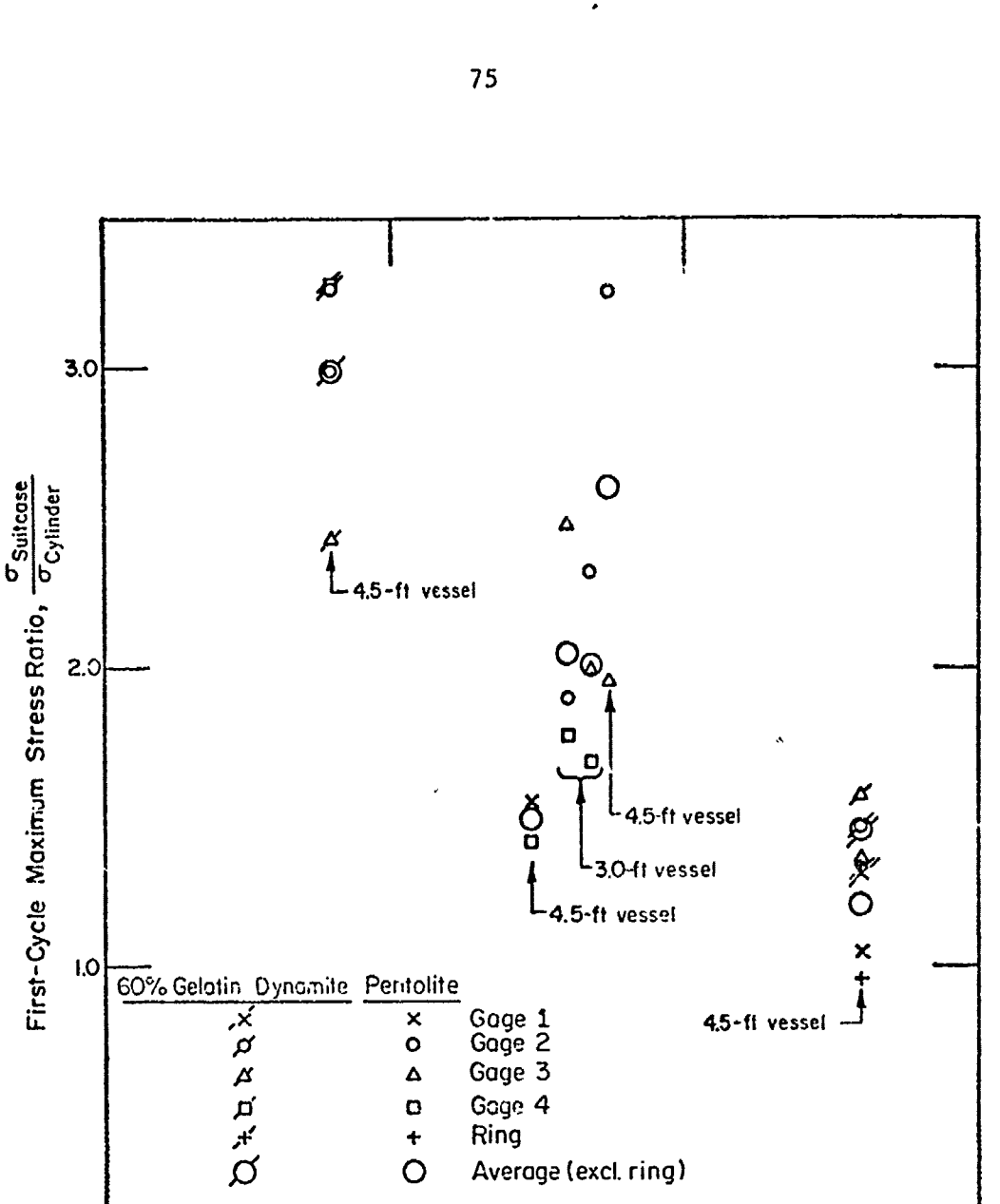

FIGURE 23. EFFECT OF CHARGE SHAPE ON FIRST-CYCLE VESSEL RESPONSE

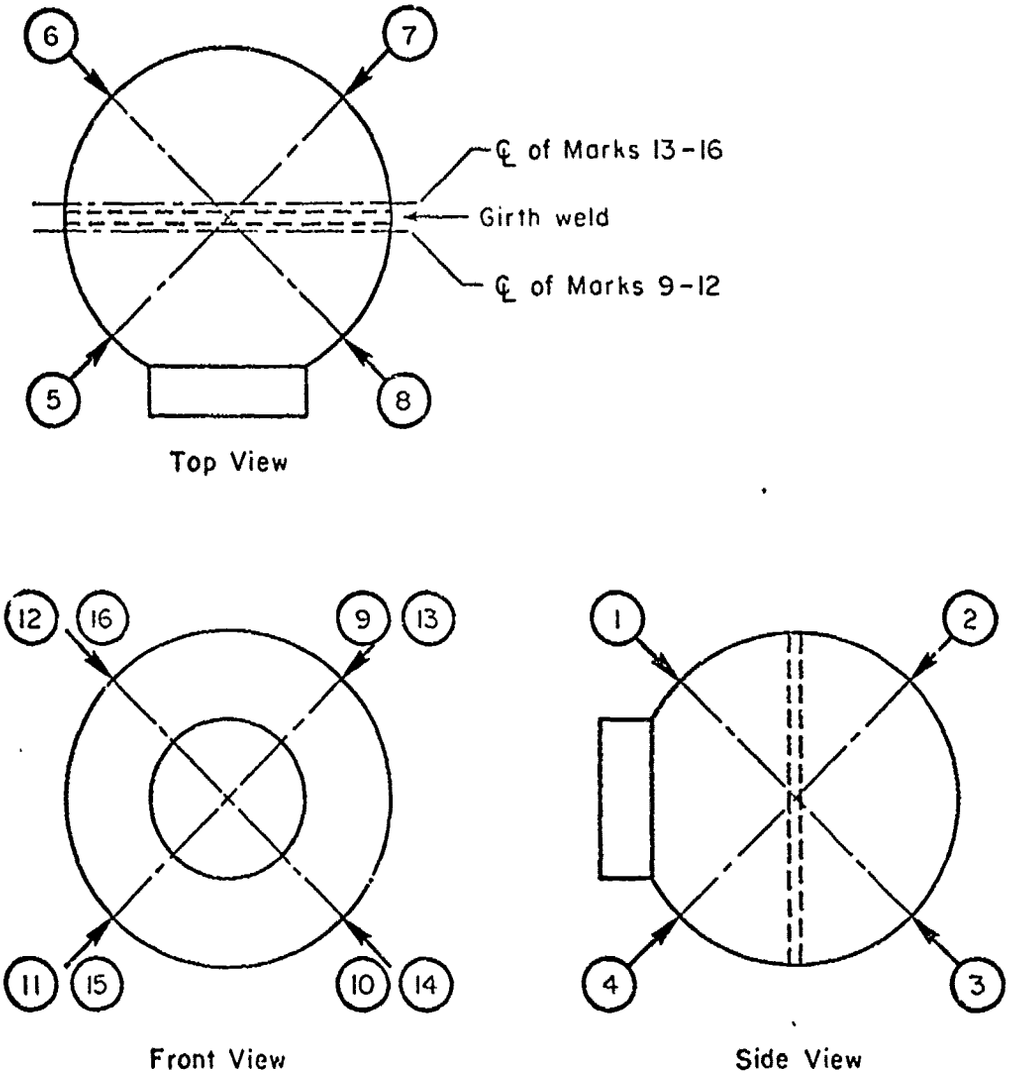

FIGURE 24. SCHEMATIC LOCATIONS OF FIDUCIAL MARKS USED TO MONITOR PLASTIC STRAIN OF VESSELS 1, 2, and 3

shot, a second 8-lb charge was fired to determine if work-hardening effects were present. Finally, a 12-lb charge was fired in the vessel, after which the maximum plastic strain had increased to 2.74 percent, and testing on this vessel was terminated. Plastic deformation of Vessel 3, between a set of fiducial marks placed on the vessel, did not begin until the charge weighing 6.5 lb was fired.

Figure 24 shows schematically the locations of the fiducial marks scribed on the surface of each vessel to follow its plastic deformation. The circled numbers in this figure are the numbers assigned to each fiducial mark. Measurements were taken between adjacent marks, as shown in each of the three views.

Figure 25 shows the total plastic strain recorded between several representative pairs of fiducial marks on the 3.0-ft vessel. The small residual strains shown for the smaller charge weights are probably the result of using a different steel tape to record the original dimensions of the vessel, than that used for the measurements shown on this figure. The accuracy of these measurements is expected to be about ±1/64 in. over the usual ∿29-5/8-in. measuring distance or about ±0.053 percent as shown on the figure. Note that the strain between marks 6 and 7 is decreasing for the higher explosive loadings. As shown in Figure 24, this strain is located transverse to the direction of the maximum strain records between Marks 2 and 3.

Figure 26 further shows the anisotropic nature of the final strain produced in this chamber. Also shown in Figure 26 in the side-view sketch is the orientation of the suitcase charges. The charge dimensions were scaled in the proportion 1X, 2X, 3X. They were oriented so that the 1X and 2X dimensions are shown in the side view sketch of Figure 26, with the 3X dimension extending out of the paper in this view. The charges were oriented in this fashion so that the normal to the largest flat face of the charges pointed directly at Gage 2 as shown in Figure 7. Note that the largest residual strains all lie in the plane of the paper for the right side view of the ball as shown in Figure 26.

Figure 27 shows two views of the 3.0-ft vessel, taken at the conclusion of testing of this vessel. The side view (Figure 27a) illustrates the method of support of the vessel during testing and the upper bulge. Distortion is most pronounced at about 10:30 hr as a reasonably localized bulge. This is adjacent to the largest flat face of the suitcase shaped charges fired in this vessel. Note also the distortion of the reinforcement sleeve where it attaches to the vessel visible along the top of the sleeve. The reinforcement sleeve was, of course, originally a straight section of round tubing.

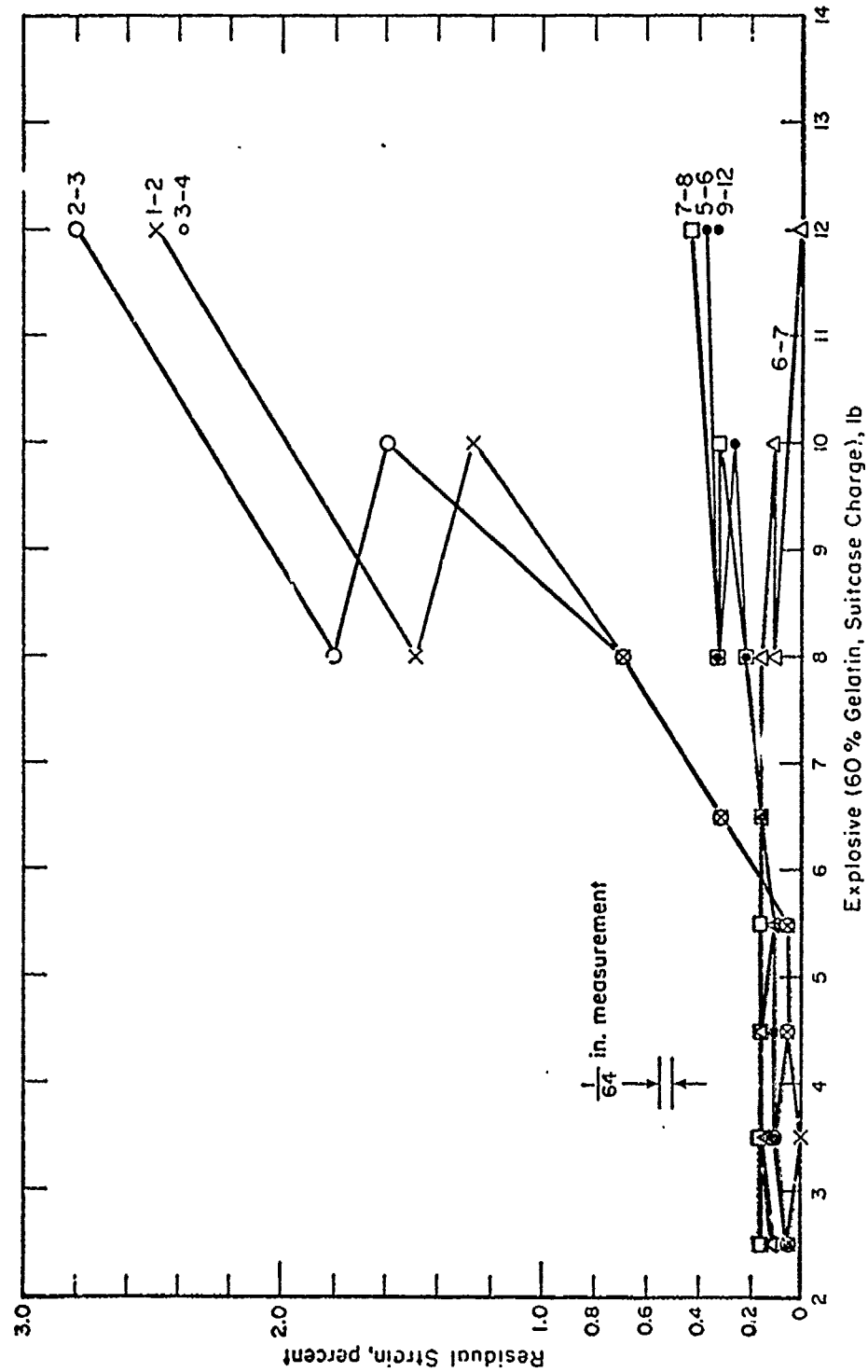

FIGURE 25. TOTAL RESIDUAL STRAIN MEASURED AFTER FIRING THE CHARGE WEIGHTS SHOWN IN THE 3.0-FT-DIAMETER SPHERICAL VESSEL

The number pairs shown on the curves refer to measurements between the fiducial marks located as shown in Figure 12.

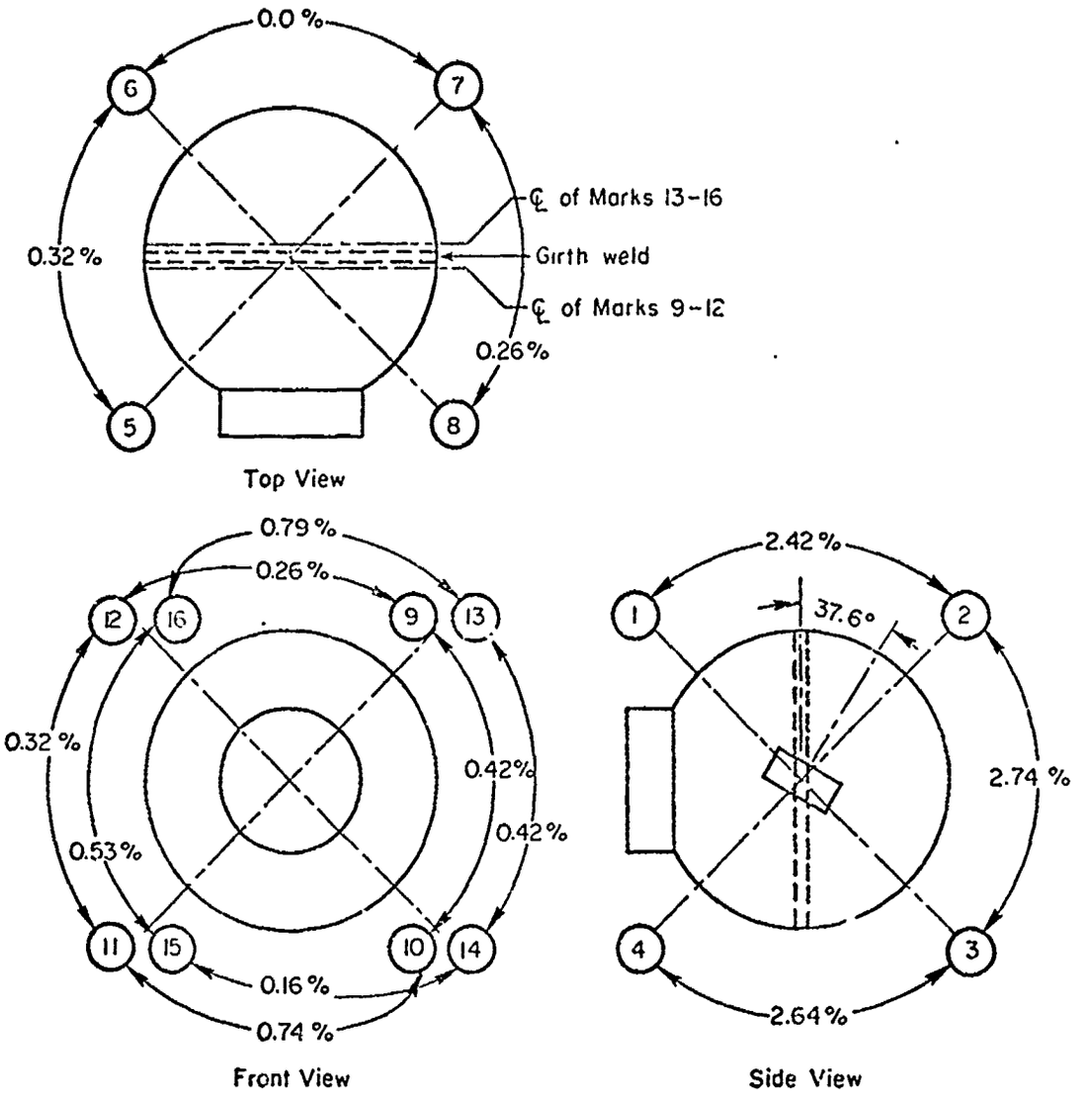

FIGURE 26. SCHEMATIC LOCATIONS OF THE TOTAL RESIDUAL STRAIN RECORDED FOR THE 3-FT VESSEL AFTER FIRING 120 LB OF SPECIAL GELATIN, 60% STRENGTH DYNAMITE

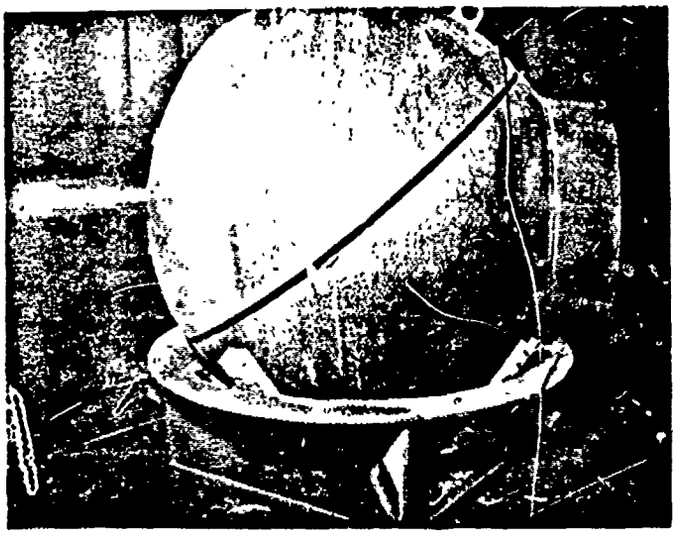

a. Side View of Vessel

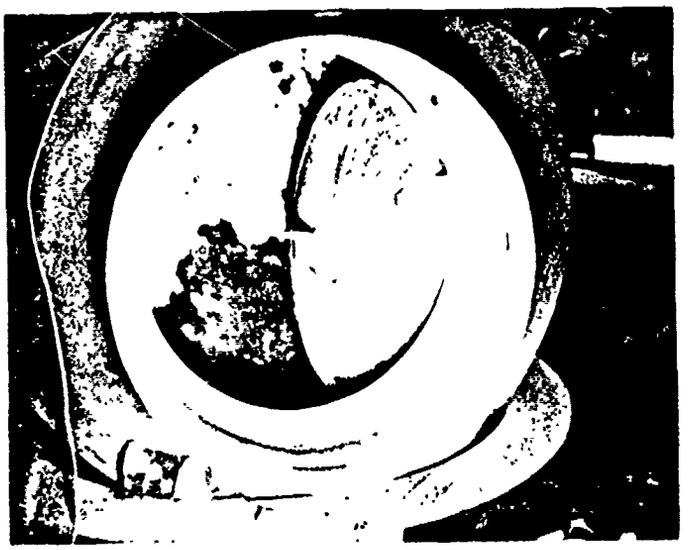

b. View of Vessel Looking Into Port

FIGURE 27. 3.0-FT VESSEL AT CONCLUSION OF TESTING

Note localized bulge at 10:30 hr (Photograph a), and the rounded curvature of the door which was originally flat (Photograph b).

Figure 27b shows a view of the vessel looking into the port. Note the smoothly rounded curvature of the partially open door, which was originally flat. When this photo was taken, the door was supported by only the upper hinge strap. The lower hinge strap broke during the 5.5-lb Shot No. 323. This view further illustrates the reinforcing sleeve distortion. The vertical diameter of the port has become ∿1 in. greater than the horizontal diameter. In addition to the stretch of the reinforcing sleeve along the circle of attachment to the vessel, the portion of the sleeve extending into the vessel has actually been reduced in diameter by the external blast loading on this part of the sleeve.

The localized bulges on the chamber corresponding to the normals from the largest flat faces of the charge show that the primary source of plastic strain in the vessel results from the reflection of, and resultant momentum transfer from, the primary shock wave generated by the expanding cloud of detonation products which are known[9] to possess such anisotropic properties, rather than the accumulated internal gas pressure, or multiple shock reflections within the vessel. This result, together with the available analysis, suggests that there exists a range of charge sizes which will produce significant plastic deformation of a containment vessel whether it is completely enclosed or has a substantial sized open port.

Of further significance is the finding in this test series that the safely containable weight of explosive charge has been demonstrated to be at least twice that which first causes measurable plastic deformation.

Plastic deformation of 4.5-ft-diameter Vessels 1 and 2 was minimal. The same set of fiducial marks was scribed on these two vessels as shown in Figure 24 for the 3-ft vessel. Vessel 1 showed no measurable change in size until after Shot 142, the first 16-lb Special Gelatin, 60% strength dynamite suitcase-shaped charge when only the distance between Marks 2-3 showed a measurable change of 3/32 in. or 0.20 percent. Shot 143, the second 16-lb Special Gelatin dynamite suitcase-shaped charge blew the reinforcing sleeve from the vessel. Post-shot measurements of the vessel could not be made on distances 2-3 and 6-7 because of the formation of a dent in this location where the vessel recoiled against the blast chamber wall. Of the remaining distances, only two showed measurable changes. These were 1-2, 3/32 in. or 0.21 percent and 3-4, 7/64 in. or 0.27 percent. Measurements of the static strain in this vessel by the strain-gage instrumentation first showed a small residual strain of 62 x 10^{-6} in./in. on Gage 3 after Shot 135, a 3.2-lb Pentolite cylinder shot. After Shot 137, a 4.4-lb Pentolite cylinder, this strain had increased to only 131 x 10^{-6} in./in. After Shot 142, the first 16-lb Special Gelatin Dynamite suitcase charge, the strains on Gages 1 and 4 had increased to 417 and 1834 x 10^{-6} in./in., respectively. These data are in agreement with the fiducial-mark measurements within experimental error.

The results of residual static strain measurements on Vessel 2 are quite similar to those of Vessel 1. The first small residual strains were recorded for Shot 210, a 3.2-lb Pentolite suitcase. They were 36 and 13 x 10^{-6} in./in. for Gages 2 and 3, respectively. Successive shots, as shown in Table 6, produced small ($<10^{-4}$ in./in.) strains up to Shot 214, a 10.0-lb Special Gelatin suitcase. This shot produced strain increments of 532 and 68 x 10^{-6} in./in. on Gages 2 and 3, respectively. Small strain increments per shot continued through Shot 216 when the total accumulated residual strains reached 672 and 469 x 10^{-6} in./in. on Gages 2 and 3, respectively. No futher data on this vessel is available.

Two-foot-diameter Vessels 3a-6a were tested with large spherical C-4 charges to determine the failure limits for this vessel design and material. A total of six shots were fired in the four vessels.

Figure 28 shows the fiducial mark layout used on these vessels. The marks consisted of fine-pointed punch marks. The distances between adjacent marks on the vessel skin were measured with a pointed vernier caliper. Hence the actual measurements were of chord distances between marks. For uniform strain in the vessel, percent changes in chord measurements are numerically equal to percent strain in the vessel surface. For nonuniform strains, the changes in chord lengths may differ from the actual vessel surface strains. No provision for this possible difference has been made nor is readily possible in the absence of additional data.

Table 12 shows the residual strain distribution in the surviving vessels after the labeled shots. Shot 402, 7 lb of C-4, in Vessel 5a produced catastrophic rupture of the vessel. Shot 406, a second 6-lb C-4 charge in Vessel 4a produced catastrophic failure of this vessel. Thus, the results of these tests show that for this vessel design the single-shot catastrophic failure limit lay between 6.5 and 7.0 lb of C-4 and, further, that the two-shot catastrophic failure limit lays between 5.0 and 6.0 lb of C-4 in the vessels tested.

Figure 29 shows the method of charge support and relative size of vessel to charge for the 6.0-lb Shot 403 in Vessel 4a.

Figure 30 shows the appearance of Vessel 5a after firing the 7.0-lb Shot 402. The vessel skin separated into four major pieces. Examination showed, by the appearance of shear lines and the accumulation of soot on the fracture surface, that the fracture of this vessel originated in two separate locations before either crack had time to run very far. The locations of the crack origins are indicated by arrowpoints on the figure. The upper origin was along the edge of the doubler plate installed to reinforce the main support pin and adjusting bolts. The lower origin was at the corner of a caster attachment farthest from the port.

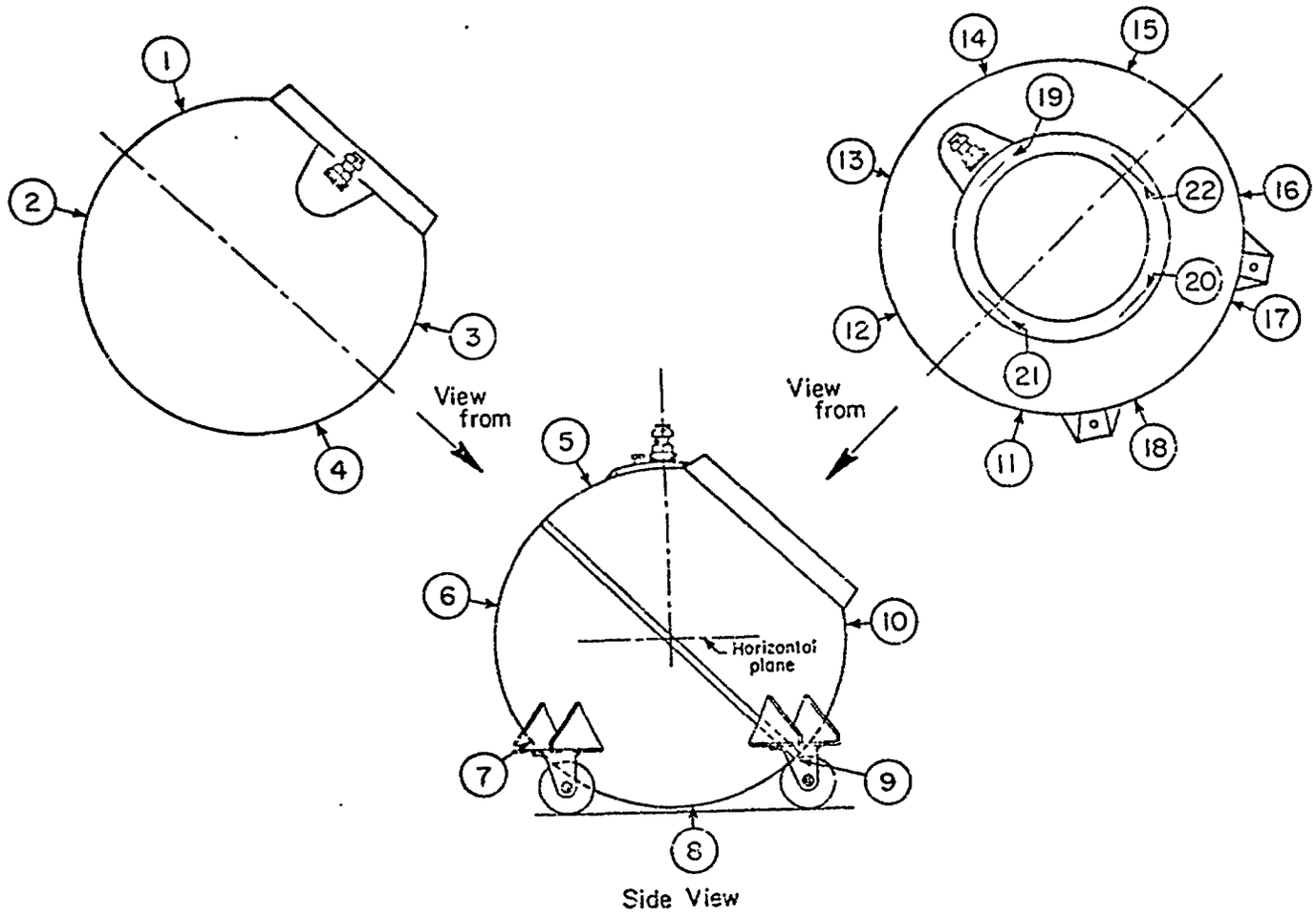

FIGURE 28. FIDUCIAL MARK LAYOUT USED ON 2.0-FT VESSELS 3a THROUGH 6a

TABLE 12. RESIDUAL STRAINS IN 2-FT-DIAMETER VESSELS

Fiducial Mark Pair	Strain in Vessel Indicated, percent				
	Vessel 3a			Vessel 4a	Vessel 6a
	Shot 401 (5 lb)	Shot 404 (5 lb)	Total Shots 401-404	Shot 403 (6 lb)	Shot 405 (6.5 lb)
Vessel Surface[a]					
1-2	2.1	1.2	3.3	3.4	4.0
3-4	1.9	1.6	3.4	3.2	3.6
5-6	2.9	1.7	4.6	3.4	3.9
6-7	3.5	2.2	5.7	4.8	6.2
7-8	4.9	3.1	8.1	6.1	7.5
8-9	4.1	2.3	6.5	5.3	6.1
9-10	3.2	0.9	4.0	3.7	3.8
11-12	2.8	1.6	4.4	3.7	4.7
12-13	3.2	1.9	5.1	4.0	4.7
13-14	3.7	1.7	5.4	3.6	5.5
14-15	3.1	1.6	4.7	3.7	5.0
15-16	2.5	1.5	4.0	4.3	4.8
17-18	2.6	1.3	3.9	3.1	4.4
Average	3.11	1.73	4.84	4.03	4.86
Reinforcing Ring[b]					
19-20	0.49	1.00	1.49	0.93	0.71
21-22	0.30	0.90	1.20	1.12	0.60
Average	0.39	0.95	1.35	1.03	0.66

(a) Nominal gage length = 10 in.

(b) Nominal gage length = 13.3 in.

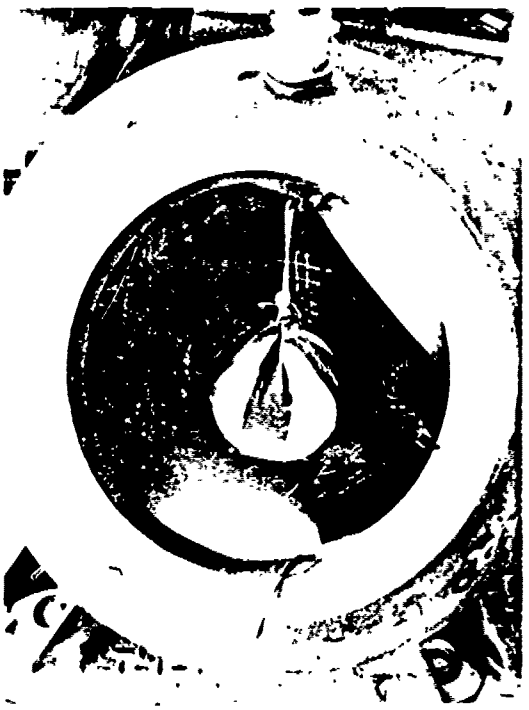

FIGURE 29. VIEW LOOKING INTO VESSEL 4a SHOWING 6-LB SHOT 403

FIGURE 30. VESSEL 5a AFTER FIRING 7.0-LB SHOT 402

Arrows indicate the location of crack origins.

Figure 31 shows the appearance of Vessel 4a after firing the second 6.0-lb C-4 shot in this vessel. The vessel skin separated into three major pieces. Both photos (a and b) show arrows pointing to the single fracture origin. Figure 31b shows a close-up of the crack origin at the corner of a caster farthest from the port. This fracture origin is at the same relative location and has the same appearance as the lower fracture origin point of Vessel 5a.

An ultrasonic thickness survey[10] on another vessel from the same manufacturing lot showed that the thinnest portion of the vessel is near this location. In the surveyed vessel, wall thicknesses varied from 0.532 to 0.569 in. adjacent to the weld, to 0.494 in. at center fo the hemisphere, with the thinnest region near the location of the casters most distant from the port. At four measurement locations around the center of the hemisphere this thinnest region varied from 0.444 to 0.476 in. in thickness. The average thickness of the surveyed vessel was 0.514 in. based on the assumption of circular symmetry of wall thickness for each hemisphere. Thus, for the surveyed vessel, wall thickness variations of +10.7, -13.6 percent from the average were observed. It is not known whether variations of this type are typical of these vessels, but there is no evidence at present to the contrary. Hence, it appears likely that an origin of fracture for both vessels which failed catastrophically was located in the thinnest portion of the vessels, and that the welded attachment of the caster-wheel supports played a role in the fracture initiation.

Figure 32 shows a plot of the residual plastic strain data for Vessels 3a-6a. The data points show the average vessel skin residual strains. The error bars show the maximum and minimum residual strains recorded for each shot. The curves shown on the figure are computed residual strains for Pentolite shock-wave parameters and a Composition C-4 mock-up for the confined explosion gas pressure for the assumed wall thickness and yield strengths shown. In these calculations the work-hardening coefficient was held constant at 80,000 psi. However, for these relatively small strains, the results are insensitive to the value chosen for the work-hardening coefficient. The three solid curves show the variation in predicted performance for the three values of yield strength shown, for the estimated average wall thickness of the vessels. The dashed curve shows the predicted performance for the estimated minimum wall thickness of the vessels. It appears that the 80,000-psi yield strength model describes the observed performance of these vessels reasonably well. Thus, it appears that there is a strong strain-rate effect on the mechanical properties of the steel vessel material even in the face of uncertainties in the true blast-wave parameters for Composition C-4 explosive compared to those of the Pentolite data used in the calculations. (Lacking detailed information, there is reason to expect these two explosives to be very similar in this respect[4].)

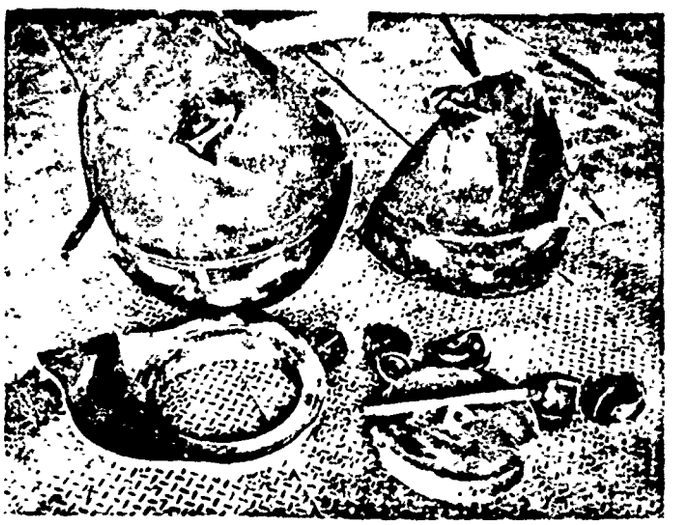

a. Overall View

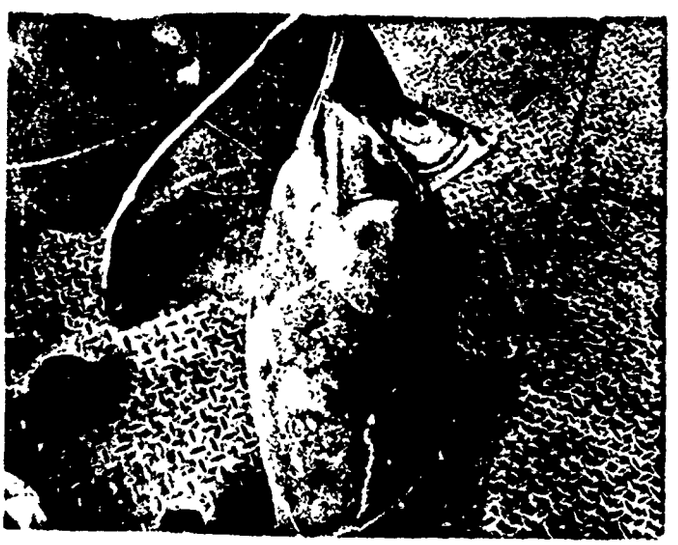

b. Close-up of Origin of Crack

FIGURE 31. VESSEL 4a AFTER FIRING SECOND 6.0-LB C-4 SHOT

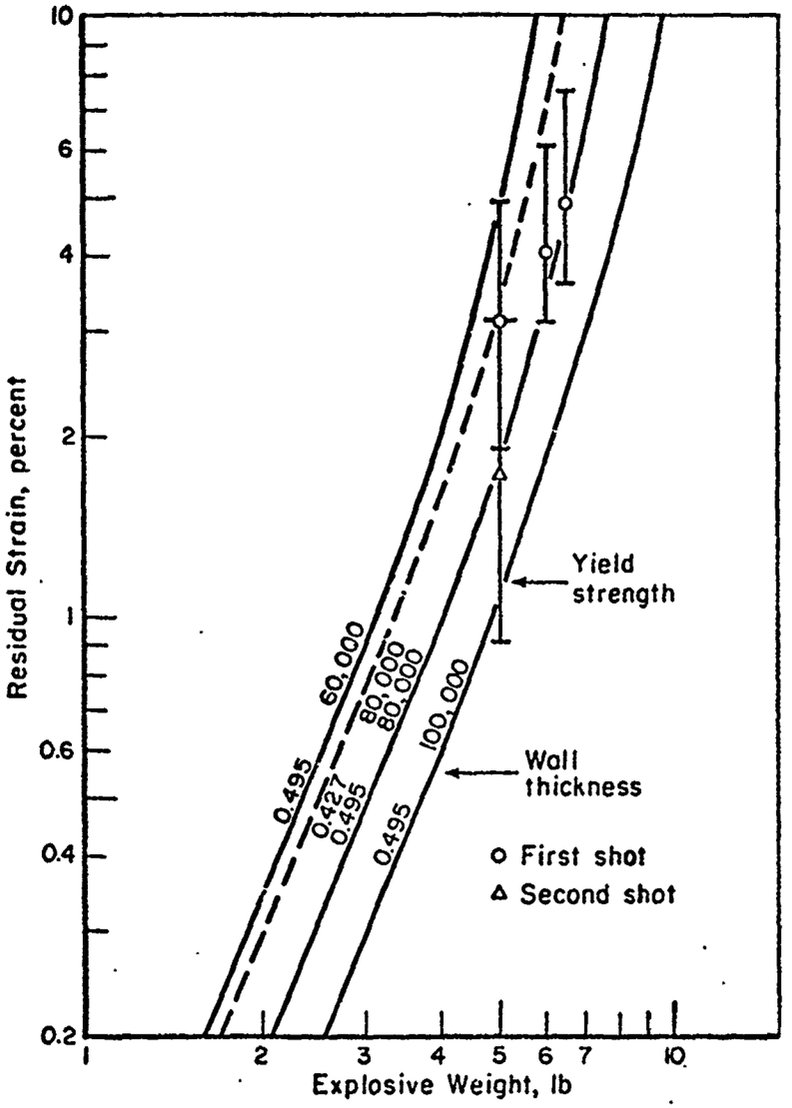

FIGURE 32. RESIDUAL PLASTIC STRAIN IN 2.0-FT-DIAMETER VESSELS 3a-6a

Estimated average wall thickness was 0.495 in.

With the agreement demonstrated between residual plastic strain and calculations, one must question why the catastrophic failure of the vessel occurred at a predicted residual strain of ∿6.5 percent for the 80,000-psi yield model. The Battelle-developed computer code includes subroutines for the calculations of the confined explosion gas pressure (CEGP)* as developed by J. F. Proctor.[4] Composition C-4 was mocked-up in this program by a mixture of 91.0 percent RDX and 9.0 percent wax. Calculations of the CEGP for this mixture suggest that the Composition C-4 CEGP is about 12 percent higher than that for Pentolite. The calculations show that the static stress produced by the CEGP in a 2.0-ft-diameter, 0.427-in.-thick wall spherical vessel is 74,000 psi for a 6.5-lb C-4 charge and 76,800 psi for a 7.0-lb C-4 charge. These calculated stresses bracket the ultimate strength of 75,300 psi given in the test certificate for this lot of hemispheres supplied by the manufacturer. In view of the approximations made in the calculations, and uncertainties in the true minimum wall thickness, the agreement in bracketing the ultimate strength of the material by calculated static stresses from explosive loads which bracket the ultimate failure of a vessel is probably fortuitous. This result does suggest, however, that the CEGP plays an important part in the ultimate single-shot failure of these vessels and, further, that the vessel design and construction were such that the ultimate properties of the material used for their construction were realized within experimental and analytical uncertainties.

Other significant details of the 2.0-ft-diameter vessel tests which relate to the design of these vessels are as follows. The sealing of the vessels was such that the 5-lb Shot 401 vented gases for ∿50 sec, while the 6-lb Shot 403 vented gases from the vessel for ∿1 min, 55 sec. The venting gases were not especially noisy and did not burn on venting.

The 6.5-lb Shot 405 blew one of the two 1/2-20 door adjusting bolts from the vessel, causing a reduction in the venting time to ∿7 sec. The second 5-lb shot (404) in Vessel 3a blew both adjusting bolts out of the vessel and reduced the venting time to <5 sec. No other adjusting bolts were lost even from the vessels which suffered catastrophic failure. These bolts were originally threaded through nearly 1 in. of vessel material including the doubler. The tap used, however, provided a relatively loose original fit of the bolts in the vessel. In both cases of bolt blowout, the recovered bolts still had threads present on them, and in the case of Vessel 6a, which contained the 6.5-lb shot, the lost

---

*This quantity is the steady-state gas pressure which would exist inside a sealed vessel after the shock waves have subsided, allowing for reaction of the gas products with the originally contained air and establishment of thermal equilibrium between the gases but no heat loss to the container.

adjusting bolt was screwed back into the original threads and held tightly enough to allow the door to be adjusted to a good fit in the port as before the shot. The combination of elastic and plastic stretching of the vessel which enlarged the adjusting bolt hole, together with the internal pressure in the vessel and original loose fit of the bolts, allowed loss of the bolts. Due to the marginal nature of these failures and the long engaged thread length available, it appears likely that this failure could be avoided in future vessels of this design by the use of coarser threads (i.e., 1/2-13 NC) and a tighter original fit of the bolts.

The damage to the door support and operating mechanism other than the adjusting bolts as a result of the large charges fired in these vessels was minimal. The principal damages to the mechanism were elongation of the holes for the cross-pin in the door supports and enlargement of the hole for the main pin (see Figure 5), with the result that as the door was lowered away from the adjusting bolts and reinforcing ring by rotation of the operating nut, the door was allowed to swing down toward a more vertical position. This damage did not appear to affect the strength or integrity of the vessels for blast containment. It merely required readjustment of the adjusting bolts to reseat the door against the ring in the closed position and a few more turns of the operating nut to open and close the door.

A final point regarding the design is that the shock loads transmitted to the floor through the caster wheels were sufficient to cause some damage to the caster-wheel supports and hard rubber tires used for the caster wheels. In the surviving vessels, this damage was sufficiently slight that the caster wheels were still operable, but with some difficulty. In this size vessel it is expected that the provision of slightly larger pneumatic-tired casters would alleviate this problem.

Effect of Blast-Attenuating Filler Materials

Several shots were fired in 4.5-ft-diameter Vessel 2 to investigate the effect of two blast-attenuating filler materials. These were expanded vermiculite of the variety commonly available for home insulation and small glass bottles in 1 to 8-oz sizes. Vermiculite was evaluated because of its lightweight crushable nature together with its low cost, availability, and nonflammable character. The small glass bottles were chosen for evaluation because of the large forces required to fracture, the large free volume, and ready availability. The glass bottles, however, turned out to be relatively heavy and inconvenient to handle.

Table 13 presents the principal results of tests of vermiculite and glass bottles filling the 4.5-ft vessel as a shock-

TABLE 13. EFFECT OF BLAST-ATTENUATING FILLERS ON DYNAMIC RESPONSE OF 4.5-FT VESSEL

Shot No.	Fill[a]	Pentolite Weight, lb	First-Cycle Maximum Response								Cycle No.	Average[b] Stress Filled / Stress Empty
			Gage 1		Gage 2		Gage 3		Gage 4			
			Time, ms	Stress, psi	Time, ms	Stress, psi	Time, ms	Stress, psi	Time, ms	Stress, psi		
227-230	Empty	1.94-2.0	0.45	22,710[3](c)	0.4	11,520[3]	0.45	19,800[1]	0.6	14,130 15,920	1st cycle 2nd cycle	
233	1/2 Filled, V	2.0	?	24,050?	?	7,182?	0.55?	8,015?	0.6	3,760 12,300	1st cycle 2nd cycle	0.588
225	Filled, V	1.95	1.9	2,900	2.0	2,020	2.0	515	1.7	7,440	1st cycle	0.214
217,232	Empty	8.0	0.4	66,470[2]	0.4	39,660[2]	0.4	69,620[2]	0.45	30,480[2] 67,890[2]	1st cycle 2nd cycle	
234	1/2 filled, V	8.0	0.45	62,820	0.45	18,730	NR	NR	NR	NR		0.709
226	Filled, V	8.05	1.6	35,400	1.4	23,770	1.7	45,520	1.3	26,490	1st cycle	0.664
236	Filled, G	8.0	NR	NR	NR	NR	3.0 3.5	18,210[d] 76,626	1.9	28,060	1st peak 2nd peak	0.591 1.011
223	Empty	10.0	0.35	73,370	0.40	69,740	0.40	89,920	0.5	50,690 82,500	1st cycle 2nd cycle	
235	Filled, V	10.0	1.2	30,200		NR	1.1	51,590	0.9	23,760?	1st cycle	0.495

(a) V is vermiculite, G is assorted small glass bottles, 8-oz capacity and less.

(b) Average stress ratio is calculated from $1/n \sum_{i=1}^{n} \frac{(\text{Stress filled})_i}{(\text{Stress empty})_i}$

The average extends over all gages for which both empty and filled stress data exist.

(c) Superscript numbers in parentheses are the number of shot records averaged to obtain recorded number.

(d) Some smaller disturbance arrives before this time. (See Figure 34.)

absorbing filler. The "first-cycle maximum response" is the first maximum tensile response noted from the dynamic strain-gage records. The strain at the first maximum is often not the largest strain observed, but it is the strain value which can be correlated with theory, at least for the empty vessel, and is the maximum strain which occurs for shots large enough to produce plastic deformation of the vessel.

The residual plastic strain data for these tests are incomplete. However, the average plastic strain increments recorded for the four strain gages for Shots 232 and 235 were 335 x 10^{-6} and 68 x 10^{-6}, respectively. Thus, a much smaller (although both are small) plastic strain was produced by 10 lb of Pentolite with a vermiculite fill than 8.0 lb in the empty vessel.

Figure 33 shows the dynamic strain-gage response observed for 8-lb shots of Pentolite. It will be recalled that the Pentolite being used here is low-density, <1.0 g/cm^3 material. Shot 217 shows records typical of those obtained for the empty vessel. Shot 226 shows the response observed for the vessel filled with vermiculite. In both shots, the oscilloscope time zero corresponds to initiation of detonation of the charges. Note the delayed response of the vessel when filled with vermiculite. This effect is also shown in the columns labeled "time" in Table 13 which give the time to reach the first maximum after charge detonation.

Figure 34 shows the dynamic strain-gage response observed for the 8-lb shot in the vessel filled with small glass bottles. The glass bottles delay the arrival of the first large stress pulse even more than the vermiculite, however, when the major stress pulse does arrive, its amplitude is apparently larger than for the vermiculite. A small plastic strain of 313 microstrain was observed at the Gage 3 position after this shot, although the other gages showed none.

It may be seen from examination of the data in Table 13 that the effectiveness of vermiculite as a shock-mitigating medium decreases with increasing charge size from 2 to 8 lb. It is believed, at present, that the vermiculite attenuation capability at the 10-lb level is probably about equivalent to its capability at 8 lb of Pentolite detonated in the vessel, based on the meager data available. It should be pointed out that the vermiculite fill used for the initial 2- and 8-lb Pentolite shots was from one lot of vermiculite, while the vermiculite for the 1/2 filled and 10-lb Pentolite shots was from another lot procured about 10 months later. This may be a factor influencing the apparent change in attenuation effectiveness between the 8- and 10-lb shots.

The intermediate average ratio of filled-to-empty stresses shown by the shots in the vessel 1/2 filled with vermiculite are of

Gage 2, 1200 microstrain per division

Gage 3, 1600 microstrain per division

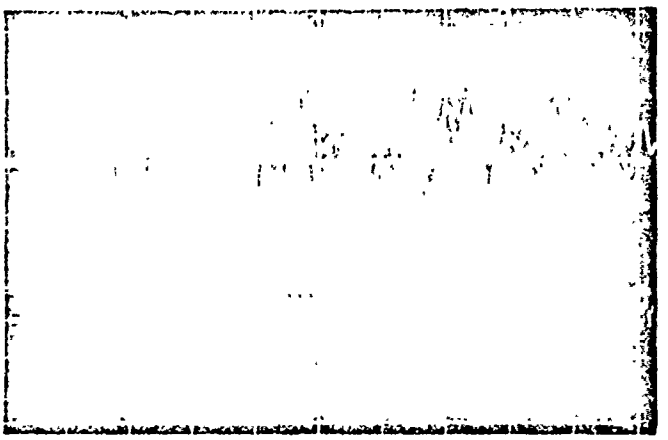

Gage 4, 1000 microstrain per division

Gage 1, 1000 microstrain per division

Shot 217, Empty

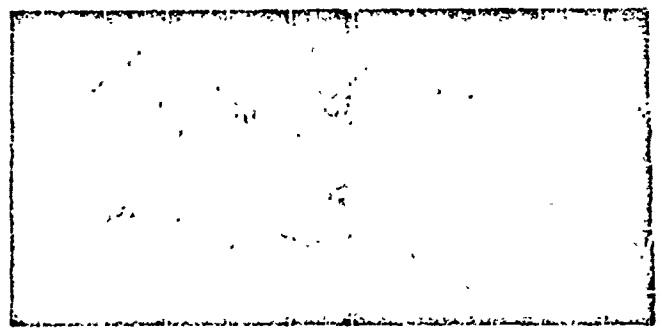

Gage 1, 1000 microstrain per division

Gage 2, 1200 microstrain per division

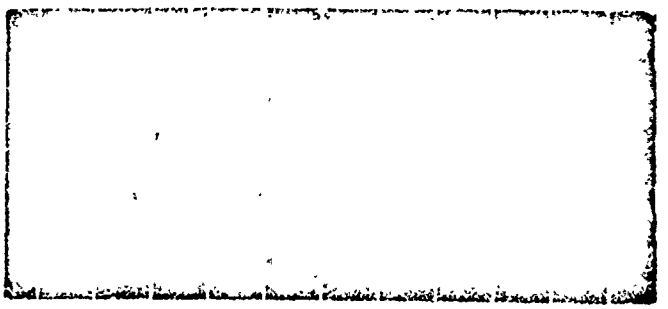

Gage 3, 1600 microstrain per division

Gage 4, 1000 microstrain per division

Shot 226, Vermiculite Filled

FIGURE 33. DYNAMIC RESPONSE OF VESSEL TO 8.0 LB OF PENTOLITE

Sweep speed is 1 ms per division.

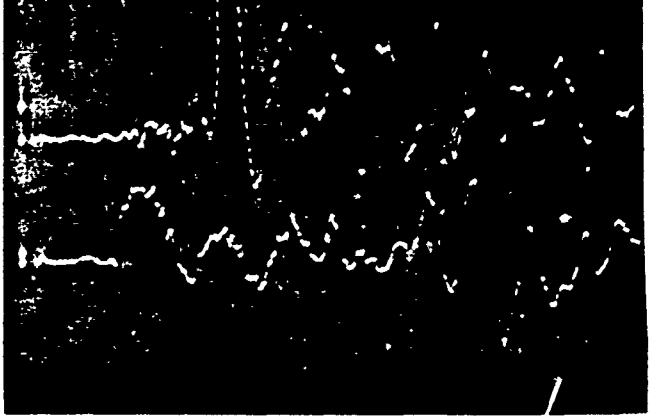

Gage 3, 600 microstrain per division

Gage 4, 600 microstrain per division

FIGURE 34. DYNAMIC RESPONSE OF VESSEL FILLED WITH SMALL (<8 OZ) GLASS BOTTLES

Shot 236; sweep speed was 1 ms/division.

little significance from the standpoint of vessel damage. Due to the location of the strain gages on this vessel (see Figure 8), only Gage 1 was well above the vermiculite fill level with a direct air shock path available from the explosive. This gage shows stress levels essentially the same as those from the empty vessel at both the 2- and 8-lb explosive levels. Thus the 1/2 fill of vermiculite appears to have little or no effect on the upper part of the vessel, while mitigating the shock to the lower part.

The performance of the glass as a blast-attenuation medium was not particularly encouraging and, due to the handling difficulties, no further shots were conducted with this material.

CONCLUSIONS AND RECOMMENDATIONS

(1) Design criteria for spherical blast containment chambers were developed and demonstrated experimentally.

(2) An elastic-plastic analysis of the behavior of spherical blast containment vessels was developed and demonstrated good agreement with experiment in both the elastic and plastic ranges of compact charge loads, for a particular steel (A-537, Class 1 or A-516, Grade 70)

(3) The maximum effect of a suitcase-shaped charge relative to a compact charge was shown to be a function of the scaled distance from the charge to the vessel wall. Further work, both experimental and analytical, is needed in this area for both suitcase and other charge shapes, and in the range of smaller scaled distances.

(4) The effect of two 60% strength dynamites relative to low-density Pentolite on containment vessels was determined approximately in the range of elastic vessel response. The relative effectiveness was found to be a function of the scaled distance. Further work is needed to determine the reason for this behavior and to refine and extend the data to smaller scaled distances for design purposes.

(5) Large, late-time strain cycles were observed for relatively small charges which could lead to low-cycle fatigue failures in the absence of residual plastic deformation. For applications in which repeated detonations in containment vessels are anticipated, this area requires considerable additional investigation to determine safe operating lifetimes.

(6) The single-shot catastrophic failure limit of 2.0-ft-diameter vessels was found to correspond with exceeding the static ultimate strength of the vessels at their thinnest part by stresses from the calculated confined explosion gas pressure. The effect of attachments to the vessel also apparently contributed to the crack origin. Further work on the effect of attachments which may influence vessel failure is needed for applications in which the failure limit load of a vessel is to be approached. Although it is expected that the analytical scaling developed in the program should provide reasonable failure limit estimates, further experimental work to show the importance of size effects on ultimate failure is needed.

(7) When rigid quality controls on manufacture are imposed for the steel employed in these studies, it appears that there may be a factor of three possible increase in the charge load which produces measurable (~0.1 percent) residual plastic strain before the single-shot failure load is exceeded for thin-walled vessels in the small size range investigated. This statement needs experimental verification in the larger vessel sizes.

REFERENCES

(1) Baker, W. E., J. Appl. Mech., 27, 139 (1960).

(2) Baker, W. E., et al., "Engineering Feasibility of Contained Detonation (U)", Air Force Weapons Laboratory Report No. AFWL-TR-65-96 (October 1965), p 29.

(3) Goodman, H. J., "Compiled Free-Air Blast Data on Bare Spherical Pentolite", Ballistic Research Laboratory Report BRL No. 1092 (February, 1960).

(4) Proctor, J. F., "Internal Blast Damage Mechanism Computer Program", Naval Ordnance Laboratory Report NOLTR 72-231 (31 August 1972).

(5) Theory of Plates and Shells, Timoshenko, S., and Woinowsky-Krieger, S., Second Edition, McGraw-Hill Book Company, New York (1959).

(6) Flügge, W., Stresses in Shells, Fourth Printing, Springer-Verlag, New York Inc. (1967).

(7) Roark, R. J., Formulas for Stress and Strain, Fourth Edition, McGraw-Hill Book Company, New York (1965).

(8) Lubahn, J. D., and Felgar, R. P., Plasticity and Creep of Metals, Wiley, New York (1961).

(9) The JANNAF Hazard Working Group, "Chemical Rocket/Propellant Hazards", Vol. 1: "General Safety Engineering Design Criteria" CPIA Publication 194, Chemical Propulsion Information Agency, The Johns Hopkins University, Applied Physics Laboratory (October 1971), p 2-11.

(10) Final Report on Contract No. N000174-74-C-0219 to the Naval Explosive Ordnance Disposal Facility from Battelle-Columbus Laboratories (July 1975), to be published.

APPENDIX A

WELDING PROCEDURE SPECIFICATION

WELDING PROCEDURE SPECIFICATION (WPS)

Welding Procedure Specification No./ Revisions P-75-A Date 3/28/75 Supporting PQR No(S) PQ-75-1

Welding Process(es) Gas-metal-arc in combination with shielded metal arc Types Semi-automatic (GMA and Manual (SMA)

JOINTS

Groove design Single U

Backing

Other

FILLER METALS

F No. 4 and 6 Other

A No. 1 Other

Spec. No. SFA 5.5 SFA 5.20 SFA, SFB AWS No. E7018 E70T-1 Class

Size of Electrode E7018 - 1/8" dia. E70T-1 - 3/32" dia.

Size of Filler

Flux Composition

Particle Size

Electrode Flux Composition

Consumable Insert

Other

BASE METALS

P No. 1 to P No. 1

Thickness range 3/16" to 3"

Other

POSITION

Position of Groove Flat

Welding progression

Other

PREHEAT

Preheat Temp. 250 F min.

Interpass Temp. 250 F min.

Preheat Maintenance

Other

POSTWELD HEAT TREATMENT

Temperature

Time Range

Other

WELDING PROCEDURE SPECIFICATION (WPS)
(Continued)

Welding Procedure Specification No. P-75-A Date 3/28/75

GAS

Shielding Gas(es) Carbon dioxide

Percent Composition _____ (mixtures)

Flow Rate 50 cfh

Gas Backing _____

Trailing Shielding Gas Composition _____

Other _____

ELECTRICAL CHARACTERISTICS

Current DC (AC or DC) Polarity Reverse

Amps. E7018 160 to 18^ E70T-1 380-400 (Range) Volts 26 volts E70T-1 (Range)

Travel Speed _____ (Range)

Other _____

TECHNIQUE PROCEDURES

String or Weave Bead String

Orifice or Gas Cup Size _____

Initial & Interpass Cleaning Initial: hand-held power grinder; Interpass: powered wire brush

Method of Back Gouging Power grinder

Oscillation _____

Contact Tube to Work Distance _____

Multipass or Single Pass Multipass (per side)

Single or Multiple Electrodes Single

Other _____

PROCEDURE QUALIFICATION RECORD (PQR)

Procedure Qualification Record No. PQ-75-1 Date 3/28/75

WPS No. P-75-A

Welding Process(es) Shielded metal-arc for passes 1 thru 3, gas metal-arc for balance

Types Semi-Auto (GMA) and Manual (SMA)
(Manual, Automatic, Semi-Auto.)

JOINTS

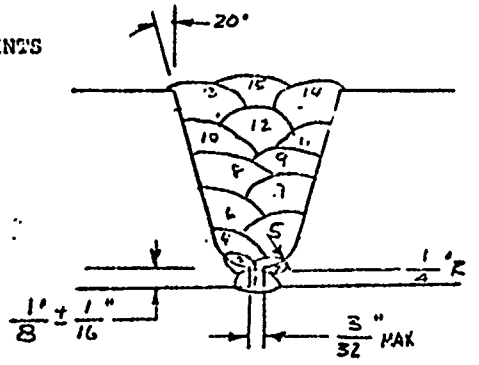

Groove Design Used

BASE METALS

Material Spec. A537A

Type or Grade

P No. 1 to P No. 1

Thickness 1-1/2 inches

Diameter

Other

FILLER METALS

Weld Metal Analysis A No. 1
Size of Electrode E7018 1/8"; E70T-1 3/32"
Filler Metal F No. 4 and 6
SFA Specification 5.5 and 5.20
AWS Classification E7018 and E70T-1
Other

POSITION

Position of Groove Flat
Weld Progression
(Uphill, Downhill)
Other

PREHEAT

Preheat Temp. 250 F
Interpass Temp. 250 F
Other

POSTWELD HEAT TREATMENT

Temperature
Time
Other

GAS

Type of Gas or Gases Carbon dioxide
& Composition of Gas Mixture
Other 50 cfh

ELECTRICAL CHARACTERISTICS

Current DC
Polarity Reverse
Amps. * Volts 26 volts - E70T-1
Travel Speed
Other

TECHNIQUE PROCEDURES

String or Weave Bead String
Oscillation
Multipass or Single Pass Multiple
(per side)
Single or Multiple Electrodes Single

* 170 amps 7018
380-400 amps E70T-1

PROCEDURE QUALIFICATION RECORD (PQR) PQ-75-1 3/28/75
(Continued)

TENSILE TEST RESULTS
SPECIMEN DIMENSIONS PER FIGURE QW 462.1d, Section IX, ASME Boiler Code

Specimen Number	Dimensions Width(1)	Thickness(2)	Area sq. in.	Ultimate Load, lb	Stress, psi	Character and Location of Failure
1			0.202	16,025	79,406	Weld metal
2			0.202	15,925	78,880	Base metal
3			0.200	16,000	79,880	Base metal
4			0.201	15,750	78,511	Base metal

(1) Record outside diameter if a full pipe section is tested.
(2) Record wall thickness if a full pipe section is tested.

GUIDED BEND TEST RESULTS
SPECIMEN DIMENSIONS PER FIGURE QW 452.2a, Section IX, ASME Boiler Code

Specimen Number	Type	Bend Radius	Results	Specimen Number	Type	Bend Radius	Results
1	Side	1-1/4"	No defects	4	Side	1-1/4"	No defects
2	Side	1-1/4"	No defects				
3	Side	1-1/4"	No defects				

Toughness Tests

Specimen No.	Notch Location	Notch Test Type	Notch Test Temp.	Impact Values	Lateral Exp. %Shear	Lateral Exp. Mils	Drop Weight Break	Drop Weight No Break

Type of Tes _____
Deposit Analysis _____
Other _____

Fillet Weld Test

Result - Satisfactory _____ (Yes, No) Penetration into Parent Metal _____ (Yes, No)

Type and Character of Failure _____ Macro Results _____

Remarks

The results of the bend and tensile tests met the requirements of Section IX, ASME Boiler and Pressure Vessel Code, 1974. Welds made by W.H. Stefanov.